ADDIS ABABA UNIVERSITY

AFRICA CENTER OF EXCELLENCE
FOR WATER MANAGEMENT

VALIDATING SATELLITE BASED RAINFALL PRODUCT AND HYDROLOGICAL MODELING IN BLUE NILE: JEMMA SUB-BASIN

M. Sc. Thesis

Getaw Endayilalu

Addis Ababa University

September, 2021

Addis Ababa, Ethiopia

ADDIS ABABA UNIVERSITY

AFRICA CENTER OF EXCELLENCE
FOR WATER MANAGEMENT

VALIDATING SATELLITE BASED RAINFALL PRODUCT AND HYDROLOGICAL MODELING IN BLUE NILE: JEMMA SUB-BASIN

A thesis submitted to Africa Center of Excellence for Water Management in partial fulfillment of the degree of Masters of Science in **Water Management (Hydrology and Water Resources)**.

By:

Getaw Endayilalu

Addis Ababa University

September, 2021

Addis Ababa, Ethiopia

Declaration

I Getaw Endayilalu, the undersigned, declare as this thesis is my own original work, and it is not presented in any University on behalf of any similar degree award. And all materials used in this thesis work were properly acknowledged and referred according to regulations and practices accepted internationally.

Getaw Endayilalu Mekte	.....	.....	getawe21@gmail.com
Name:	**Date:**	**Signature:**	**E-mail:**

Certification

The undersigned certify that he has read the thesis entitled **VALIDATING SATELLITE BASED RAINFALL PRODUCT AND HYDROLOGICAL MODELING IN BLUE NILE: JEMMA SUB-BASIN**, and hereby recommends for acceptance by Africa Center of Excellence for Water Management in partial fulfillment of the requirements for the degree of Master of Science.

.....

Dr.-Ing. Adane Abebe (Advisor)

.....

Date:

ADDIS ABABA UNIVERSITY

AFRICA CENTER OF EXCELLENCE FOR WATER MANAGEMENT

VALIDATING SATELLITE BASED RAINFALL PRODUCT AND HYDROLOGICAL MODELING IN BLUE NILE: JEMMA SUB-BASIN

A thesis submitted to Africa Center of Excellence for Water Management in Partial fulfillment of the Degree of Masters of Science in **Water Management (Hydrology and Water Resources)**.

By:

Getaw Endayilalu

Approved by Board of Examiners

Nigus Gabbiye (PhD) **Chair man:**	..... Date:	..... Signature:
Adane Abebe (PhD) **Advisor:**	..... Date:	..... Signature:
Alemseged Tamiru (PhD) **Internal Examiner:**	..... Date:	..... Signature:
Getachew Tegegne (PhD) **External Examiner:**	..... Date:	..... Signature:

Acknowledgment

First of all almighty God, crutch of all weak and hope of all dishearten, I do not frustrate with you forever. Your endless and measureless love persisted me throughout my life. Let your name is praised and blessed forever.

Dr.-Ing. Adane Abebe deserves my private thanks for his role as a course instructor and as my principal thesis advisor from the starting of the proposal development.

I would like to extend my gratitude to Dr. Fasikaw Atanaw, for his introductory guide as this thesis document is to be written with R-markdown, without which the compilation of this document actually may not be easy.

I would also want to acknowledge my sponsoring University, Aksum, and my hosting University, Addis Ababa, which facilitated the chance of carrying out my graduate study in the indicated hosting University, Addis Ababa.

GetawEndayilalu

Abbreviations and Acronyms

μm	micrometer
AMW	Active Microwave
Arc-GIS	Geographical Information System
ASC2DSS	American Standard Code to Data Storage System
ASCII	American Standard Code for Information Interchange
CN	Curve Number
CSI	Critical Success Index
CTT	Cloud Top Temperature
DEM	Digital Elevation Model
DMC	Double Mass Curve
DOS	Disk Operating System
DSS	Data Storage System
EM	Electro Magnetic
ETS	Equitable Treat Score
FAQ	Frequently Asked Question
FAR	False Alarm Ratio
GeoHMS	Geospatial Hydrologic Modeling system
GIS	Geographical information system
GPS	Geographical position system
GRDs	Ground Rain gauge Data
GSFC	Goddard Space Flight Center
HEC	Hydrologic Engineering Center
HEC-DSS	Hydrologic Engineering Center's-Data Storage System
HEC-DSSVue	Hydrologic Engineering Center's-Data Storage System Visual Utility Engine
HEC-HMS	Hydrologic Engineering Center's-Hydrological Modeling System
HEC-SSP	Hydrologic Engineering Center's-Statistical Software Package
IDW	Inverse Distance Weighted
IDWM	Inverse Distance Weighted Method
IR	Infrared
Km^2	Square Kilometer
LEO	Low Earth Orbit
LULC	Land Use Land Cover
m	Meter
MAE	Mean Absolute Error

ME	Mean Error
METEOSAT	Meteorological Satellite
mm	millimeter
MoWIE	Ministry of Water Irrigation and Electricity
MSE	Mean Square Error
MW	Microwave
NetCDF	Network Common Data Form
NASDA	National Space Development Agency of Japan
NMSA	National Meteorological Service Agency
P24	Daily precipitation
PM	Passive Microwave
POD	Probability of Detection
POFD	Probability of False Detection
R^2	Coefficient of determination
R-PL	R-Programming Language
RC	Raster Calculator
RMSE	Root Mean Square Error
RS	Remote Sensing
SCS	Soil conservation Service
SREs	Satellite rainfall estimate
TIR	Thermal Infrared
TLGCE	Travel Length Grid Cell Exporter
TMI	TRMM Microwave Imager
TMPA	TRMM Multisatellite Precipitation Analysis
TRMM	Tropical Rainfall Measurement Mission
US	United State
USGS	United State Geological Survey
UTM	Universal Transverse Mercator
VIRS	Visible and Infrared Scanner
VIS	Visible
WWRP	World Weather Research Program

Abstract

Water resource management absolutely depends on water resource data like rainfall and stream flow. Better quality of such data are obtained by direct measurement via interconnected gauging instruments. Due to limited resource, gauging instruments' distribution are not dense enough, in turn causes water resource data scarcity. Currently, Satellite rainfall estimates are available with good spatial and temporal resolutions. However, they are estimates rather than direct measurements. Thus, as the study was begun to evaluate the performance of satellite based rainfall product, TRMM_3B42; it was validated in Jemma sub-basin, and its raw and combined version was evaluated as input of distributed type of HEC-HMS model in Gumerrow catchment. For the achievement of the objectives, collected hydro-meteorological, satellite remote sensing and Arc-Info data were processed with appropriate tools like R-programing language, Arc-GIS model builder, HEC-HMS and others. Results also were presented using graphical techniques, categorical and continuous statistics, and model evaluation statistics. The Satellite based rainfall product and Ground rain-gage data were comparable except some important variations. In categorical rainfall values, the overall accuracy of Satellite rainfall estimate was greater than 78.7%, which was observed in Light rain type of daily timescale. However, the stated algorism has faced special difficulty in daily timescale with more false alarms. In continuous rainfall values, Positive linear association was detected in daily, monthly and seasonal timescales with correlation coefficient values of 0.52, 0.915 and 0.926 respectively. And an average underestimation of Satellite rainfall estimate was discovered in all timescales. Among seven HEC-HMS model parameters, Potential max retention factor (S) was obtained as the most sensitive parameter in Gumerrow catchment. Raw Satellite rainfall estimate showed poor performance in calibration period of (2003-2006) with NSE, PBIAS, RSR and R^2 values of 0.406, 24.26%, 0.771 and 0.417 respectively. However, the performance had improved significantly to good enough with NSE, PBIAS, RSR and R^2 values of 0.532, 14.83%, 0.684 and 0.554 respectively when combined version was used as input of HEC-HMS model. Relative to calibration period, improved performance was discovered in validation period of (2007-2008) with NSE, RSR and R^2 values of 0.452, 0.74 and 0.477 respectively for raw Satellite rainfall estimate, and 0.56, 0.663 and 0.618 respectively for combined version.

Keywords: Jemma sub-basin, TRMM_3B42, combined version, Gridded data, distributed HEC-HMS model.

List of Tables

List of Figures

Contents

1 INTRODUCTION

1.1 Background

Even if the beginning of water cycle is not determined, precipitation is the main input of global water balance either in the ocean or continental basin level. Liquid part of it, water, is one of the basic element of nature. Without water, nature is unexpected dream to exist. Plants, animals and things within a universe all alive with water, and it is needed in different quantity, quality and forms. So, water directly controls the diversity of all on the earth. However, because of natural and anthropogenic effects, its pattern and distribution varies with space and time.

Global water balance has been believed as a constant amount. However, world population and his demand for water is increasing continuously due to different natural and artificial factors. As a result, people are now navigating water resource in remote areas, and investing huge investment to treat surface water to satisfy their demand. Not only this, penetrating very deep ground water wells and extracting ground water became the usual reaction for the scarce and unmet demands. Even if these reactions are relaxing the temporal demands, still there is scarcity for different purposes (Drinking Water supply, Irrigation, Hydropower, green environment and the like).

Conversely, there is time which excess water becomes rejected like flood in summer seasons (Ethiopia). Therefore, quantifying the temporal and spatial water availability is decisive precondition for compromising such demand imbalance and extreme events through water management tool. Precipitation and stream flow are the common and usual water resources need to be quantified.

The best and nearly accurate way of quantifying water resource potential is direct measurement through interconnected rain gauge and stream flow gauging network. But, installing dense enough network and making continuous record is no viable, especially for low income countries. Conventionally, rain gauge observation is an accurate way of measuring precipitation at a point. But, due to financial and other limitations, the network is not dense enough, and not reliable to represent the actual rainfall distribution (Liu et al., 2015). Not only this, also could be affected by natural and artificial obstacles. Sometimes, wrong data report is another defect being observed in rain gauge measurement.

Another contemporary method of estimation of precipitation is satellite algorisms, which able to provide temporally and spatially continuous retrieve. But, the measurement is on

surrogate variables like reflectance, brightness temperature and back scatter. Even, these variables are being measured above ground surface on the air, and may not exactly represent the precipitation on the ground surface. The algorisms are calibrated locally, and may not work the same in another areas. Sampling and bias correction processes in SREs also induces different uncertainties. Thus, SREs also have their own weakness on the side of their merit, like that of conventional method (Rahmawati and Lubczynski, 2018).

The precipitation passes through number of interconnected hydrological processes to reach to the outlet of drainage basin such as interception, infiltration, evaporation, transpiration and percolation. The remaining part of precipitation finds its way to flow as runoff over watercourses. It is another fundamental Water resource need to be quantified. Usually measurement of stream flow is done through installing gauging instrument on appropriate position of the river. But, installing and operating stream flow gauging stations in each rivers continuously is not an easy task financially. It may fail frequently and maintenance also is a challenging issue. Following that, hydrologists are applying different hydrological models. However, precipitation is still an indispensable input. Therefore, verifying and assuring the level of accuracy of SREs should be an important precondition of professionals.

1.2 Problem statement

The global water balance has been assumed as a constant amount. Because of continuous population growth, water however is highly demanding from time to time. Different technological advancements also demanding extra water. Global climate change due to natural and anthropogenic effect became new hot issue, which directly affect the normal rainfall distribution. Extreme events (flood and drought) are also appearing in different parts of the world with sever disaster. Human beings are trying to react otherwise adapt such issues through different techniques, and generally it could be said water management.

Accurate and near real-time water resource data is the vital input of such water management reactions. However, this data is highly scarce especially in low income countries, even the available are questionable due different reasons. Even if ground rain gauge is in use, Ethiopia is highly exposed country for the scarcity of water resource data . Because, the available rain gauge network is not dense enough (Tesfatsion and Dinku, 2015), and it is also easily affected by natural and artificial activities. Not only this, the available gauging stations are limited along roadways. Currently, near real-time contemporary Satellite rainfall algorisms are available globally with high spatial and temporal resolution. But, it is not direct way of measurement like that of ground rain gauge. Otherwise, it is estimation of precipitation from

surrogate variables indirectly, and which is problems of all SREs (Shrestha et al., 2008).

As the Satellite algorisms are an indirect method of precipitation estimation, direct application of such products for water resource quantification in turn for water resource management is wastage of resource in addition to causing to wrong conclusions (Zambrano-Bigiarini et al., 2017). Thus, this research was initiated to evaluate and validate the spatial and temporal performance of Satellite rainfall estimates, and to combine with rain gauge data so as to consider their respective advantages in application of distributed type of hydrological models.

1.3 Objective

1.3.1 General objective

The general objective of this study is to evaluate the performance of satellite based rainfall estimate, TRMM_3B42.

1.3.2 Specific objectives

The specific objectives of the study are;

- To verify the latest version of TRMM_3B42 satellite based rainfall estimate.
- To evaluate the performance of TRMM_3B42 as an input of distributed type of HEC-HMS hydrological model.
- To realize the effect of combined version of TRMM_3B42 on the model output.

1.4 Research questions

- Does the latest version of TRMM_3B42 agrees with ground rain gauge data?
- Does TRMM_3B42 performs well as an input of the model?
- Does the combined version of TRMM_3B42 has an effect on the model output?

1.5 Significance of the study

Even if the rain gauge has better accuracy at a point, its distribution is very limited to represent the spatial rainfall. As a result, this study helps to evaluate TRMM ability to use

instead of rain gauge in turn as a potential source of hydrological model. Also it may be helpful for researcher, algorism developers, Students and any other interested bodies.

1.6 Scope of the study

This study is restricted on verifying the latest version of TRMM_3B42 data for Blue Nile, Jemma Sub Basin, and on evaluating this data with HEC-HMS hydrological model for Gumerrow catchment. To do so, TRMM_3B42 data was verified and compared with graphical techniques, categorical and continuous statistics; raw TRMM_3B42 data was then used as input of distributed type of HEC-HMS model, and finally, the combined version of TRMM_3B42 data was used as input of the HEC-HMS model.

2 LITERATURE REVIEW

In hydrological and watershed modeling, remotely sensed data along with advancement of computer technology are found to be more valuable for providing cost-effective data input and for estimating model parameters. And hydrologist have gradually started using GIS-based distributed modeling approaches. It has become an efficient method to integrate the spatial and non-spatial database for hydrological modeling. Thus, remotely sensed data and GIS tools were used fundamentally. And this part of the document presented related and relevant literature works around the world, and accessible previous studies done within the proposed study area.

2.1 Remote sensing

Remote sensing is the science of obtaining information about an object through the analysis of data acquired by a sensor that is not in contact with the object (Lillesand et al., 2004). Propagating electromagnetic energy from the sun through the atmosphere is the main source of energy which remote sensing is being employed. This energy interacts with earth surface features, and retransmit through the atmosphere to (air or space) borne platform that is deployed various application sensors over it. Accordingly, these Sensors acquire data on the way various earth surface features emit and reflect electromagnetic energy. And these data are being analyzed with computer to provide information about the resource that is under investigation. As data being analyzed, remotely sensed data may be supported and verified by ground truth through field surveying.

2.2 Satellite based rainfall estimates

Satellite-based precipitation estimation, the effect of remote sensing, has been one of the most research topics in multiple disciplines like Meteorology, Hydrology and Agriculture. Nowadays, rainfall data from satellite products are found in high spatial and temporal resolutions including near real time data for different purposes. The main problem of all SREs are estimation of precipitation from cloud signals indirectly (Shrestha et al., 2008). Satellite-based rainfall estimates (SREs) provide a new opportunity for a wide range of hydrological applications, from water resources modelling to extreme event monitoring such as droughts and floods (Zambrano-Bigiarini et al., 2017). However, SREs has their own uncertainties. A great deal of research was made in last two decades on methods of estimating

rainfall from infrared and microwave satellite observations; now there are several operational and semi-operational satellite algorithms available from national centers and universities to produce rainfall estimates for time periods ranging from half-hourly to monthly (Shrestha et al., 2008).

Satellite rainfall can be estimated from geostationary satellites using VIS and IR sensors data, as well as from Low earth orbiting satellites using Passive and Active microwave sensors data. Most common sensing systems operate in one or several of the visible, IR, or microwave portions of the spectrum (Barrett, 2000). Barrett (2000) also presented as VIS, IR (thermal) and MW electromagnetic radiation from the target are the proven methods of estimation of rainfall from environmental satellites. Upadhyaya and Ramsankaran (2014) divided the techniques available for rainfall estimation from remote sensing into three basic categories: VIS/IR techniques, Microwave techniques and Blended techniques. These techniques are based on their sophisticated sensors, mostly developed to measure electromagnetic spectrums outside the visible range.

Visible and infrared

VIS and IR techniques have a long historical development and depends upon the relationship between cloud top characteristics and the rainfall falling from their bases (Kidd et al., 2003). Visible portion of EM spectrum is extremely small (0.4-0.7)μm, but IR is (0.7-14)μm. VIS and TIR sensors carried by Geo-stationary satellites provide very high temporal resolution. But, these sensors are not having direct relation with rainfall (Upadhyaya and Ramsankaran, 2014). Within the IR portion of the spectrum, only thermal IR (3-14)μm is directly related to the sensation of heat (Lillesand et al., 2004). In case of visible images, the clouds which appear bright are tending to be thick, and thick clouds are likely to be associated with rainfall. But, major drawback of this band is that the data is available only during day time. In case of the IR regions, the principle is based on the cloud top temperature (CTT). CTT is inversely proportional to the rainfall rate. Colder clouds are associated with the heavier rainfall. It has an advantage over visible spectrum as the data is available 24 hrs. The main drawback of IR-based techniques is that they relate the surface rainfall from the cloud-top characteristics. However, more direct measurements of rainfall can be done with algorithms utilizing PM data. These algorithms exploit the observation of the hydrometeor particles themselves (rather than the cloud tops) to produce estimates of rainfall (Kidd et al., 2003).

Passive microwave

The portion of this EM spectrum is 1mm to 1m (Lillesand et al., 2004). In microwave region, the EM radiations penetrate through the cloud and hence it can be used to estimate rainfall

more accurately than VIS and IR techniques (Upadhyaya and Ramsankaran, 2014). Rainfall estimates produced by using PM techniques are more direct, since they are primarily sensitive to the concentration of ice particles or droplets associated with precipitation (Kidd et al., 2003). LEO satellites can carry sensors operating in the microwave band because the short distance from the target allows to obtain a good spatial resolution. As these LEO satellites carry sensors in microwave spectrum more accurate rainfall estimates can be provided, but the disadvantage associated with this is its coarse temporal resolution.

Active sensors

Unlike passive sensors, Active sensors are designed to have their own artificial source of radiation in addition to measuring reflected EM waves. Precipitation Radar is the first AMW instrument on board of satellite which provides three dimensional profile of rainfalls (Mishra, 2012). It was launched in 1997 by joint Japanese and US Tropical Rainfall Measuring Mission (TRMM) satellite (Barrett, 2000). Providing vertical distribution of rainfall for the investigation of its three-dimensional structure; obtaining quantitative measurements over land and oceans; and improving the overall retrieval accuracy by the combined use of the radar, TMI and VIRS instruments was the aim of this sensor (Levizzan et al., 2002). The principle of estimating rainfall from AMW is the same as that of Ground based Rader.

Blended techniques

This technique combines strengths of different sensors explained above, may be by incorporating rain gauge observations also. The recent SREs are multi-sensor techniques which combines advantages of both geostationary (high temporal resolution) and polar orbiting satellites (direct relation) data (Upadhyaya and Ramsankaran, 2014). Blending is done by different algorisms (Doan et al., 2014) to produce better SREs accuracy.

In the last few years, satellite-based precipitation datasets were believed to be a potential source of inputs in driving hydrological models especially in complex terrain areas or ungauged basins where ground gauges are sparse or nonexistent (Alazzy et al., 2017). But these SREs are being obtained from different sources, different sensors and having different resolutions. Even the algorisms are calibrated with local rain gauge data. Therefore, before using any satellite rainfall products in the extension of other areas, their performance should be evaluated.

2.3 Satellite rainfall estimate (TRMM_3B42v7)

TRMM is a joint space mission between NASA and the Japan Aerospace Exploration Agency (JAXA) launched on November 27, 1997, and designed to monitor and study tropical and

subtropical precipitation and the associated release of energy (Bayissa et al., 2017, Alazzy et al., 2017). It is the first space mission dedicated to measure tropical and subtropical rainfall through microwave and visible/infrared sensors, including the first spaceborne rain radar (NASDA, 2001). According to Liu et al. (2015), TRMM satellite carries five rain measuring instruments (Figure 2.1) such as Microwave Imager (TMI)⇒ Provides information on the integreted column preciptation content, cloud liquid water, cloud ice, rain intensity, and rainfall types; Visible Infrared Scanner (VIRS)⇒ Provides high resolution observations on the cloud coverage, cloud type, and cloud top tempratures; Precipitation Radar (PR)⇒ Measures 3D rainfall distribution; Lightning Imaging Sensors(LIS)⇒ Observes the distribution and variablity of lightning over earth; the clouds and Earth's Radiant Energy System(CERES)⇒ Measures emited and reflected radiative energy from the earth's surface and the atmosphere and its constituents. However, on 7 October 2014, the TRMM Precipitation Radar data was precluded due to the satellite altitude descendant (Huffman, 2018). CERES was out of service due to mechanical failure (Liu et al., 2015).

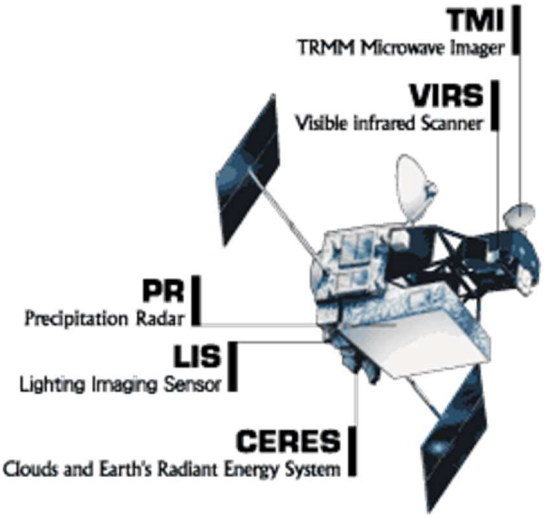

Figure 2.1: Overview of TRMM Satellite (Japan Aerospace Exploration Agency, 2017)

According to Huffman et al. (2007), TMPA (the accurate precipitation estimate of satellite), were produced by merging three types of observations such as PMW, IR, and PR from multiple LEO and Geo satellites and ground observations at a spatial and temporal resolutions of $0.25^oX0.25^o$ and 3hr respectively. However, PR, PMW, and IR operate within the global latitude belt of 35^oN to 35^oS, 40^oN to 40^oS, and 50^oN to 50^oS, respectively.

The NASA Goddard Space Flight Center (GSFC) developed the Multisatellite Precipitation analysis (TMPA) algorithm (Zeng et al., 2018) from a wide variety of modern satellite borne precipitation related sensors (Mauricio Zambrano-Bigiarini et al., 2017). As example: TRMM

Microwave Imager (TMI) sensor on TRMM satellite; Special Sensor Microwave/Imager (SSM/I) and Special Sensor Microwave Imager/Sounder (SSMIS) on Defense Meteorological Satellite Program (DMSP) satellites; Advanced Microwave Scanning Radiometer for the Earth Observing System (AMSR-E) on Aqua; Advanced Microwave Sounding Unit (AMSU) on the National Oceanic and Atmospheric Administration (NOAA) satellite series; and Microwave Humidity Sounders (MHS) on later NOAA-series satellites and the European Operational Meteorological (MetOp) satellite (Huffman et al., 2009; Zambrano-Bigiarini et al., 2017; Zeng et al., 2018) could be listed. Many more satellite sensor data may also be incorporated.

The products are continuously reprocessed, and algorisms are improved to the next version, when new issues are identified in the previous version by TRMM (Rossi et al., 2017). The TRMM Combined Instrument (TCI) estimate (TRMM 2B31 product) uses data from the precipitation radar (PR) and the TRMM Microwave Imager (TMI) sensors onboard the TRMM satellite to derive optimal precipitation estimates for TRMM (Wei et al., 2017). On October 7, 2014 the satellite descended to an altitude that precluded useful TRMM Precipitation Radar data (Huffman, 2018). TRMM Microwave Imager (TMI) however continued to function with slowly changing characteristics until it was shut down on 8 April 2015 (Huffman, 2018). Version-7 of 3B42 algorism which is based on multi-satellite precipitation analysis is the latest version of TRMM products (Alazzy et al., 2017). After more than 17 years of data collection, the instruments on TRMM were turned off on 8 April 2015, but the TMPA 3B42 product will continue to be produced through early 2018 (Zambrano-Bigiarini et al., 2017; https://pmm.nasa.gov/data-access/downloads/trmm).

TMPA algorithm could be executed using the following three steps: first, the PMW precipitation estimates are calibrated and combined to generate the most accurate estimation from PMW; second, the calibrated PMW are used to create IR precipitation estimates; and finally, both the PMW and IR precipitation estimates are merged to provide the best TMPA precipitation estimates. The TRMM 2B31 product was used as a satellite calibrator for the production of 3B42 and 3B43 products until October 2014 when the routine production of TRMM TCI precipitation estimates was terminated due to the gradual orbital descent of the TRMM spacecraft. As a result, after October 2014, climatological satellite calibrations were instead adopted for real-time TMPA products (Wei et al., 2017, Ren et al., 2018). TMPA is available in two products real time (3B42RT) and Post real time (3B42).

Among different types of satellite missions, the most extensive and most widely used for rainfall study of tropical regions, TRMM (Woldemeskel et al., 2013) and its latest version product, TRMM_3B42v7, which was released in May 2012 (Alazzy et al., 2017) was used.

2.4 Ground-based rain gauge observation

Ground rain gauge observation is a method of measuring rainfall depth at a point location. Liu et al. (2015) presented unreliability of ground data at sparse rain gauge network in South East Asia. While appreciating the advantages of SREs, they also observed a remarkable limitation of point rain gauge data on the application of distributed hydrological model. Installing and operating rain gauge networks in every remote areas may not viable economically, especially in low income countries. The network density of conventional stations does not adequately reflect the various climatic zones of the country/Ethiopia (Tesfatsion and Dinku, 2015). Accurate estimation of spatial rainfall is vital for modelling hydrological systems and planning and management of water resources (Woldemeskel et al., 2013). In addition to its spatial coverage problem, it can be easily affected by natural and artificial activities (vegetation, mountains, buildings, measurement errors, and wind effect). Even while spatial rainfall can be estimated using dense rain gauge measurements, it is not as such easy task to operate reliably to get reliable data.

2.5 Methods of verifying satellite rainfall estimates

Estimated satellite rainfall products have to be verified and compared with relatively accurate rain gauge data. Various verification scores are used to verify precipitation estimated by satellites. Details of these scores can be found at world weather research program (WWRP, 2009) and from the (WWRP, 2008). World weather research program (2009) described standard verification methods as eyeball, categorical and continuous. These methods are also described by (Mariani, 2008).

2.5.1 Eyeball or Visual or Graphical verification

Eyeball method, which is said one of the oldest and best verification methods, is looking at the forecast and observations side by side and use human judgment to differentiate the forecast errors. It is always recommended before starting any statistical verification, especially if only few forecast fields have to be compared, that is, if forecast verification is performed in a case-study context (Mariani, 2008). According to Mariani, this kind of subjective interpretations is useful to recognize forecast errors; to detect possible observed errors; to qualitatively evaluate the spatial displacement of the forecast field with respect to the observed field; to identify missing data, etc. It is not quantitative; could be exposed to subjective bias of interpretation, and advised to use with caution (WWRP, 2009). This method was illustrated with example

Table 2.1: Contingency table

		Observed Values		
		Yes	**No**	**Total**
Forcasted Values	**Yes**	Hit	False alarm	Forcasted Yes
	No	Miss	Correct Negative	Forcasted No
	Total	Observed Yes	Observed No	**Total**

on WWRP (2009). Eyeball method is very important if there is only a few forecasts, or have enough time, or not interested in quantitative verification statistics. Even when quantitative statistics are used, it is a very good idea to look at the data from time to time. Common ways to present data are time series and maps (WWRP, 2009).

2.5.2 Categorical verification

Categorical verification statistics measure the correspondence between the estimated and observed occurrence of events (Levizzani et al., 2007). When forecasts are discrete or expressed in terms of categories or classes, categorical skill score is valid approach. These categories can be defined in terms of ranges of continuous forecast values by introducing several thresholds. When only one threshold is introduced, we are dealing with categorical dichotomous forecasts (Mariani, 2008). A dichotomous forecast says, "Yes, an event will happen", or "No, the event will not happen" (WWRP, 2009). Rain and fog prediction are pointed out as example which required yes/no forecasts. To verify this type of forecast it is started with a contingency table (Table 2.1) that shows the frequency of "yes" and "no" forecasts and occurrences. The four combinations of forecasts (yes or no) and observations (yes or no) called joint distribution are:

- Hit - event forecast to occur, and did occur
- Miss - event forecast not to occur, but did occur
- False alarm - event forecast to occur, but did not occur
- Correct negative - event forecast not to occur, and did not occur

The total numbers of observed and forecasted occurrences and non-occurrences on the lower and right sides of the contingency table (Table 2.1) are called marginal distribution.

A perfect forecast system would produce only hits and correct negatives, and no misses or false alarms. Highly recommended statistics (WWRP, 2008) such as Accuracy, BIAS, POD,

FAR, and CSI are selected to use, and their formulas, ranges and perfect scores are tabulated in Table 3.5.

2.5.3 Continuous verification

Verifying forecasts of continuous variables measures how the values of the forecasts differ from the values of the observations (WWRP, 2009). Continuous verification often includes exploratory plots like scatter plot and box plots. Continuous verification concerned on quality of continuous variables like rain amount (WWRP, 2008). Correlation coefficient (r), Mean Error (ME), Mean Absolute Error (MAE) and Root Mean Square Error (RMSE) are highly recommended statistics (WWRP, 2008).

2.6 Hydrological modeling

Model is simplified representation of the actual phenomena to understand the real world system. Hydrologic models are simplified representations of actual hydrologic systems that allow us to study the functioning of watersheds and their response to various inputs, and gain a better understanding of hydrologic processes (Tiwari et al., 2013). Hydrological models are simplified and conceptualized representation of hydrologic cycle that serve as a tool to transform the meteorological forcing (rainfall and evapotranspiration) into the hydrological response of a catchment (runoff). According to hydrologic modeling system HEC-HMS technical reference manual, Feldman (2000), A model relates something unknown (the output) to something known (the input). In rainfall-runoff modelling, the known input is rainfall, the unknown output is runoff characteristics (peak discharge, volume, time to peak, etc.) or the known input is upstream flow and the unknown output is down stream flow, and the watershed is the system being modelled.

2.6.1 Classification of hydrological models

There are number of ways of classifying models, which generally based on the method of representation of the hydrological cycle or a component of the hydrologic cycle. Due to the complex nature of rainfall-runoff processes, different hydrologists have different modelling approaches even to the same hydrological system. According to Jajarmizadeh et al. (2012), classification of hydrological models are not exact, and different hydrologist may give different definitions; the reason is that the nature of models is often the same but many models

have overlapping characteristics. According to Pechlivanidis et al. (2011), hydrological models can be classified based on their model structure, spatial distribution, randomness, and spatial-temporal application.

2.6.1.1 Structure based model classification

Depending on the degree of complexity and physical completeness in the formation of the structure, hydrological models can be broadly classified into three categories: Empirical or Black Box, Conceptual or Grey-Box, and Physically based distributed or White-Box models.

Empirical (Black Box) models: These models are built upon observation of input and output without seeking to represent explicitly the process of conversion (Feldman, 2000). The parameters of the model do not have any physical meaning. According to Xu (2002), sometimes they are called input output models, and parameters can be estimated only by using concurrent measurements of input and output. They do not account for the catchment behavior. They consider the catchment as a lumped unit, without taking into account the spatial characteristics of the basin.

Conceptual (Grey Box) models: It is built up on a base of knowledge of the pertinent physical, chemical and biological processes that act on the input to produce the output (Feldman, 2000). Hydrologic models are considered as conceptual if the form of the function of equations are suggested by consideration of the physical processes acting upon the input variables to produce the output variables. Generally, conceptual models consider physical laws, but in highly simplified form. These models are intermediate between physical and empirical models (Xu, 2002). It Includes semi empirical equations with a physical basis (Devi, 2015).

Physically based (White Box) models: According to Xu (2002), physical based model has a logical structure similar to the real-world system and may be helpful under changed circumstances. This is a mathematically idealized representation of the real phenomenon. In this method huge amount of data such as soil moisture content, initial water depth, topography, topology, dimensions of river network etc. are required, and it can overcome many defects of the other two models because of the use of parameters having physical interpretation (Devi, 2015).

2.6.1.2 Spatial distribution based model classification

Lumped models: It does not account for spatial distribution of input variables or

parameters to represent the heterogeneity in vegetation, soil or other watershed characteristics. These models either average or ignore spatial catchment characteristics. HEC-HMS model primarily lumped models; the Mod-Clark model is an exception (Feldman, 2000).

Semi-distributed models: In semi-distributed model, watershed is divided into smaller computational elements (or sub-basins), and hydrologic computation is carried out for each element (Paudel, 2010). There is a wide variation on how these computational elements are formulated. Again Paudel (2010) stated as some of the models use natural watershed-divides as the criterion for dividing a watershed, and some use land use and soil characteristics.

Distributed models: In this model, spatial (geographic) variations of characteristics and processes are considered explicitly (Feldman, 2000). According to Paudel (2010), distributed models divide the basin into elementary unit areas such as grid cells and solve basic physical equations to simulate the watershed processes. Distributed model can be used to account for the spatial variation of precipitation, land use, or soil type within a watershed (Paudel, 2010).

2.6.1.3 Timescale based model classification

Single event models: An event model simulates a single storm (Feldman, 2000). Rainfall-runoff process in a catchment is simulated for a single rainfall or stream flow event with durations ranging from several hours to several days (Hossain et al., 2019). According to their conclusion event based modelling performs better than continuous simulation modelling in reproducing both total runoff hydrograph and direct runoff hydrograph.

Continuous event models: These types of models use time series of number of years relative to event types of models. In Continuous modelling the rainfall-runoff process is simulated for a long time period ranging from a couple of months to several years, including both dry and wet seasons (Hossain et al., 2019). Generally, in event-based models, the rainfall losses mainly due to infiltration are computed. However, in continuous hydrologic models, the rainfall losses due to evapotranspiration are mainly computed because they constitute the largest part of the rainfall losses on a long-term time basis (K and V, 2014).

2.6.1.4 Randomness based model classification

Deterministic models: Results are uniquely determined through known relationships between the conditions and data. A single result is produced from a model with a single set of input data and parameter values, and a given input will always produce the same output, if the parameter values are kept constant (Pechlivanidis et al., 2011).

Stochastic models: Random variables are used to represent process uncertainty. According to Pechlivanidis et al. (2011), it produces different results from one set of input data and parameter values when they run under clearly seen identical conditions.

2.6.2 Hydrologic model selection

Hydrological model selection depends on the objective of the modeler and the availability of hydro-meteorological as well as other necessary data. Furthermore it may depends on simplicity, acceptability, versatility, stability and powerfulness of the model in addition to its cost.

2.6.3 Significance of hydrological modelling

Hydrological modeling is very advantageous to know water resource potential and in turn for management of surface as well as subsurface water resources by saving time, labor and money that will be invested in direct watershed runoff measurement. Apart from that, it helps to understand hydrological system more.

2.7 HEC-HMS hydrological modeling system

Over view

Mathematical model means the equations that represent the behavior of hydrologic system components. For examples the combination of the continuity and momentum equations together form a model of open channel flow for routing. If the equations of a mathematical model are too numerous or too complex to solve with pencil, paper and calculator, they are translated into computer code and an appropriate equation solver (an algorism). The result is a computer program. Thus, HEC-HMS is a computer program that includes variety of models, which was developed at the Hydrologic Engineering Center of the US Army Corps of Engineers (Feldman, 2000).

2.7.1 Model components

HEC-HMS model computes runoff volume by computing the volume of water that is intercepted, infiltrated, stored, evaporated, or transpired, and subtracting it from the precipitation. Interception and surface storage are intended to represent the surface storage of water by trees

or grass, local depressions in the surface ground, cracks and crevices in parking lots or roofs, or a surface areas where water is not free to move as overland flow. Infiltration represents the movement of water to areas beneath the land surface. Interception, infiltration, storage, evaporation, and transpiration collectively referred to as loss in the program. Subtracting the sum of all these losses from the precipitation results runoff volume within the specified watershed.

In HEC-HMS, a project consists of a basin model, a meteorological model, and control specifications. The basin model is composed of a schematic, a loss model, a transform model, and a base flow model. The meteorological model contains the rainfall data. Control specifications set the starting time and date, the ending time and date, and the computational time interval. Methods and model components used in this study are summarized in Table 2.3.

2.7.1.1 Loss method

The soil conservation service (SCS) curve number model estimates precipitation excess as a function of cumulative precipitation, soil cover, land use, and antecedent moisture using the following equations:

$$P_e = \frac{(p - I_a)^2}{(p - I_a + S)} \text{.....(2.1)}$$

where,

- P_e = Excess precipitation (runoff) (mm);
- P = Rainfall (mm);
- I_a = Initial abstraction (mm); a total amount of loss that occurs in the watershed before the surface runoff begins, and it includes water retained in surface depressions and water intercepted by vegetation, evaporation, and infiltration (Paudel, 2010); and
- S = Potential maximum retention (mm); a measure of the ability of a watershed to abstract and retain storm precipitation. SCS developed empirical relation of I_a and S from experiment like I_a=0.2 S.

Therefore the watershed runoff is

$$P_e = \frac{(p - 0.2S)^2}{(p + 0.8S)} \text{.....(2.2)}$$

The maximum retention, S, and watershed characteristics are related trough an intermediate parameter, Curve Number (CN)

$$S = \frac{25400}{CN} - 254 \quad \text{.....(2.3)}$$

Curve number ranges from 100 for water body to approximately 30 for permeable soil with high infiltration rates. CN for a watershed can be estimated as a function of land use, soil type, and antecedent watershed moisture using table published by SCS. For watershed consist of several soil types and land use, composite curve number can be calculated as:

$$CN_{composit} = \frac{\sum_{i=1}^{n} A_i * CN_i}{\sum_{i=1}^{n} A_i} \quad \text{.....(2.4)}$$

HEC-HMS model allows modelers to choose among different loss methods. However, only Gridded Curve Number method allows spatially distributed infiltration calculation (Knebel et al., 2004). In this option the subdivisions of watershed are grid cells. Each cell in the database has the following descriptions;

- Location of the cells
- Travel distance from the watershed outlet
- The cell size and
- The cells' curve number (CN)

The program compute precipitation excess (runoff) for each cell independently using Equation (2.2), and routes the excess to the watershed outlet using Mod-Clark transform method.

2.7.1.2 Transform method

Model could be lumped or distributed based on variability of spatial characteristics. In HEC-HMS modeling system, Mod-Clark is an exceptional distributed transform method, which considers variations in travel time to the watershed outlet from all regions of watershed. It is based on the Clark conceptual unit hydrograph. It fundamentally represents the basin as a collection of grid cells (Feldman, 2000). Prior HEC-HMS version 4.3, it was not possible to utilize the gridded precipitation option for areas of outside of United State due to limitation in how gridded data was stored in HEC-DSS (https://www.hec.usace.army.mil/training/materials.aspx). The HEC-DSS grid data libraries have been modified to include storage of gridded data in the Universal Transverse Mercator (UTM) spatial reference system (Scharffenberg et al., 2018). With this method, a grid is superimposed on the watershed.

For each cells of grid representation of the watershed, the distance to watershed outlet is specified. Translation time to the outlet is computed as

$$t_{cell} = t_c * \frac{d_{cell}}{d_{max}} \text{.....(2.5)},$$

- t_{cell}= time of travel for each cell;
- t_c= time of concentration for a watershed;
- d_{cell}= travel distance from a cell to outlet;
- d_{max}= travel distance from a cell that is most distant from the outlet

Grid cell area is one of the grid cell parameters in the grid cell file, and having this grid area, the volume of inflow to the linear reservoir for each time interval is computed as a product of area and precipitation excess. Excess precipitation is the difference in mean average precipitation on a cell and losses in that cell. Thus, the computed inflows are routed through linear reservoir, and yielding an outflow hydrograph for each cell. The program combines these cell outflow hydrographs to determine the basin direct runoff hydrograph.

GHARIB et al. (2018) used mod-Clark method to simulate flood in Tangrah watershed, Iran, with comparison of SCS transformation method. The Mod-Clark method has been simulated more accurately than the SCS method. Bhattacharya (2012) used mod-Clark transformation for spatially distributed flood hydrograph modeling investigation. He also prepared the input data for the gridded SCS loss model in addition to gridded precipitation for his study. Generally he obtained an excellent result, and calibrated hydrographs matched the observed hydrographs well in the shape with largest error of about 9%.

2.7.1.3 Routing method

In HEC-HMS, routing is a method of modeling channel flow. Muskingum is among different methods available in HEC-HMS that uses a simple finite difference approximation of the continuity equation. It considers the reach storage as the sum of prism storage and wedge storage (Feldman, 2000). Prism storage is the volume of a steady-flow water surface profile, while wedge storage is the additional volume under the profile of the flood wave. Furthermore, detail descriptions of this method could be referred in HEC-HMS technical reference manual.

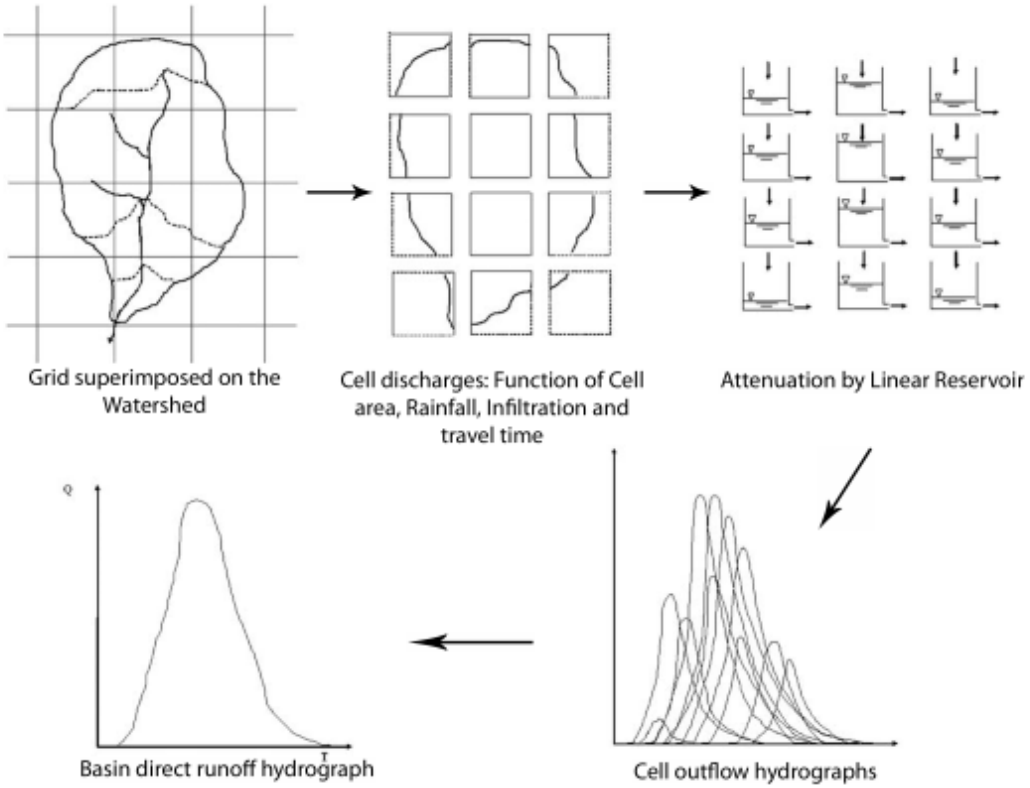

Figure 2.2: Structure of the ModClark model (Kull and Feldman-1998)

2.8 Satellite based rainfall and ground rain gauge data combination

The performances of different satellite based rainfall products are evaluated by incorporating ground rain gauge data. Dinku et al. (2013) observed significant modification of merged product than satellite estimate alone over Ethiopia. According to their discovery, there was no significant difference between gridded gauge and the merged product over regions with relatively dense station network, when merged product performs much better over data-sparse parts of the country. Ajmar et al. (2012) highlighted the benefits of integrating rainfall data analysis with RS.

2.9 Hydro-meteorological data quality analysis

The quality of hydro-meteorological data highly determines quality of results of hydrological analysis and hydrological modeling's. Therefore, maintaining hydro-meteorological data quality is the precondition of hydrologist they have to check and make. According to Caldera et al. (2016) Consistency and continuity of rainfall data series are very important for obtaining reliable results from water studies. Absence of observers, problems with measuring devices,

loss of records and any others may be the reason of such errors.

Continuity: Data which is not continuous and interrupted are missed meteorological data. Such data weakens the performance of hydrological models perfectly. Arithmetic Mean, Normal Ratio, Inverse Distance Weighting, Linear Regression are methods of managing missed records from near stations. Inverse distance weighting method is simple and most commonly used for estimation of missing data (Suhaila et al. 2008). Detail of these and other complex methods described in literatures (Caldera et al., 2016; Suhaila et al., 2008; Silva et al., 2007; Sattari et al., 2016).

Consistency: The trend of the rainfall records at a station may slightly change after some years due to coming of a new building, fence, planting of trees or cutting of forest nearby, which affect the catch of the gauge due to change in the wind pattern or exposure (Raghunath, 2006). This inconsistency of data may also arise from: Damage and replacement of a rain gage; Change in the gage location or elevation; Change in measurement procedure, or; Human, mechanical, or electrical error (Zemadim, 2010). Unless the inconsistency shown by the double-mass curve starts at the same time as a change in method of data collection, and unless the direction of the change shown by the curve could reasonably result from the change in method, no adjustment should be applied to the observed data, because the inconsistency could be due to other causes, such as works of man or vagaries of nature (Searcy and Hardison, 1960). A double mass curve technique is a method of detecting inconsistency of data and adjustment also could be done by multiplying the broken slope data with ratio preceding slope to succeeding slope. It is a plot of average cumulative precipitation of surrounding stations with cumulative precipitation of target station. First the data have to be in reverse order from recent to early time.

2.10 Previous studies in Blue Nile (Abay)

2.10.1 Satellite rainfall verification

Dinku et al. (2013) used European Meteorological Satellite METEOSAT data to compare with ground observation in Ethiopia, and concluded with good agreement. However, investigations carried out on Blue Nile, mostly pertinent SREs, were presented in table 2.2.

Table 2.2: Previous SREs (focusing TRMM) assessed within the Blue Nile/Abay

SREs	**Methods used**	**Main Results**	**References**
TMPA_3B42v7	CREST	Encouraging performance	
CMORPH	model	Better performance	Lakew (2017)
CHIRPS v2.0,		Satellite derived	
TARCAT v2.0	Continuous	rainfall products	Bayissa et al. (2017)
TRMM_3B42	statistics	showed good agreement	
& PERSIANN			
TMPA_3B42,	Categorical	All datasets need	
CMORPH,	and Continuous	improvement interms of	
PERSIANN,	statistics	high rainfall intensity	Sahlu et al. (2017)
MSWEP			
& ECMWF ERA			
CMORPH,	Graphical	All the SREs underestimate	
TMPA_3B42RT	technique	rainfall across almost	Romilly &Gebremichael (2011)
& PERSIANN		all elevations.	
CMORPH,	Categorical	Underestimate at highland	
TMPA-RT v7,	and continuous	Miss more rainfall at highland	
&TMPA-RP v7	statistics	Underestimate heavy rain rates	Gebremichael et al. (2014)

Table 2.3: Previous studies done with HEC-HMS within the Blue Nile/Abay

Components	**Sub-components**	**Basic Results**	**References**
Loss model	Deficit and Con	The results obtained	
Transformation	Synder's UH	were satisfactory and	Gebre (2015)
Routing model	****	accepted for simulation of	
Base-flow model	E. Recession	runof	
Meteorological Model	Areal precipitation		
Loss model	SCS-CN	Was very good	
Transformation	SCS-UH	and appropriate	Tassew et al. (2019)
Routing model	Muskingum	for hydrological	
Base-flow model	****	simulation	
Meteorological Model	Areal precipitation		
Loss model	SMA	Satiafactory model	Bashar and Zaki (2009)
Transformation	Clark UH	performance was	
Routing model	Linear Rese	obtained	
Base-flow model	****		
Meteorological Model	****		
Loss model	Gridded SCS-CN		New
Transformation	Mod-Clark		New
Routing model	Muskingum		*
Base-flow model	None		*
Meteorological Model	Gridded Rainfall		New

2.10.2 Satellite based rainfall estimate-ground rain gauge data

As elaborated in the previous section, different authors have evaluated the performance of different satellite algorisms in the Blue Nile basin. The satellite rainfall estimate-ground rain gauge data combination is relatively new technique of incorporating ground rain gauge data in SREs.

2.10.3 HEC-HMS hydrological modeling

Previous studies carried out within the Blue Nile basin using HEC-HMS model, and the unique components of HEC-HMS model incorporated in this study are tabulated in table 2.3.

3 MATERIALS AND METHODS

3.1 Description of the study area

3.1.1 Location

Jemma Sub-Basin is located in central highlands of North East part of Ethiopia and situated in the begging of Blue Nile Basin with a total drainage area of 15,330 Km^2. And geographically it is between 1016872.9m to 1212665m N latitude and 423308m to 589334m E longitude in terms of Universal Transverse Mercator (UTM) coordinate system. The Addis Ababa-Debre Birhan-Debre Sina and the Addis Ababa-Fitche-Debre Markos roads are the main asphalted roads that accesses along the eastern and western part of the Sub-Basin. The location map is showed in Figure 3.1.

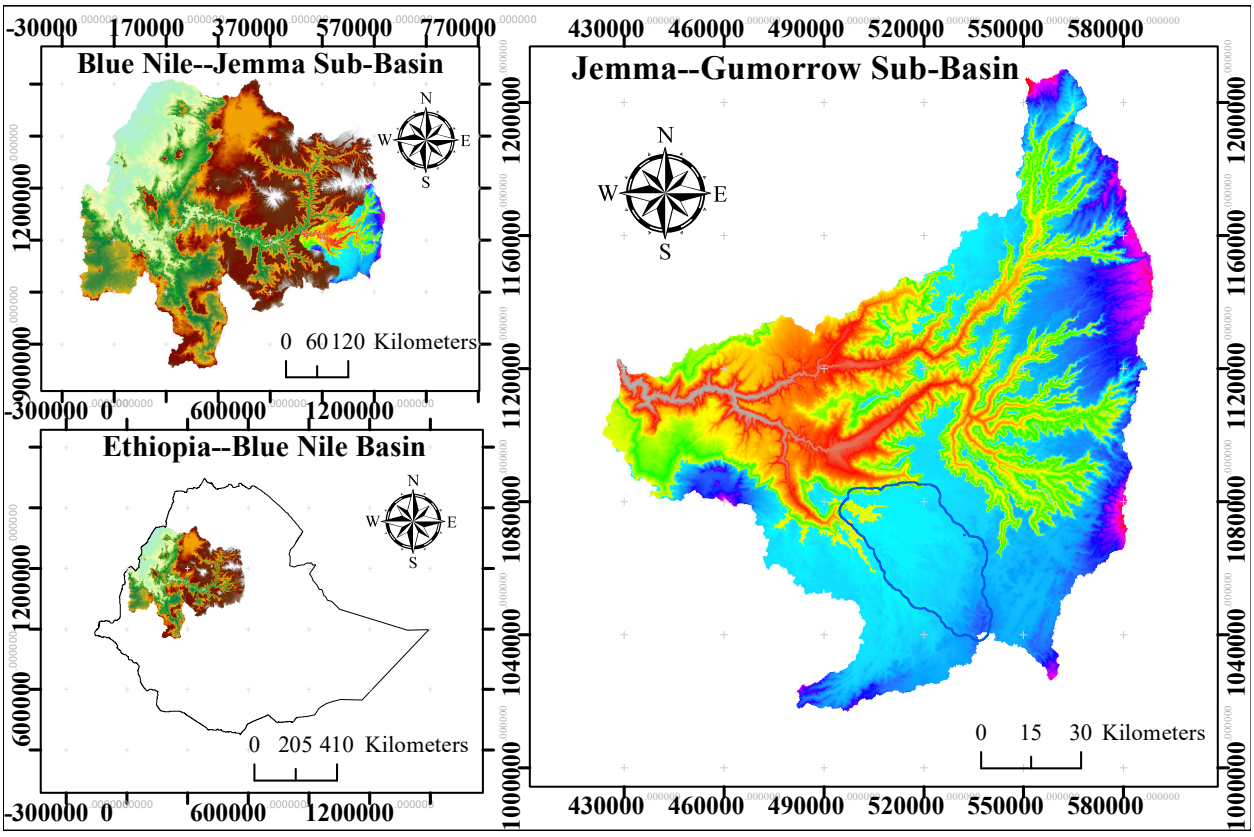

Figure 3.1: Location map of Jemma Sub-Basin

3.1.2 Topography

Jemma Sub-Basin has marked river network which drains from its highlands to lowlands. The river network is surrounded with highland topography with one clear outlet. As it can be observed in Figure 3.2, the Sub-Basin has narrow river width in highlands that became wide at the middle, and ends with narrow gorge. Based on SRTM DEM, the elevation of the Sub-Basin ranges from highest of 3842m to lowest of 1040m above sea-level.

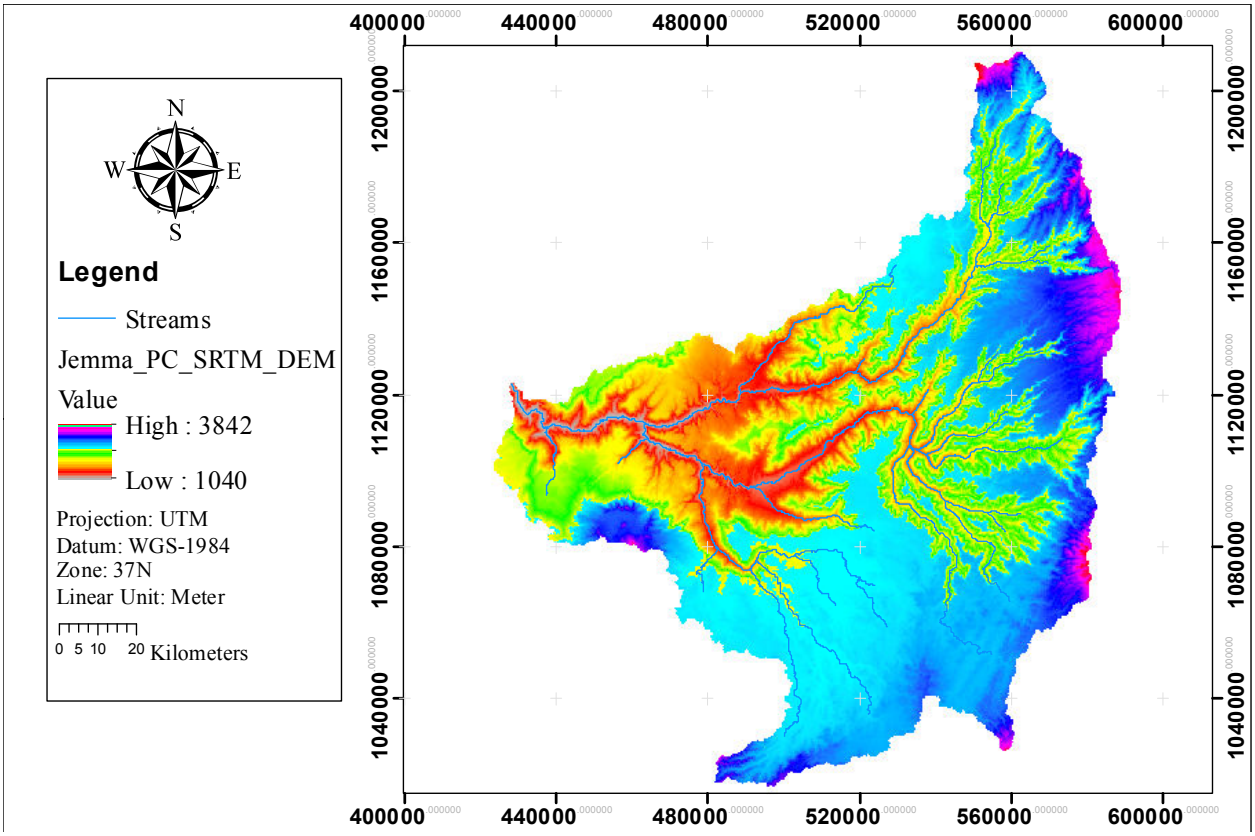

Figure 3.2: Digital Elevation Model map of Jemma Sub-Basin

3.1.3 Slope

Slope is one of the basic factors which can influence the velocity of surface runoff. Higher slope results higher velocity of flow, therefore the runoff drains quickly from the Sub-Basin through its outlet. Slope map of Jemma Sub-Basin was generated from SRTM Digital Elevation Model to see its topographical characteristics. Based on the slope map showed in Figure 3.3 the highest slope is observed near river network as well as in highland areas. And someone can clearly see as riverbanks.

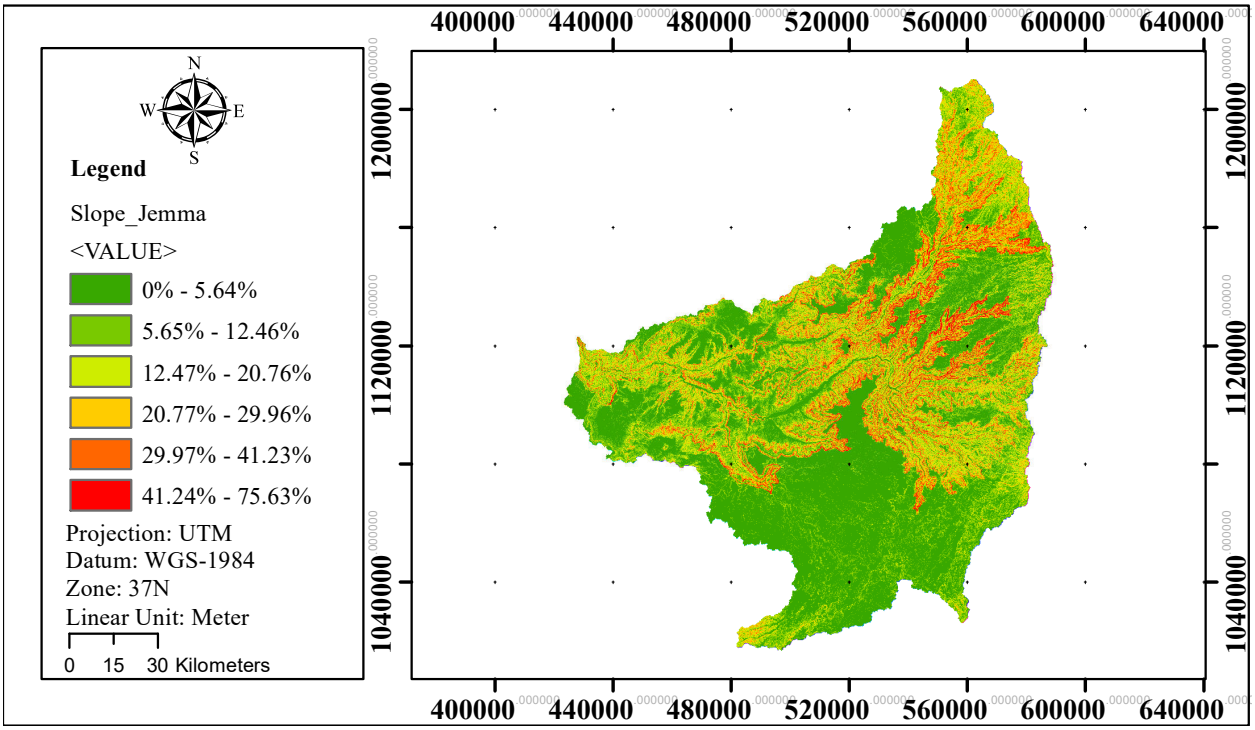

Figure 3.3: Slope map of Jemma Sub-Basin

3.1.4 Climate condition

Jemma Sub-Basin has a total of 30 meteorological stations inside it. Due to their bad measurement eleven of them were discarded. The location of meteorological stations is showed in Figure 3.4. The annual average rainfall of the meteorological stations is presented in Figure 3.5. The annual average rainfall of the Sub-Basin is 1123.59mm. Annual average Minimum and maximum temperature is 7.36^oC and 21.38^oC respectively. Monthly average rainfall distribution of the stations also could be seen in Figure 3.6. All this is based on the analysis made over six years of data (2003 to 2008) taken from National Meteorological Service Agency of Ethiopia (NMSA).

3.1.5 Soil

The Sub-Basin has different soil classes like: Lithic Leptosols, Vertic Cambisols, Eutric Vertisols, Eutric Leptosols, Rendzic Leptosols, Eutric Cambisols, Chromic Luvisols, Humic Nitisols and Haplic Luvisols. However, the most dominant soil types were Lithic Leptosols, Vertic Cambisols, Eutric Vertisols consecutively in their dominancy. The soil map is showed in Figure 3.7.

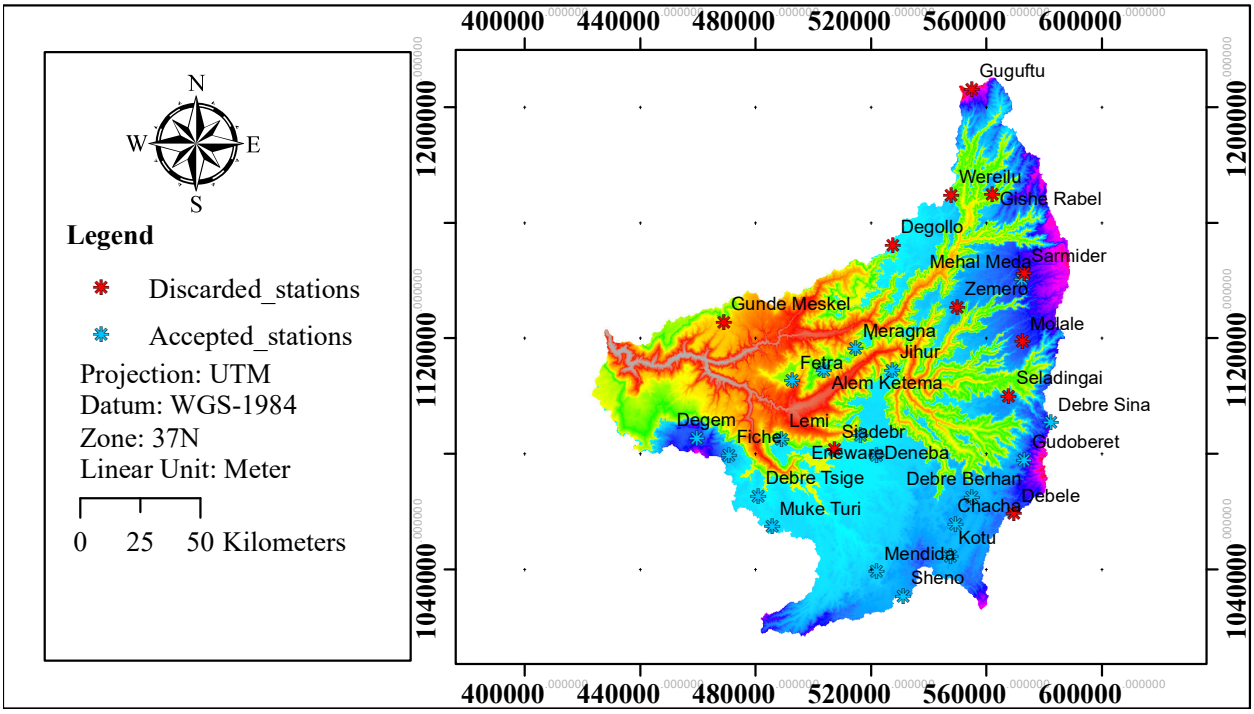

Figure 3.4: Location of meteorological stations within Jemma Sub-Basin

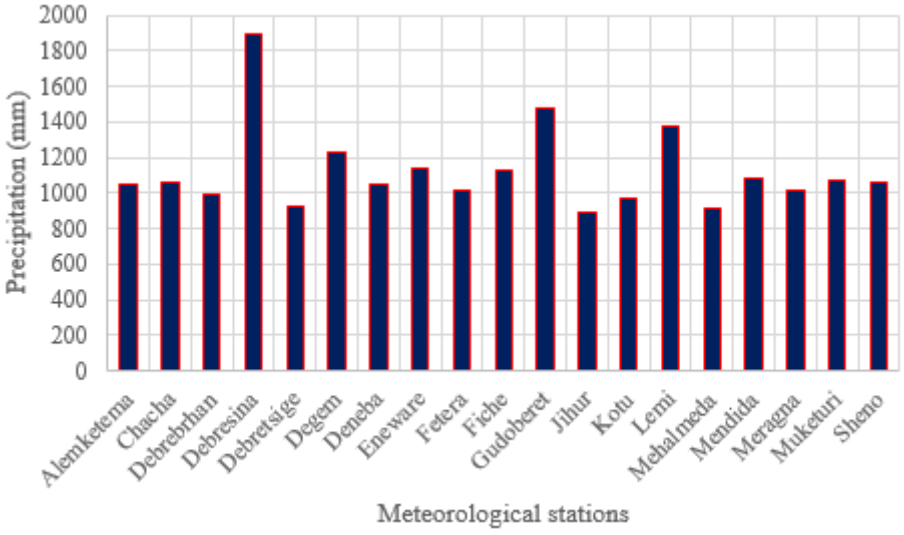

Figure 3.5: Annual average precipitation of the stations (2003-2008)

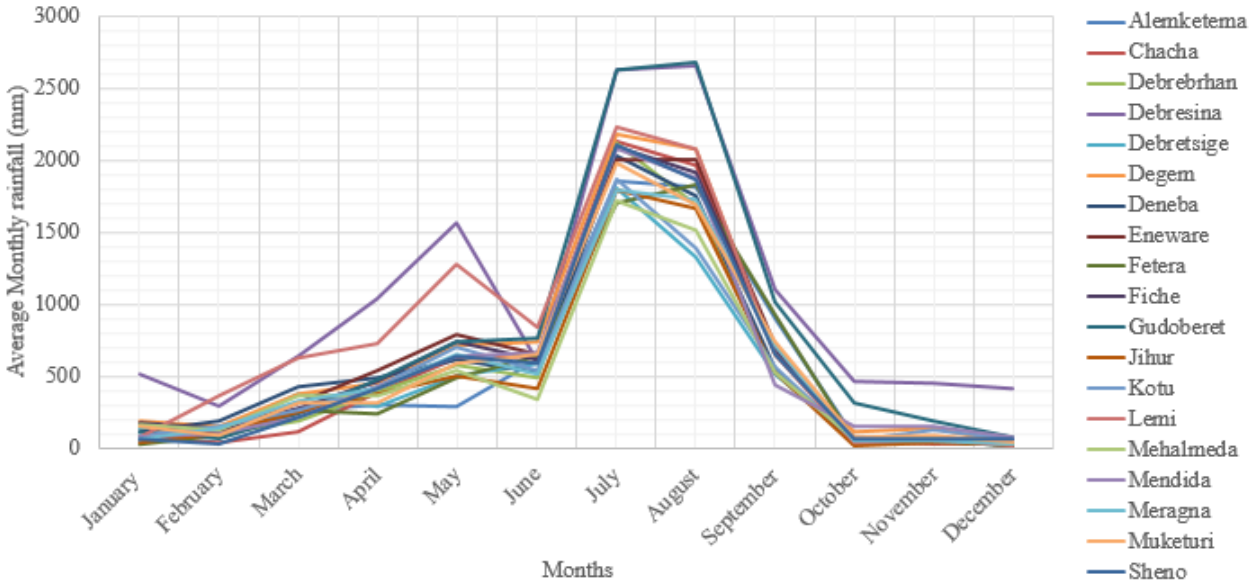

Figure 3.6: Monthly average rainfall distribution of the stations (2003-2008)

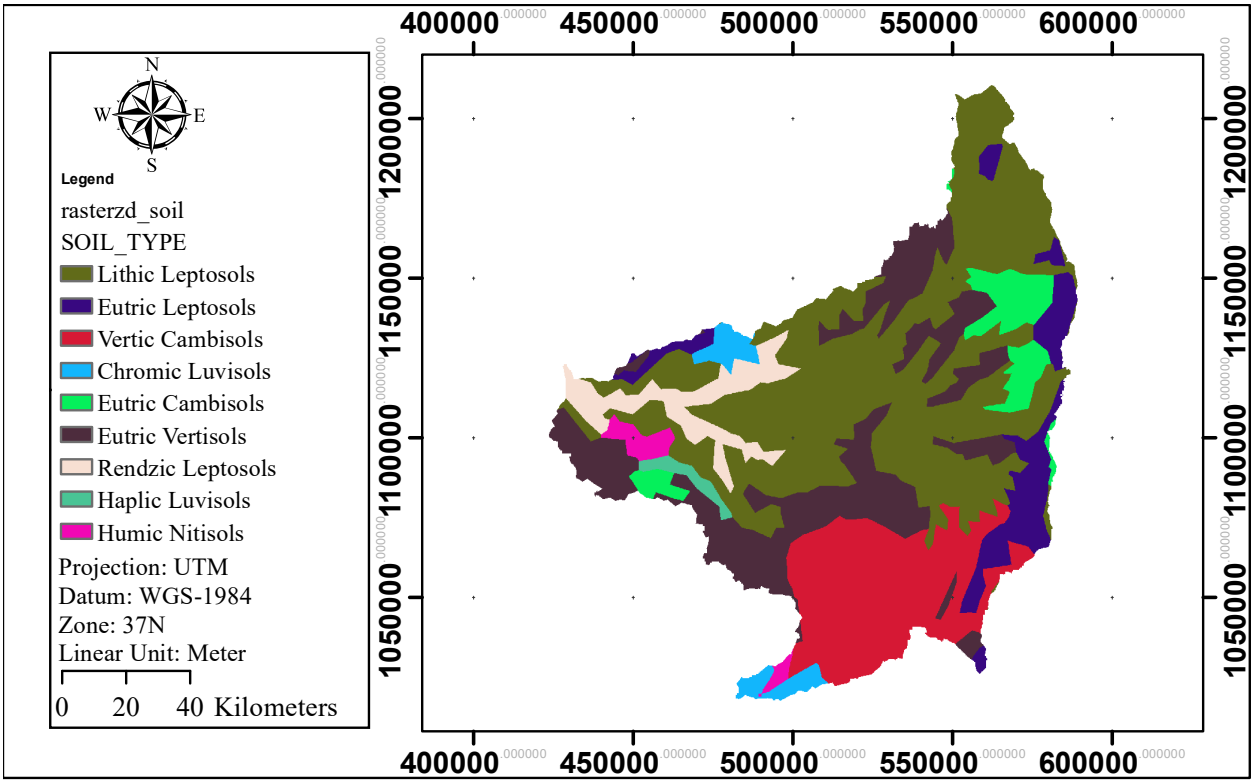

Figure 3.7: Soil map of Jemma Sub-Basin

3.1.6 Land-use land-cover

Generally, the land use land cover of Jemma Sub-Basin is characterized by six categories like: cultivated land, Grassland, Urban area, Shrub land, Plantations and Bushland. The most dominant land use is Cultivated land with dominantly and moderately cultivation. Shrub land is the second dominant land cover relative to others coverage. Grassland and Bushland have nearly the same proportion within the Sub-Basin as showed in Figure 3.8. Plantation which is an artificial forest is found in the eastern highland part of the Sub-Basin. Minor areas coded with red colors are sparsely urban areas within the Sub-Basin.

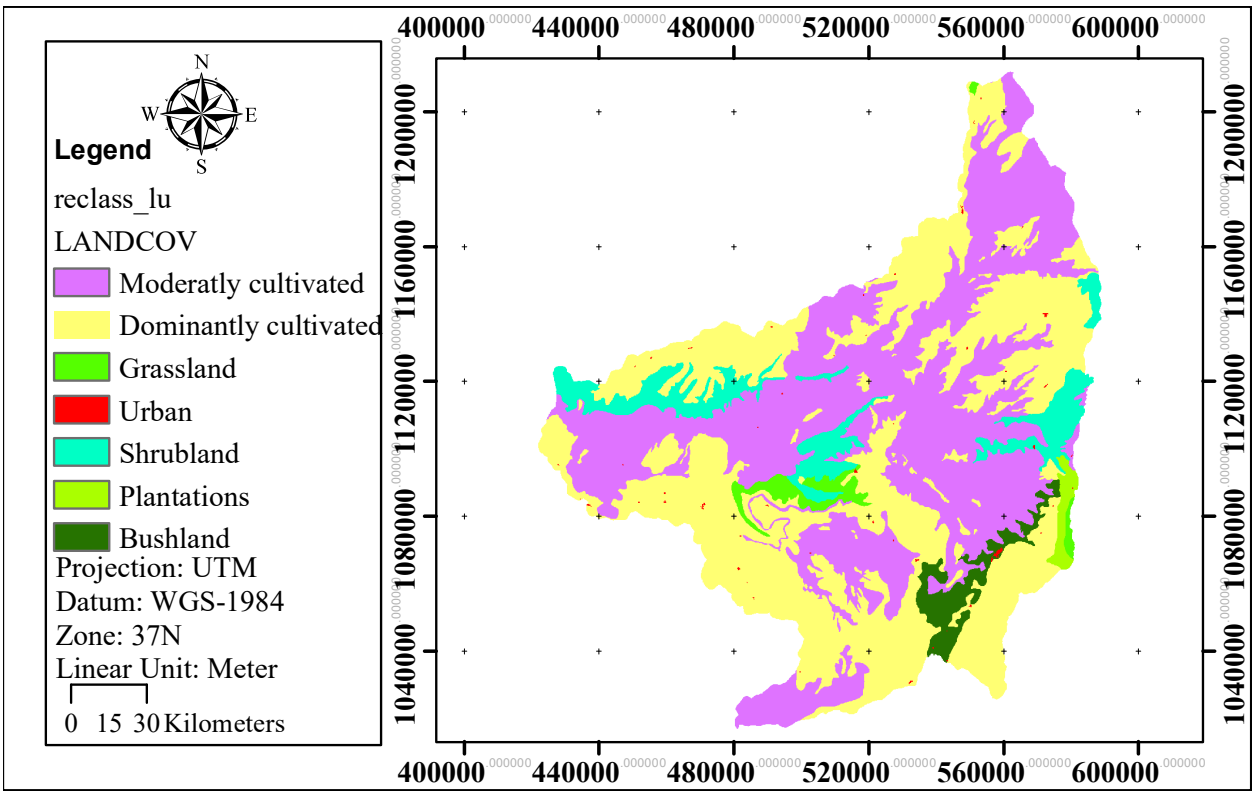

Figure 3.8: Land Use Land Cover map of Jemma Sub-Basin

3.2 Data collection

To achieve the objectives of the study, different datasets were collected from different relevant sources. Among these DEM, Soil data and LULC data were spatial datasets. Meteorological data was point and temporal data for each stations, and SREs were both spatial and temporal dataset. Other basic dataset collected during data collection was hydrological data, which is time series/temporal data type.

3.2.1 Meteorological data collection

Daily timescale meteorological data such as precipitation, Temperature within and around the watershed were collected for a period of 2003 to 2008 from National Meteorological Service Agency (NMSA) of Ethiopia. That was point data file with Microsoft excel version for all meteorological stations. These meteorological data were used to extract information and describing the study area through processing to their required level. Especially precipitation was used as base dataset while combined version of SREs is made. Meteorological stations within the study area were showed in Figure 3.4 with their acceptability.

3.2.2 Hydrological data collection

Hydrological data, which is Stream flow, is one of the boundary condition when rainfall runoff simulation is performed. For this study, stream flow data was necessary for sensitivity analysis, calibration and validation of the rainfall-runoff model. And a Microsoft excel version of it was collected from Ministry of Water, Irrigation and Energy of Ethiopia (MoWIE) for the period of 2003 - 2008.

3.2.3 Soil data collection

Soil data in Arc-info format was collected from Ministry of Water, Irrigation and Energy (MoWIE) of Ethiopia. Physical properties of the soil such as soil type, soil texture and hydrological soil group (HSG) was contained in soil data. Hydrological soil group (HSG) was used for generation of runoff CN grid in conjunction with LULC, sink filled DEM and Soil Conservation Service Curve Number (SCSCN) table.

3.2.4 Land use Land cover data collection

The other necessary and important dataset collected from Ministry of Water, Irrigation and Energy (MoWIE) of Ethiopia was LULC data. It was an Arc-info data format, and different land use land cover classes/categories were contained in this LULC data. The collected data was in Abay basin level, and it was clipped in to the study area level with the required shape files.

Table 3.1: Summary of major software's and Tools used throughout the research

S.No	Software and Tools	Major functions and tasks were executed
1	Arc-GIS 10.3	Spatial data analysis, Mapping, Model building, Conditional analysis
2	ASC2DSS Tool	ASCII to DSS conversion
3	Edraw Max	To prepare Flow chart diagram
4	Geo-HMS Tool	Soil-Land use data analysis, CN Grid preparation
5	HEC-HMS 4.6	Basin processing, Grid cell file generation, modeling, visualize results
6	HEC-DSSVue [HEC-SSP]	DSS data visualization and monitoring
7	Microsoft excel [MS]	Mathematical calculation, Figure preparation, Conditional analysis
8	R-PL (version 4.1.1)	SREs processing, statistical calculation, Document preparation
9	TLGCE Tool [Vortex]	Grid cell file to shapefile conversion
10	Wget	To download TRMM data

3.2.5 Satellite remote sensing data collection

3.2.5.1 Digital Elevation Model (DEM)

Shuttle Radar Topography Mission Digital Elevation Model (SRTM-DEM) with 30m resolution was downloaded from United States Geological Survey (USGS) website (https://earthexplorer.usgs.gov/). DEM was necessary to delineate the watershed and analyze the drainage pattern and characteristics of the study area. Sink fill, drainage processing, stream identification and grid cell file generation were done from this DEM. The clipped DEM is depicted in Figure 3.2.

3.2.5.2 Satellite rainfall estimates (SREs)

TRMM-3B42_V7 satellite based rainfall in daily timescale was downloaded from https://mirador.gsfc.nasa.gov/ using Wget software. The length of the data was same as the meteorological and hydrological data. The unique behavior of this data was its *netCDF4* format, and each day of the time series had their own individual dataset with spatial data type. It was fundamental dataset used for rainfall-runoff simulation input (Raw SREs) through performing different level of processes.

3.3 Data processing and analysis

Generally, different software's and tools were used for data collection, data processing and analysis, and data as well as result visualization. For major software's and tools used, including their Major functions, Table 3.1 is summarized.

3.3.1 Hydro-meteorological data analysis

Before beginning any further analysis, collected hydro-meteorological data were analyzed and tested for different errors. Tested and qualified data were then used for overall process and analysis of the study.

3.3.1.1 Meteorological data

Meteorological data of six years collected for period of 2003 to 2008 had miss records, and were estimated from other stations around the missed record station. According to (Subramanian, 2013) and (Zemadim, 2010), if the normal precipitation at the adjacent stations differs by greater than 10% of the normal precipitation of the station under consideration, the missing records of the precipitation stations were recommended to be estimated by using normal ratio method. However, to calculate normal precipitation of a meteorological station, it requires about thirty years of full data (Subramanian, 2013). Getting such full record is almost unusual. Thus, the most commonly used method (Suhaila et al. 2008), which is Inverse Distance weighted Method (IDWM) (Equation **3.1**), was used to manage missed records.

Daily precipitation (P_{24}) at a point **m** with geographic coordinates of X and Y could be estimated from the daily precipitation of the nearest gauging stations with geographic coordinates of X and Y. Using the coordinates of target station and surrounding stations, the distance of each surrounding stations from the target station easily obtained . In this method weight for each samples are inversely proportional to its squared distance from the point being estimated (Equation **3.2**). Arc-GIS and Microsoft excel programs were used for mapping the coordinates and calculating the weights of the stations respectively.

$$P_m = \frac{\sum_{i=1}^{N} P_i * W_i}{\sum_{i=1}^{N} W_i} \quad \text{.....(3.1)}$$

$$W_i = \frac{1}{d_i^2} \quad \text{.....(3.2)}$$

- P_m is the precipitation at the target station **m**
- P_i is the precipitation at surrounding station i
- W_i is the weight of surrounding station i
- d_i is distance of target station from surrounding stations

- N is the number of surrounding stations

Missing records of the remaining meteorological variables such as Temprature were estimated using simple arithmetic mean of the adjacent gauges (Equation **3.3**). If the missing data at **X** is P_X and P_1, P_2, P_3 ... P_n are meteorological variables at N surrounding stations:

$$P_X = \frac{\sum_{i=1}^{N} P_i}{N} \quad \text{.....(3.3)}$$

The stations location could be observed in Figure 3.4

3.3.1.2 Hydrological data

Stream flow data shows strong serial correlation in its time series than rainfall data. That means, flow in a day is closely related to the flow on the previous and the next days, especially during periods of low flow/recession time. Some gaps were detected on stream flow data, and these gaps were very short. A linear interpolation technique was used to fill such gaps found in between two existing values.

3.3.1.3 Data statistical tests

Consistency of the precipitation records: Before using for further analysis with a sequence of observations made at a particular rain gauge, it should be tested weather it is consistent or not with its surrounding stations. Double mass curve (DMC) analysis was used for this particular task. It is a plot of accumulated annual precipitation of the target station and the accumulated of mean annual precipitation for a group of surrounding stations (Zemadim, 2010). Further description about double mass curve could be referred on (Searcy and Hardison, 1960).

Trend analysis: Before applying the stream flow data for sensitivity analysis, calibration and validation of the model, the time series was tested for absence of trend by using Spearman's Rank-Correlation Method (Equation **3.4**). If R_{sp} is zero, there is no trend and jumps in the data and no need to check further, but if R_{sp} is greater than or less than zero, the student's t-distribution is required (Equation **3.6**).

$$R_{sp} = 1 - \frac{6 * \sum_{i=1}^{n} D_i * D_i}{n * n(n-1)} \quad \text{.....(3.4)}$$

Table 3.2: Trend analysis of stream flow with Spearman's Rank-Correlation

Years	i=x	Stream Flow(m^3/s)	Y=Ranked flow	Kxi	Kyi	Di	Di^2
2003	1	4586.772	2111.507	1	6	-5	25
2004	2	3579.227	3207.739	2	3	-1	1
2005	3	3207.739	3579.227	3	2	1	1
2006	4	6850.036	3701.245	4	5	-1	1
2007	5	3701.245	4586.772	5	1	4	16
2008	6	2111.507	6850.036	6	4	2	4
						Sum	48
						R_{sp}	-0.371
						t_{cal}	-0.800
						t_t	-2.78

$$D_i = Kx_i - Ky_i \text{.....(3.5)}$$

$$t_{cal} = R_{sp} * [\frac{n-2}{1-R_{sp} * R_{sp}}]^{0.5} \text{.....(3.6)}$$

If t_{cal} full fill the condition t(v,2.5%) $< t_{cal} <$ t(v,97.5%), the time series has no trend for given year and degree of freedom. If the time series does have a trend, the data cannot be used for frequency analyses or modelling. Where,

- D is difference
- i is the chronological order number
- K_{xi} is the rank of the variable x, chronological order number of the observations
- K_{yi} is chronological transformed series for observation y
- n is the total number of data

3.3.2 CN Grid Computation and analysis

Curve Number (CN) grid is one of the basic hydrologic parameters used in HEC-HMS rainfall runoff simulation. It is a computational result of LULC data, soil data and DEM. These three datasets were clipped in to the required study boundary. The two datasets, soil and land use, were then merged using Arc-GIS 10.3 software. Grid codes, which refers different land use classes, and hydrological soil groups (HSG), which refers different Soil textures were the required components of land use and soil data respectively. Merging these two datasets resulted one feature class that contains hydrological soil group and grid code as a common

Table 3.3: CN Look-up Table

RowID	LUValue	DESCRIPTION	CN values for HSG			
			A	B	C	D
1	1	Moderetly Cultivated land	61	73	81	84
2	3	Grass land	30	58	71	78
3	4	Urban area	77	86	91	94
4	5	Shrubland	30	55	70	77
5	6	Plantations	32	58	72	79
6	7	Bushland	30	48	65	73
7	2	Dominantly Cultivated land	62	71	78	81

attribute. Based on SCS curve number table, CN look-up table (Table 3.3) was prepared, that contains different CN values for a combinations of different grid code (LUValue) and hydrological soil group. Considering this CN look-up table for different soil group and land use, CN values were populated and its grid was generated using HEC-GeoHMS. The result is shown in Figure 4.2. Using sink filled DEM was also not ignored while CN is generated.

Once CN grid is prepared, it was projected to UTM, and resampled to a grid size of 2000m. Hence, it can overlays and fits over 2000m grid cell file (Section 3.3.3.1). Then it was converted in to ASCII file format. By creating batch file with a **.bat** extension, and incorporating parameters like: Input file name, Output file name, Path name, Grid type, Zone, Data unit and Data type, a DSS file which contained Gridded CN was generated. This DSS file conversion relies on using the asc2DSSGrid utility program. Finally, the DSS could be read by HEC-DSSVue for inspection.

3.3.3 Satellite remote sensing data analysis

3.3.3.1 Digital elevation model (DEM)

DEM was imported in to HEC-HMS, and coordinate system of the basin model was defined. Through terrain preprocessing, sink fill and sink location layers were created. Similarly, flow direction and flow accumulation layers were also created. By specifying a threshold value of $65km^2$, Streams were identified. By specifying a Break Point at a point of outlet the watershed was delineated.

Grid cell file, the base of distributed model type, was generated in text file format by using flow direction as an input. UTM and 2000m was selected for Projection and cell size respectively. This grid cell file specifies which grid cells are in which sub basin and the properties of each cell including location, area within the sub basin, and the distance to the sub basin outlet.

Travel-length-grid-cells-exporter utility program found in HEC-Vortex was used to convert the grid cell text file into a shapefile. It can be downloaded from https://github.com/HydrologicEngineeringCenter/Vortex/releases. By providing the grid cell text file, projection, and cell size as input into the utility, a grid cell shapefile was produced and added as a map overlay showing the gridded representation of the catchment (Figure 4.4).

3.3.3.2 Satellite rainfall estimates (SREs)

SREs, downloaded from https://mirador.gsfc.nasa.gov/ was processed into the final DSS file that can be used as input of HEC-HMS model. Conversion of NetCDF4 files to Geo-tiff raster; Coordinate System projection and grid resampling; conversion of raster to ASCII file, and DSS file preparation are fundamental steps involved in SREs analysis. Except the NetCDF4 file conversion, all these steps were done with **Model Builder** in Arc-GIS 10.3. Model Builder could process multiple files with single iterative model. But for NetCDF4 file conversion, **MakeNetCDFRasterLayer** tool under Multidimension Tools of ArcTookbox was used. NetCDF4 raster files are called one by one in Arc-GIS 10.3, and were exported as Geo-tiff raster.

Geo-tiff raster data were projected to UTM Zone 37N and the resolution also resampled to equal size of the grid cell file, which is 2000m. Following that, precipitation grid would be aligned over grid cell file. About two thousands of daily precipitation raster files were projected with Model builder model, and it in turn converted to ASCII files with the same name as the input file names. By creating batch file like it was done in CN processing, relying on using ASC2DSSGrid DOS utility program, DSS file was generated, and it could also be read by HEC-DSSVue.

3.4 Satellite rainfall estimates comparison and verification

So many Satellite rainfall products are available and accessible in different characteristics like resolution, file format, algorism. As their advantage is preserved, these products are just models rather than direct rain collection as of ground rain gauge. To use these products in hydrological and other related applications, their performance have to be tested and verified. In this study Eyeball comparison, categorical statistics and continuous statistics were used as a methods of comparison and verification, based on their point-to-pixel values. Comparison by means, assessment and quantification of the satellite estimates' relation, resemblance and difference with observed rain gauge value.

3.4.1 Eyeball comparison

Even if it is a subjective method of interpretation, a simple side by side comparison of accumulated values (Monthly, Seasonal, and annual) was made. It was an ideal method to see the spatial variation of the precipitation in the form of map; and the magnitude of accumulated precipitation values in the form of time series plot and bar chart. Which means Maps and plots were the appropriate illustration methods for spatial and temporal variations respectively.

Pixel values of SREs at the rain gauge locations were extracted with R programing software. Now both SREs and ground rain gauge data are daily point data, and were accumulated in to Monthly, Seasonal, and annual timescales. For precipitation distribution comparison, these accumulated point values were then converted in to their respective spatial maps using Inverse Distance Weighted interpolation method (IDW) except the monthly accumulation. But for temporal comparison, these accumulated point values were drawn as time-series plots and charts. Before side by side viewing performed, as it is necessary, same color-ramp had been assigned for two comparable spatial maps (SREs and GRDs). Simple visual interpretation was then made from these maps and plots.

3.4.2 Categorical statistics

It is a quantitative method of verification relative to visual interpretation. Ranges of threshold values were fixed for Daily, Monthly, and Seasonal timescales (Table 3.4) as a function of their maximum average rainfall. Yellow marks in the first row of Figure 3.17 shows threshold values, and the first two columns show a pair of SREs and GRDs. Based on the threshold values, distributions of "Yes" "No" and joint distributions of forecasts and occurrences were populated using Microsoft excel program. The conditional statement used to populate joint distributions of forecasts and occurrences could be observed at the top of Figure 3.9. The sum of frequency of each joint distributions (HIT, MISSES, FALSE ALARM, and NULL) can be tabulated as contingency table. Categorical statistics like: Accuracy, bias score (BIAS), Probability of Detection (POD), False Alarm Ratio (FAR), and Critical Success Index (CSI) describing detection capability of SREs were calculated by using their respective formulas (Table 3.5).

Accuracy: Accuracy is one of the recommended indices that answers the question of what fraction of the forecasts were correct? That means, it Indicates fraction of estimated values which are correct.

Table 3.4: Rainfall threshold values (mm) and their descriptions for different timescales

S.No	Daily	Monthly	Seasonal	Description
1	[0-1)	[0-6)	[0-13)	No rain
2	[1-7)	[6-46)	[13-90)	Light rain
3	[7-21)	[46-138)	[90-270)	Moderate rain
4	[21-42)	[138-277)	[270-540)	Heavy rain
5	≥42	≥277	≥540	Violent rain

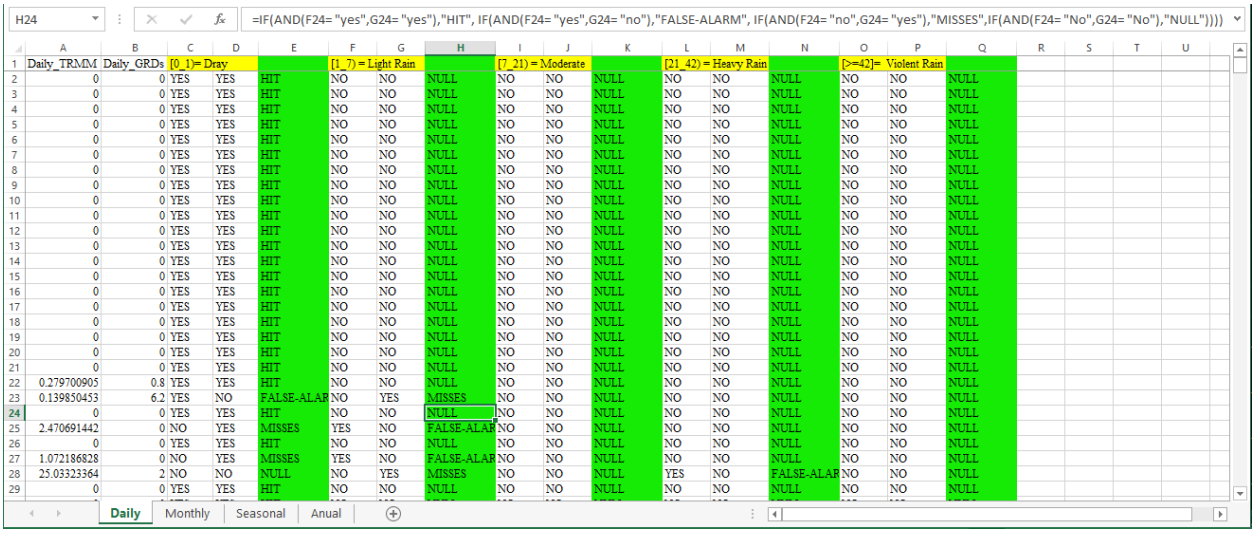

Figure 3.9: "Yes" " No" and Joint distributions of forecasts and occurrences

Table 3.5: Categorical and continuous statistical indices

Statistics	**Indices**	**Formulas**	**Ranges**	**Perfect Score**
Catagorical	Accuracy=	$\frac{Hits+Correct\ Negative}{Total}$	0 to 1	1
	BIAS=	$\frac{Hits+Falsealarms}{Hits+Misses}$	0 to ∞	1
	POD=	$\frac{Hits}{Hits+Misses}$	0 to 1	1
	FAR=	$\frac{False\ alarms}{Hits+False\ alarm}$	0 to 1	0
	CSI=	$\frac{Hits}{Hits+Misses+False\ alarms}$	0 to 1	1
Continous	r=	$\frac{\sum_{i=1}^{N}(F_i-\bar{F}_i)(O_i-\bar{O}_i)}{\sqrt{\sum_{i=1}^{N}(F_i-\bar{F}_i)^2}*\sqrt{\sum_{i=1}^{N}(O_i-\bar{O}_i)^2}}$	-1 to 1	1
	ME=	$\frac{1}{N}\sum_{i=1}^{N}(F_i-O_i)$	-∞ to ∞	0
	MAE=	$\frac{1}{N}\sum_{i=1}^{N}\lvert F_i-O_i\rvert$	0 to ∞	0
	RMSE=	$\sqrt{\frac{1}{N}\sum_{i=1}^{N}(F_i-O_i)^2}$	0 to ∞	0

Bias Score (BIAS): BIAS indicates weather the estimated system has a tendency to underestimate or overestimate the observed system; that means if the BIAS is less than 1 and if the BIAS is greater than 1 respectively.

Probability of detection (POD): Probability of detection measures the fraction of observed events that were correctly diagnosed or estimated, and is sometimes called the "hit rate".

False Alarm Ratio (FAR): False Alarm Ratio answers the question: What fraction of the predicted "yes" events actually did not occur? Or it indicates fraction of the estimated system which are incorrect (i.e., were false alarms).

Critical success index (CSI): Critical success index also called Threat score answers the question: How well did the forecasted "yes" events correspond to the observed "yes" events? Measures the fraction of observed and/or forecasted events that were correctly predicted.

3.4.3 Continuous statistics

It is another quantitative method used to evaluate the performance of SREs. The continuous statistics evaluate magnitude of rainfall values, while categorical statistics is frequency of occurrences. This mean, the former is concerned on the values of precipitation, while the latter is over the detected frequency of SREs. Relying on a pairs of Daily_TRMM and Daily_GRDs (first two columns of Figure 3.9), recommended continuous statics like: Correlation Coefficient (r), Mean Error (ME), Mean Absolute Error (MAE), and Root Mean Square Error (RMSE) were calculated by using their respective formulas in Table 3.5. Ranges and perfect scores are also tabulated in the table. Where,

- F_i is forecasted value at point or grid box i
- $\bar{F_i}$ is mean of forecasted values
- O_i is observed value at point or grid box i
- $\bar{O_i}$ is mean of observed values
- N is Number of pair of samples

Correlation coefficient (r): Correlation coefficient is a measure of linear association of forecasted values to observed values, which implies that, it could answer the question of "How well did the forecast values correspond to the observed values?"

Mean Error (ME): Bias or mean error measures the average direction of the deviation from the observed values. It answers the question "What is the average forecast error?"

Mean Absolute Error (MAE): Mean absolute error is same as mean error, but measures the average magnitude of the error without considering the average direction.

Root Mean Square Error (RMSE): Root Mean Square Error is another error index, which measures the average magnitude of the error like MAE, but it gives greater weight to large errors than small errors through squaring the errors before it is being averaged. This means, RMSE is important when large errors are not desired.

3.5 Satellite rainfall estimates-Ground rain gauge data combination

The advantage and disadvantage of SREs and ground gauging stations are known, and are discussed in the previous sections. Relying on the advantage of ground gauging stations, the SREs was combined with rain gauge data in order to consider their respective advantages. First of all, pixel values of satellite rainfall estimate found at points of each ground gaging stations were extracted for each daily data using the following R script:

- library(raster)
- setwd("C:\Users\Getaw_AAU\Desktop\SRE_Data") → It sets working directory
- Files<- list.files(getwd()) → lists all files found in the working directory
- Rasterdata<- lapply(Files,raster) → reads all Raster files using raster package
- Points<- read.csv("Jemma.csv") → reads Jemma.csv table contains station's coordinates
- Stacked<- stack(Rasterdata) → stacks all Raster files together
- Extracted<- extract(stacked,points) → extracts pixel values from stacked Raster at points gauging location
- Write.csv(extracted, file = "Dailly_SREs.csv") → exports extracted values with Dailly_SREs.csv file name

The daily $GRDs_i - SREs_i$ difference or ($Error_i$) were calculated using Microsoft excel program. This error is arranged the form of table that would be easily iterated and interpolated (Figure 3.18). Each arranged daily error were then interpolated spatially by Inverse Distance Weighted method (IDW) using Model-builder model (Figure 3.19). Finally each daily spatial error was re-added to their respective daily SREs ($Error_i + SREs_i$) by using the following R script: Where; i=1 to N; N is Number of days with in the years of the study.

- library(raster)
- setwd("C:\Users\Getaw_AAU\Desktop\Error")
- A<- list.files(path = "C:\Users\Getaw_AAU\Desktop\Error")
- stacked_A<- stack(A)

- setwd("C:\Users\Getaw_AAU\Desktop\SREs")
- B<- list.files(path = "C:\Users\Getaw_AAU\Desktop\SREs", pattern = ".tif")
- stacked_B<- stack(B)
- sum<- stacked_A+stacked_B
- Lists<- unstack(sum)
- setwd("C:\Users\Getaw_AAU\Desktop\R_Written")
- writeRaster (sum$layer.1 ,filename=" 2003-01-01 ", format="GTiff")
- writeRaster (sum$layer.2 ,filename=" 2003-01-02 ", format="GTiff")
- writeRaster (sum$layer.3 ,filename=" 2003-01-03 ", format="GTiff")

As a result of this, the pixel values of SREs at rain gauge locations become corrected, and finally each daily data was exported in *GTiff* format (2003-01-01; 2003-1-02; ... 2008-12-31). Pixel values of SREs farther from points of rain gauge location also get corrected based on the principle of IDW interpolation. These daily raster data were converted to ASCII in turn to DSS with model builder.

However, the error maps had insignificance pixel values in turn the combined SREs. When the raster data changed in to ASCII data format, these insignificance pixel values were labeled in scientific notation format. And the values labeled in scientific notation could not be read by HEC-HMS model. This means the HEC-HMS model does not know these values, and returns error message to run the model. Such challenge was resolved with raster calculator tool (Figure 3.20) using the conditional function "Con((("%2003-01-01.tif%") < 0.0001) & (("%2003-01-01.tif%") > -1000), 0.0001,"%2003-01-01.tif%")". This means when the value in raster data (for example 2003-01-01.tif) less than *0.0001* and greater than *-1000* make 0.0001 otherwise, put the value as 2003-01-01.tif raster data. During error calculation negative values may occur when extracted SREs exceed the corresponding GRDs in the locations of rain gauges. That is why negative boundary is incorporated in the function.

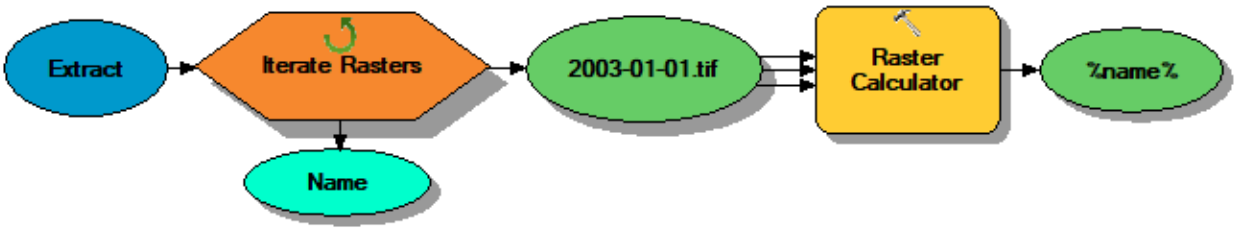

Figure 3.10: Model-builder model for raster calculetor

3.6 HEC-HMS Hydrological modeling

3.6.1 HEC-HMS model Input

Different Datasets collected during data collection were processed and analyzed with different softwares and programs, and were used as input of HEC-HMS hydrological modeling to simulate the rainfall runoff processes. Grid cell file, Gridded CN Grid, Gridded precipitation and corrected stream flow are among the basic inputs obtained from data processing and analysis.

3.6.2 HEC-HMS model Setup

The implementation of HEC-HMS model depends on its components like Basin Model, Meteorological model, Control specification and Time-Series Data Manager. Grid Data Manager, Terrain Data Manager and Grid Region Manager are others additional HEC-HMS model components for distributed model type. By using the tools under GIS menu of HEC-HMS 4.6, background shape files for the rivers and catchment as well as Grid cell file were prepared and basin model representing the physical watershed was constructed. Configuration of HEC-HMS model is then made using Loss, Rainfall to runoff transform, base flow, and routing methods.

3.6.2.1 Loss method

There are different methods available in HEC-HMS to calculate rainfall loses. For this study, Gridded Soil Conservation Service Curve number method was used. In this method, precipitation excess is estimated as a function of cumulative precipitation, soil cover, land use and antecedent moisture using Equation 2.2. The subdivisions of Sub-Basin were uniform grid cells with spatial resolution of 2000m that would fit with others gridded data Grid precipitation. The program computes the precipitation excess for each grid cells independently by subtracting losses from the precipitation depth available on each grid cell. Basically this method is selected to keep and consider spatial variation of the catchment characteristics. It could also be compromised with selected Mod-Clark transform method, which uses gridded precipitation dataset. For detail calculation technique Section-2.7 could be referred.

3.6.2.2 Transformation method

Mod-Clark is one of rainfall to runoff transformation methods in HEC-HMS. It is a linear, quasi distributed transform method that is based on the Clark conceptual unit hydrograph. In this method, separate travel time index for each grid cells are explicitly considered. Fundamentally, it represents the Sub-basin as a collection of grid cells. By contrast to Clark method, Mod-Clark method eliminates the time-area curve and instead uses a separate travel time index for each grid cells. Linear reservoir and gridded based travel-time model are accounted for storage and translation methods respectively. The area of each cell is specified, and from this the volume of inflow to the linear reservoir could be computed as the product of area of a cell and precipitation excess in it. Where precipitation excess is the difference of precipitation in a cell and loss in that cell. The outputs from the linear reservoirs of the cells are combined with program to produce the final hydrograph at the given outlet.

In this method, excess precipitation is calculated for each individual grid cells (Section 2.7). As far as spatial variations of the characteristics are intended to consider, it needed gridded data inputs like Grid cell file, gridded CN and Gridded precipitation. These gridded data are stored in HEC-DSS grid data libraries in Universal Transverse Mercator (UTM) spatial reference system, of course it was limitation of earlier versions of HEC-HMS.

3.6.2.3 Routing method

A method of modeling flow through the reaches is called routing. In this study Muskingum routing method is applied. In this method, three model parameters such as Muskingum K, Muskingum X and Number of sub reaches were considered.

Generally, in the presence of rainfall and stream flow observations, calibration is the appropriate method of selecting optimal parameter values by setting their initial values. Hence, for all parameters found in all selected modeling methods, optimal values were determined through model calibration.

3.6.2.4 Sensitivity analysis

According to Moriasi et.al. (2007), Sensitivity analysis is a process of determining the rate of change in model output with respect to changes in model inputs (parameter values). So, it enables to rank the level of sensitivity of model parameters for ease of calibration process. Each model parameters have their own contribution to simulate the rainfall runoff hydrological processes. However, not every parameter produces same influence on the model output. When one parameter changes, model output also changes. So, knowing the most

sensitive and the least sensitive parameters is important to know the influence that will be produced on the model output, when model calibration is prformed.

Hence, HEC-HMS model was run repeatedly with the starting point value, and then by multiplying with a factor of 10%, while keeping all other parameters constant at their initial values. The effect of each model parameter was inspected based on the objective functions like Nash-Sutcliffe (NSE), percent bias (PBIAS), Root means square error to Standard deviation Ratio (RSR). Thus, in this study local sensitivity analysis, which keeps other model parameters constant, was used to know the rate of change on model output while changing model parameters.

3.6.2.5 Calibration

Model calibration is a process of estimating model parameters by comparing model prediction (output) with observed data for the same conditions (Moriasi et al., 2007). To minimize the difference between observed and predicted values, calibration, which can be automatic or manual method or both could applied. Based on sensitivity analysis result, in this specific project, manual model calibration was performed to obtain the optimal value of the parameters.

3.6.2.6 Validation

Model validation is a process of verifying model performance to simulate observed stream flow with rainfall data other than used for calibration. In this process model parameters are no subjected to further adjustment, and their values are kept as the value obtained in the final model calibration.

In this study, efficiency of the model was tested using the final parameters for the validation period of two years (2007 to 2008) to validate and evaluate the accuracy of the calibrated model.

3.6.3 Model performance evaluation

The performance of models need to be evaluated for their ability to simulate the rainfall runoff hydrological processes relative to observed flow. In this study the performance of distributed based HEC-HMS model was evaluated using quantitative statistical techniques in addition to graphical comparisons; hence, the quality and reliability of the model could be determined. Model evaluation statistics such as Nash-Sutcliffe efficiency (NSE), Percent bias

Table 3.6: Model Performance critria

Statistics and Formulas	Model Performance ratings			
	Very Good	Good	Satisfactory (Fair)	Unsatisfactory (Poor)
$\text{NSE} = 1 - \frac{\sum_{i=1}^{N}(Q_{Oi}-Q_{Si})^2}{\sum_{i=1}^{N}(Q_{Oi}-\bar{Q_O})^2}$	(0.75-1]	(0.65-0.75]	(0.5-0.65]	≤0.50
$\text{PBIAS} = \frac{\sum_{i=1}^{N}(Q_{Oi}-Q_{Si})}{\sum_{i=1}^{N}Q_{Oi}} * 100$	<± 10%	[±10-±15]%	[±15-±25)%	≥±25%
$\text{RSR} = \frac{RMSE}{STDEV_{obs}} = \frac{\sqrt{\sum_{i=1}^{N}(Q_{Oi}-Q_{Si})^2}}{\sqrt{\sum_{i=1}^{N}(Q_{Oi}-\bar{Q_O})^2}}$	[0-0.5]	(0.5-0.6]	(0.6-0.7]	>0.7
$\text{r} = \frac{\sum_{i=1}^{N}(Q_{Oi}-\bar{Q_O})(Q_{Si}-\bar{Q_S})}{\sqrt{\sum_{i=1}^{N}(Q_{Oi}-\bar{Q_O})^2}\sqrt{\sum_{i=1}^{N}(Q_{Si}-\bar{Q_S})^2}}$	Generally	correlation	coefficient (r)	>0.6 is Good
$R^2 = [\frac{\sum_{i=1}^{N}(Q_{Oi}-\bar{Q_O})(Q_{Si}-\bar{Q_S})}{\sqrt{\sum_{i=1}^{N}(Q_{Oi}-\bar{Q_O})^2}\sqrt{\sum_{i=1}^{N}(Q_{Si}-\bar{Q_S})^2}}]^2$	(0.75-1]	(0.65-0.75]	(0.5-0.65]	≤0.50

(PBIAS), RMSE to standard deviation ratio (RSR), Pearson's correlation coefficient (r) and coefficient of determination (R^2) were used to evaluate the model performance both during the calibration and validation periods. The first three statistics are recommended for model evaluation, and the remaining two are commonly used model evaluation statistics but not selected for recommendation (Moriasi et.al., 2007).

NSE and R^2 indicates the ability of a model to reproduce the pattern of observed hydrographs, i.e. how well the plot of observed versus simulated data fits the 1:1 line. PBIAS indicates average tendency of the simulated data to underestimate if PBIAS is positive and overestimate if PBIAS is negative. RSR is standardized RMSE index, and lower value indicates better model performance (Moriasi et.al., 2015; Moriasi et.al., 2007). Their formulas and performance ratings are given in Table 3.6.

3.7 Conceptual framework of the study

The conceptual framework diagram shown in figure 3.22 is designed to create Schematic view of the overall techniques followed in the research work. And the route followed from the beginning of data collection to the succeeding of the study objectives is presented.

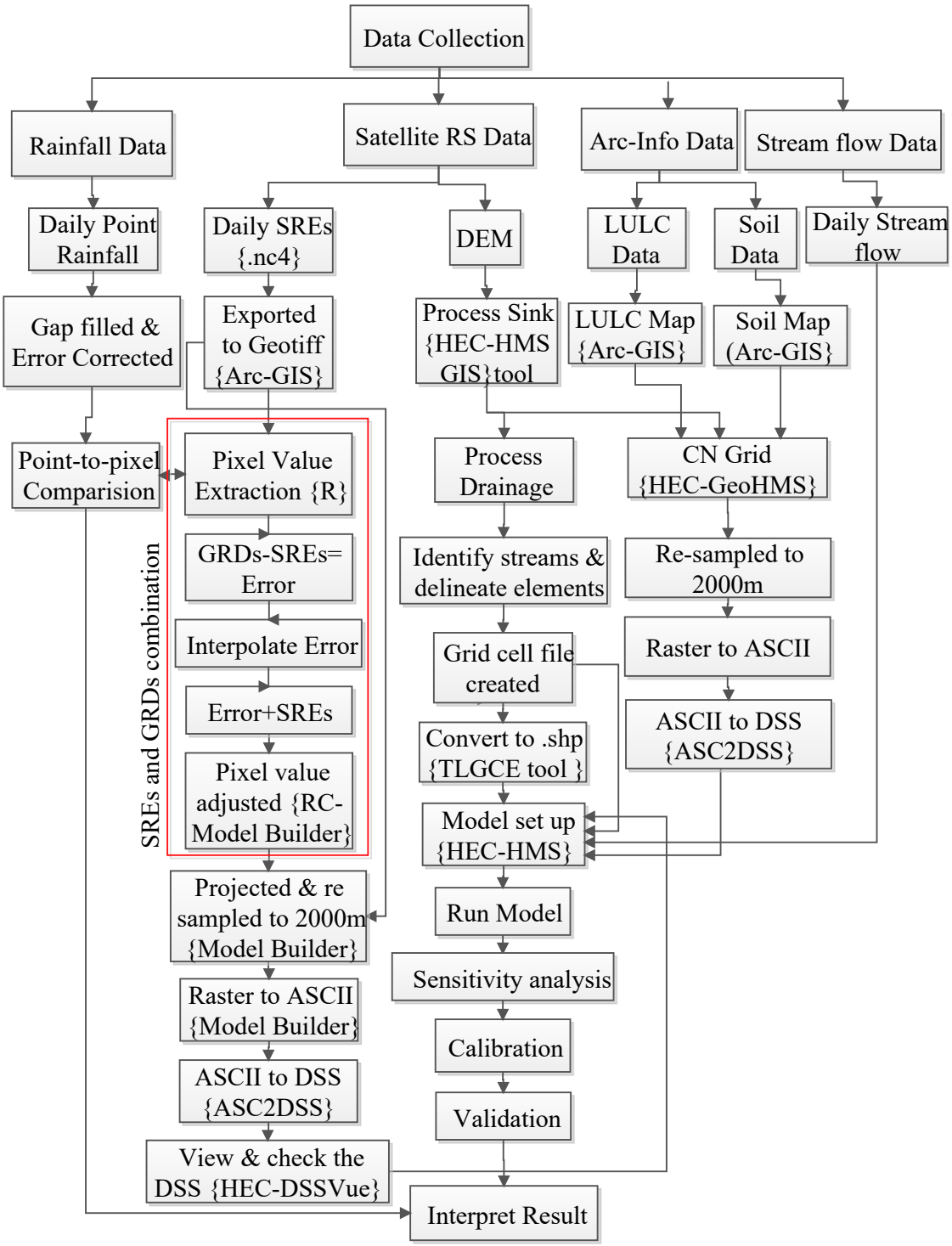

Figure 3.11: Conceptual framework diagram

4 RESULT AND DISCUSSION

In this section of the document, major findings of the study were presented in their respective headings and sub headings. Depending on the findings obtained, appropriate professional explanations were given.

4.1 Hydro-meteorological data analysis results

4.1.1 Meteorological data

All gaps found in the recorded daily rainfall data were filled and completed using Inverse Distance Weighted (IDW) method, and the slice of it with their respective meteorological stations was attached in Appendix A.

The consistency of meteorological stations' rainfall data was checked by double mass curve technique for all nineteen selected stations. Based on those double mass curve result, all meteorological stations were with no significant slope variation. The coefficient of determination (R^2) of each station was also obtained above 0.995. Thus, the data were taken as consistent and relatives. Fiche's double mass curve is shown in Figure 4.1. The associated annual average rainfall used for preparation of Double mass curve was presented (Table 4.1).

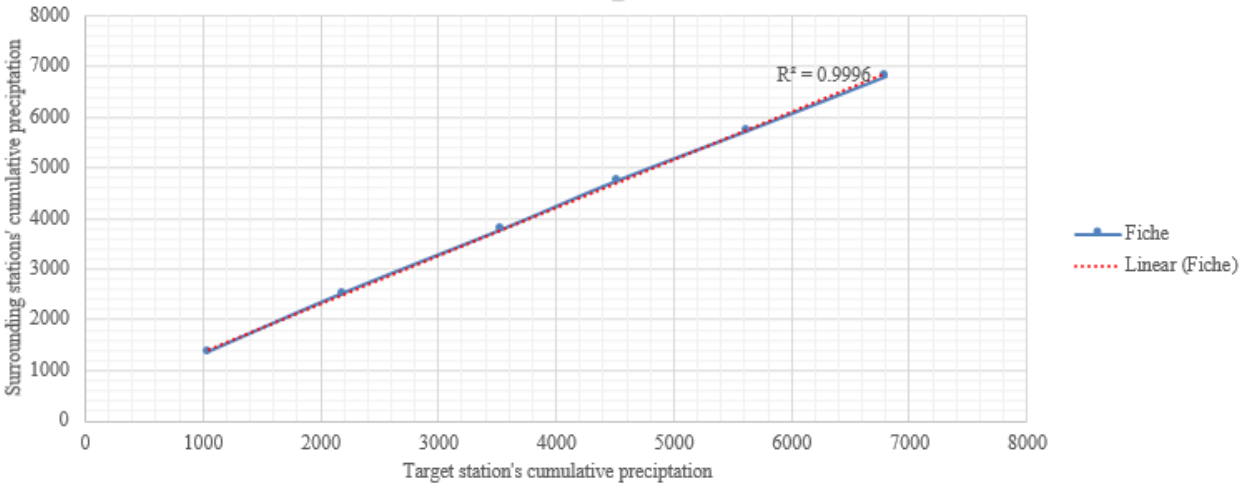

Figure 4.1: Double mass curve of Fiche station

Table 4.1: Annual average rainfall of the stations

	Years					
Stations	2003	2004	2005	2006	2007	2008
Alemketema	1005.7	870.5	1075.8	1206.9	1176.8	961
Chacha	1070.6	1206.8	929.1	1066.4	1128.7	983.4
Debrebrhan	1005.5	1023.2	932.4	948.175	1083.5	946.7
Debresina	1734.18079	2028	1952.9	2151.6	1879.8	1616.9
Debretsige	1030.3	851.7	800.4	1132.404	884.5	825.9
Degem	1344.4	968.888	1082	1441.1	1301.427	1245.8
Deneba	1292.9	932	905	1149.2	1178.1	869.3
Eneware	961.1	1157.9	995	1215.442	1478.4	1007.3
Fetera	851.480	964.8	1026.7	1161.156	1142.9	951.549
Fiche	1176.6	1103.3	982.6	1349.3	1138.6	1046.5
Gudoberet	1238.172	1548.5	929.6	1642.1	1908.3	1590.8
Jihur	934.475	979.6	911.3	980.1	786	787.6
Kotu	947.8	985.057	911.6	1054.7	1045.9	870.9
Lemi	1081.055	1159.820	963.392	1318.2	1297.575	2459.4
Mehalmeda	909.5	866.8	893.5	1027	937.2	838.606
Mendida	939.8	970.5	918.6	1216.610	1319.179	1121.2
Meragna	1171.1	895.318	982.6	1246.5	998.9	781.043
Muketuri	1171.3	978.8	1027.2	1107.4	1086.662	1053.8
Sheno	1265.9	1009.786	969	1080.998	1039.3	1003

4.1.2 Hydrological data

The gaps found in stream flow were completed using linear interpolation technique. The trend analysis also was completed with Spearman's Rank Correlation Coefficient Method, and its value is found as 0.371. The tabulated student's t-test t value is -2.78, and the calculated t value is -0.800, which shows that calculated t-test value is within the recommended range of t(4, 2.5%)=-2.78 $<t_{cal}$=-0.800< (v, 97.5%)=2.78, and the stream flow data has no trend.

4.2 Soil-Land use data analysis results

Figure 4.2 shows Curve Number grid map of Jemma Sub-Basin which is the computed result of soil, land use and sink filled DEM. The non-dimensional Curve Number value ranged from minimum of 30 to maximum of 94. Curve Number is known by a reverse relation with infiltration capacity of the soil, which means, areas of low curve number values have high infiltration capacity or low imperviousness, and areas of high curve number values have low infiltration capacity or high imperviousness.

For better understanding, Curve Number values within the sub-basin were illustrated in Column chart (Figure 4.3). As indicated in the Column chart 8.5%, 32.99%, 12.82%, 2.17%, 4.34%, 27.92% and 9.83% of Jemma Sub-Basin were possessed with Curve Number values of

30, 61, 62, 71, 73, 81 and 84 respectively. Others Curve Number values such as 32, 55, 77, 78, 79, 86 and 94 have a coverage of below 1% individually. Hence, the most dominant Curve Number value was 61 with 32.99%.

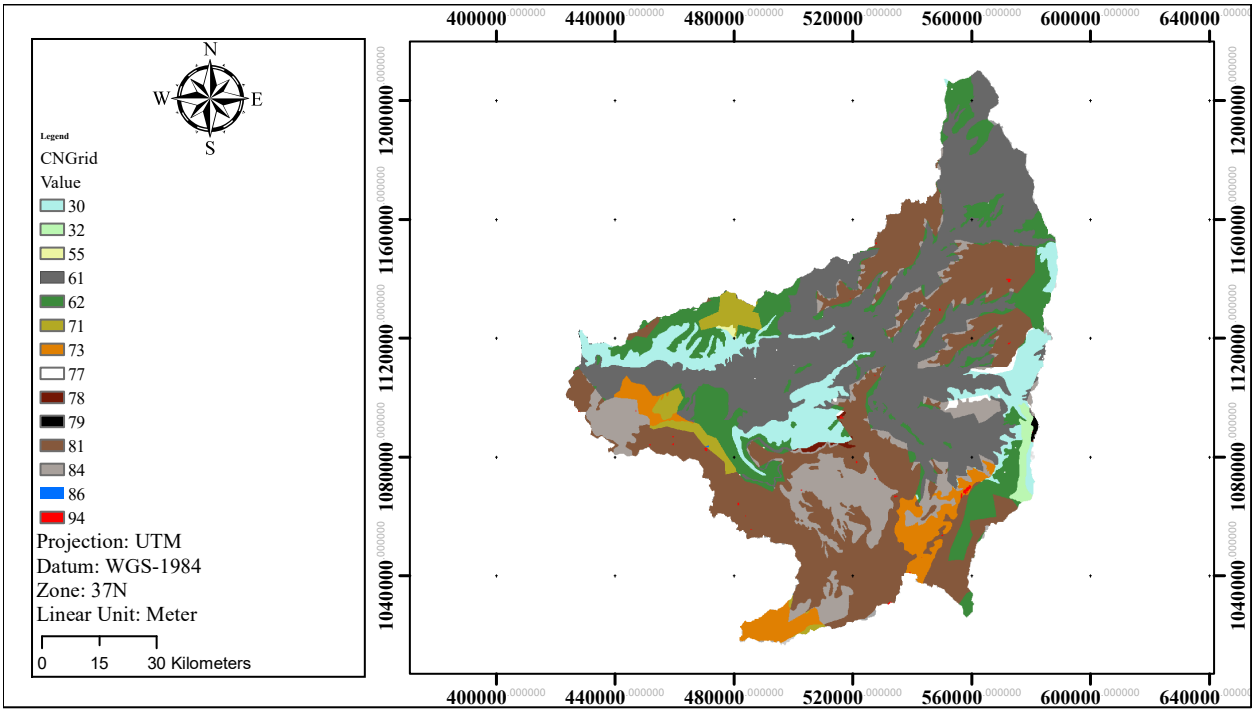

Figure 4.2: Curve Number grid map of Jemma Sub-Basin

4.3 Digital elevation model (DEM)

The Figure depicted in 4.4 is Gumorrow's catchment which was obtained from processing and analysis of 30m resolution DEM by using HEC-HMS 4.6. As shown in the Figure, it has seven sub-basins; three reaches, and three junctions. The Grid cell shapefile also overlaid over the catchment. In HEC-HMS, Grid Cell file is foot of Gridded data usage as well as distributed model type. The grid cell size shown in the Figure is 2000m, of course there are choices of standard grid sizes starting from 10m. But, high grid sizes affect the processing time and memory of processing machine. Furthermore, most maps used in the study area description are outcome of DEM.

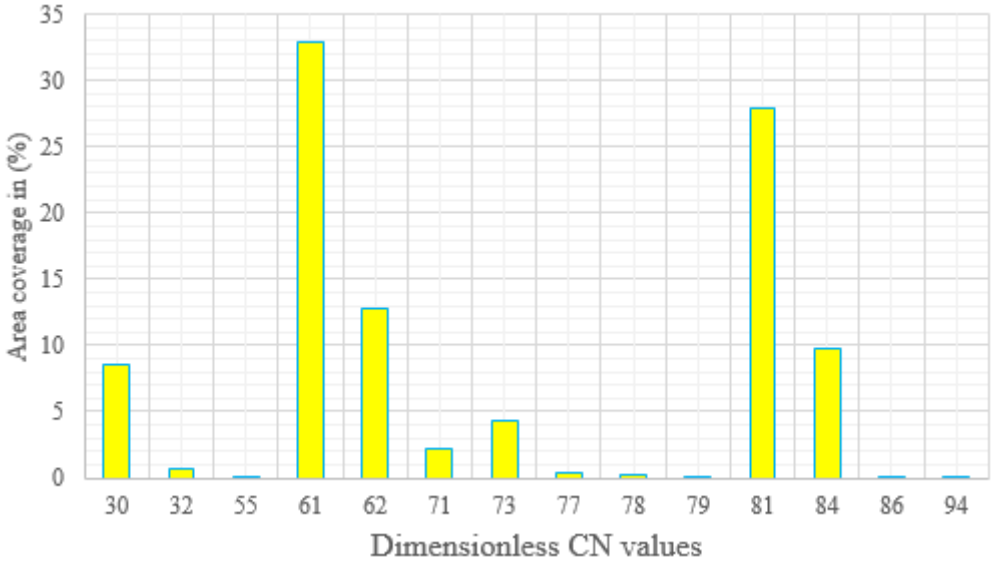

Figure 4.3: Column chart illustration of CN values for Jemma Sub-Basin

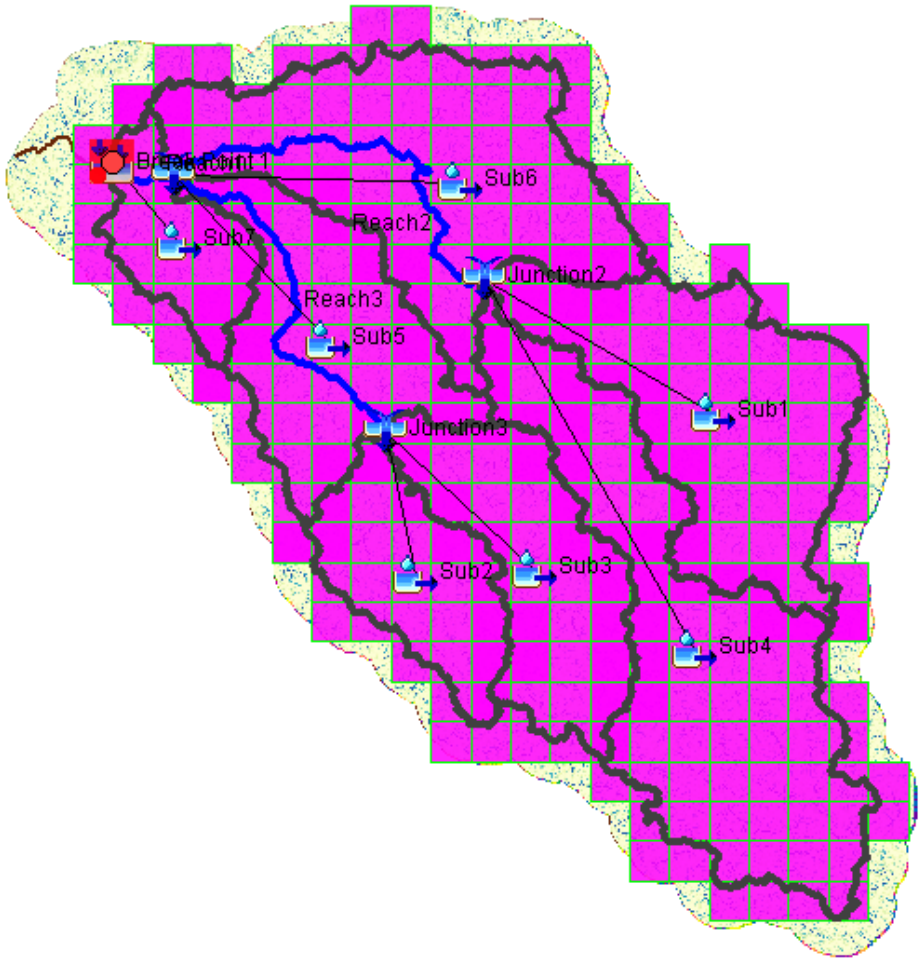

Figure 4.4: Grid cell shapefile overlied over Gumorrow catchement

4.4 SREs comparison and verification results

4.4.1 Graphical comparison

- **Maps**

Left and right-hand Maps in Figure 4.5 show the spatial distribution of precipitation for SREs and GRDs respectively, accumulated as of 2004 kiremt season. The complete spatial maps of all seasons with in the years of the study and all years (annual timescale) are illustrated in appendix B and C respectively. To produce such maps, both Satellite rainfall estimate and Ground rain gauge data were interpolated with IDW interpolation method for seasonal and annual timescale.

Based on the maps produced, most of the seasons showed comparable precipitation distribution in between SREs and GRDs except some variations. In Figure 4.5, the satellite precipitation product showed higher values in south west borders of the study area, when GRDs is showing higher values in central eastern part; hence, SREs underestimated in central eastern highlands, while overestimation is being observed in most south west borders. A total overestimation of SREs was observed in 2005 kiremt season except central eastern part. In 2006 kiremt season, underestimation of SREs was observed in the eastern highlands. Further minor variations between SREs and GRDs could be investigated from appendix B.

Similarly, Left and right-hand Maps in Figure 4.6 show the spatial distribution of precipitation for SREs and GRDs respectively, accumulated as of 2005. Based on the Figures, a total overestimation of SREs is observed except the spike of GRDs in central eastern edge. Underestimation of SREs in central eastern part is observed except 2003 and 2008; this and further minor variations could be investigated from appendix C.

Based on this qualitative type of comparison method, most of the seasonal and annual precipitation distributions of SREs and GRDs are nearly comparable except some important variations discussed in the previous paragraphs, and some further minor variations in kiremt and others seasons. This type of graphical comparison helps to understand and discover systematic errors and to identify locations where SREs are more accurate. The color ramp given in their respective appendixes could be referred as a legend for identification of the color-code levels.

- **Timeseries plots**

Based on the monthly and seasonal time-series plots, Figure 4.7 and 4.8, the SREs almost followed the trend of observed ground rain gauge data in all time. The satellite based rainfall

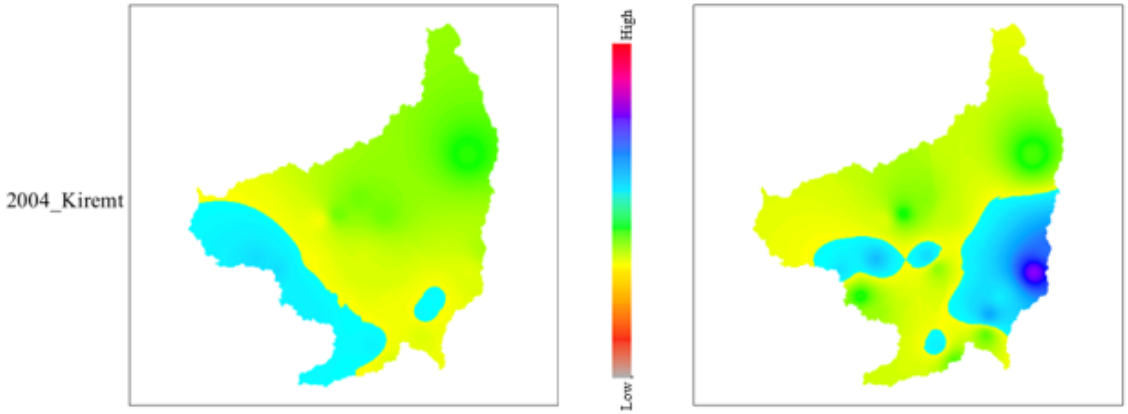

Figure 4.5: Spatial preciptation distribution of SREs and GRDs (2004 kiremt)

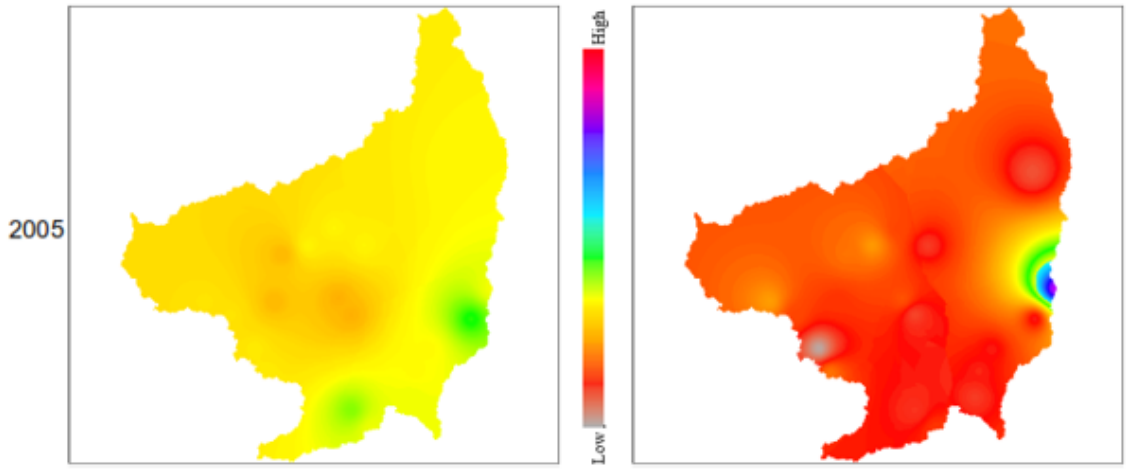

Figure 4.6: Spatial preciptation distribution of SREs and GRDs (2005)

also captured most rain occurrences. The same result is observed on the complete set of time-series plots given in appendix D and E.

The satellite rainfall estimate, where Debresina and Gudoberet stations found, practically underestimated the rainfall values throughout the time-series in both seasonal and monthly timescales. This result agrees with the result discussed in the previous paragraph, that is underestimation of SREs in central eastern part.

Uniquely, in the months of July and August of year 2005 or 2005 kiremt season, the satellite based rainfall overestimated the observed ground rain gauge data in all meteorological stations except Debresina.

Generally, the times series plots show that, satellite rainfall estimate is fairly good in prediction of GRDs, except occasional underestimation and overestimation of precipitation values in addition to variations discussed in the previous paragraphs. Hence, it does not seems that satellite rainfall retrieval faced an exaggerated difficulty to detect rainfall events except 2005 summer time.

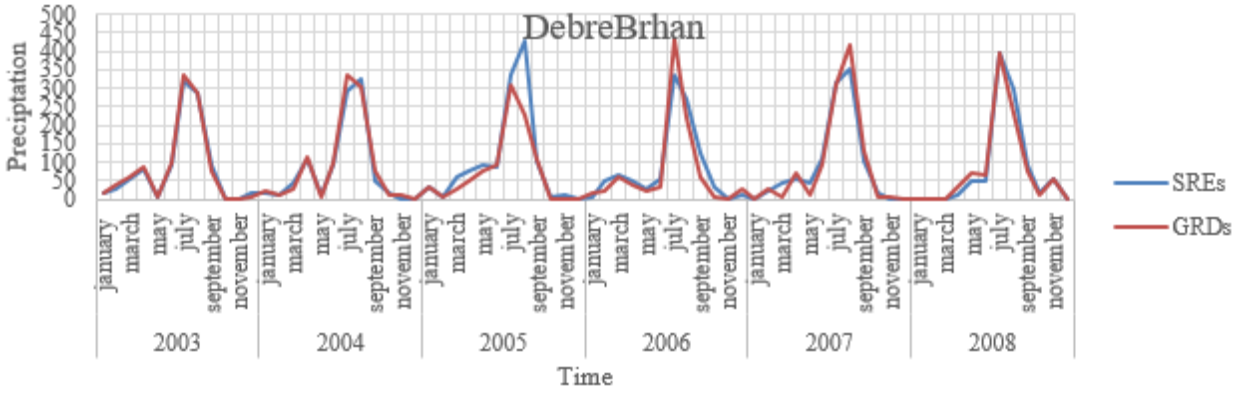

Figure 4.7: Acummulated monthly timeseries plot of the stations

4.4.2 Categorical statistics

By introducing different threshold values as different rainfall types, Categorical data analysis was completed for recommended categorical indices. However, only a piece of information is obtained from each statistic about the error, and inspecting a number of statistics is necessary to get a complete picture (Levizzani et al., 2007). To measure algorithm performance for different rain rates, it is valuable to plot the categorical scores as a function of an increasing rain threshold. Hence, Categorical statistics' results (Table 4.2) and categorical statistical plots (Figure 4.11-4.15) were used in combination for discussion.

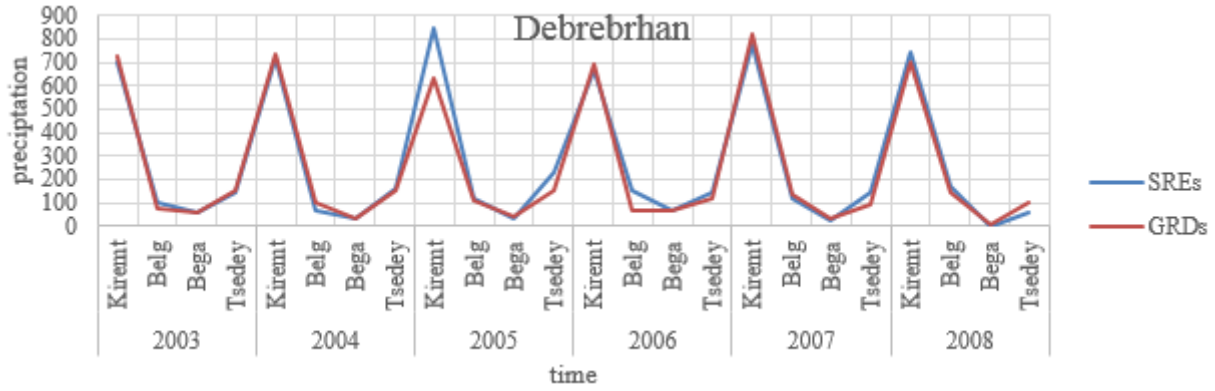

Figure 4.8: Acumulated seasonal timeseries plot of the stations

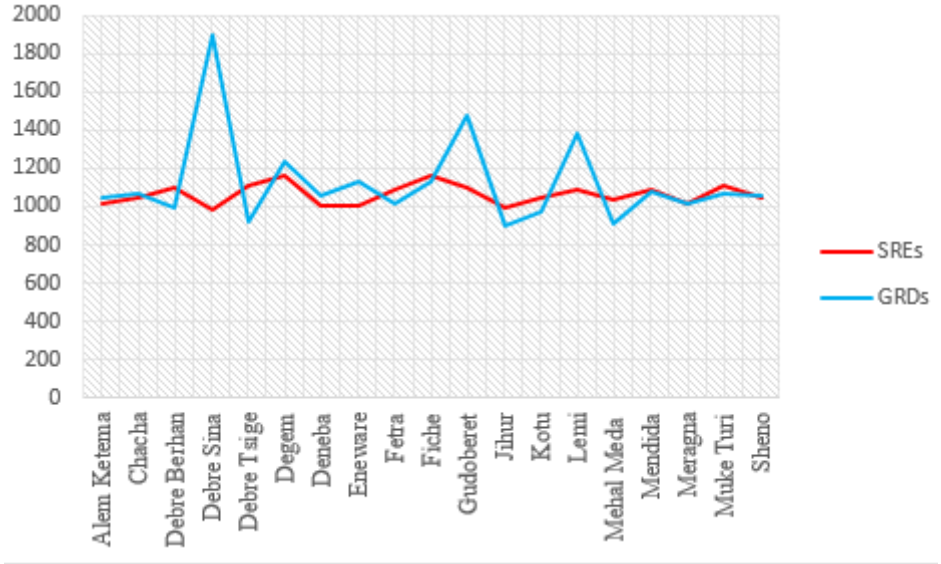

Figure 4.9: Acumulated Anual average timeseries plot of the stations

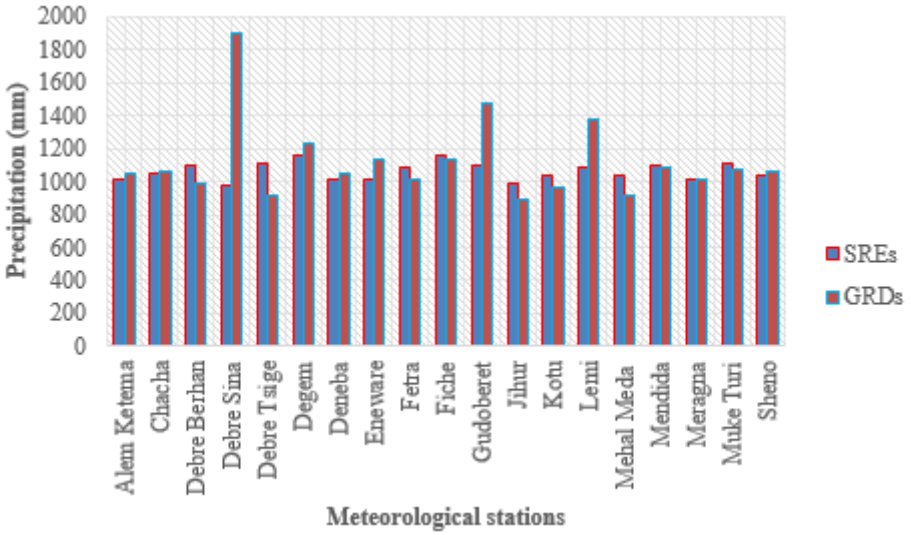

Figure 4.10: Anual average column barchart of the stations

Based on daily Accuracy plot (Figure 4.11), the accuracy fell in between 0.787 and 0.992. This implies that, (78.7-99.2%) of satellite rainfall estimate was correct. Violent type of rain ($\geq$ 42 mm/day) was highly detected with 99.2% than other rain types. Relatively, SREs accuracy was low in Light rain and No rain types with 78.7% and 81.8% respectively. In monthly timescale, lowest SREs performance was observed in Light rain with 79.5%, while highest performance was being observed in violent rain with 94.8%. In seasonal timescale, the overall accuracy was about 83.8% to 98.5%. However, lowest accuracy shifted to moderate rain, while highest accuracy is being still in violent rain type. Relative to the Monthly and Seasonal timescales, the daily timescale showed nearly uniform prediction performance (lowest gradient) for all rain types. Generally, SREs showed improved performance with increasing precipitation thresholds; that means, increased ability for intense precipitation magnitude.

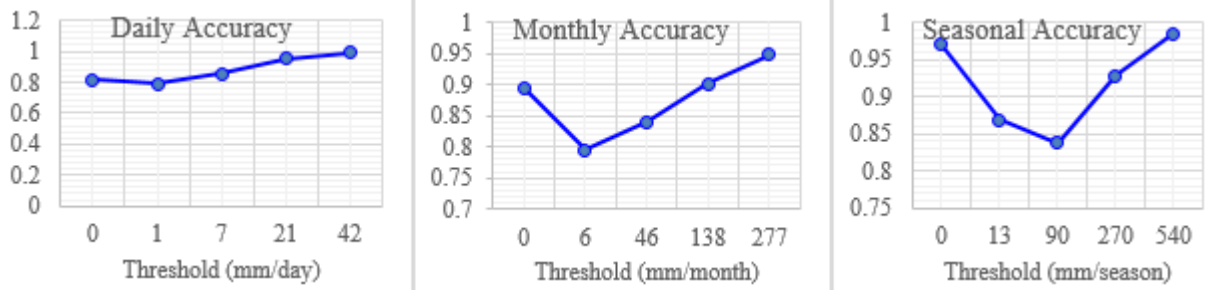

Figure 4.11: Catagorical Accuracy plot

Based on Daily BIAS plot (Figure 4.12), even though the degree of bias is different, the rainfall algorithm underestimated all rain types except the light rain. In monthly BIAS plot, SREs showed a slight overestimation of frequency of Moderate and Violent rains. Frequency

Table 4.2: Categorical verification Statistical results

Timescale	Threshold values (mm) as a function of Maximums average	Categorical Statistical values				
		Acuracy	BIAS	POD	FAR	CSI
Daily	1.5%=[0-1)- No rain	0.818	0.967	0.855	0.116	0.769
	10%=[1-7)- Light rain	0.787	1.243	0.362	0.709	0.193
	30%=[7-21)- Moderate rain	0.857	0.965	0.347	0.641	0.214
	60%=[21-42)-Heavy rain	0.952	0.836	0.186	0.778	0.113
	≥60%=42 - Violent rain	0.992	0.709	0.108	0.848	0.067
Monthly	1.5%=[0-6)- No rain	0.895	0.960	0.742	0.228	0.609
	10%=[6-46)- Light rain	0.795	1.031	0.650	0.37	0.471
	30%=[46-138)- Moderate rain	0.84	1.142	0.788	0.311	0.581
	60%=[138-277)-Heavy rain	0.902	0.422	0.215	0.491	0.178
	≥60%=277 - Violent rain	0.948	1.142	0.853	0.254	0.661
Seasonal	1.5%=[0-13)- No rain	0.97	0.818	0.591	0.278	0.481
	10%=[13-90)- Light rain	0.868	1.112	0.776	0.303	0.580
	30%=[90-270)- Moderate rain	0.838	1.076	0.838	0.221	0.677
	60%=[270-540)-Heavy rain	0.928	0.207	0.034	0.833	0.029
	≥60%=540 - Violent rain	0.985	1.008	0.973	0.035	0.940

of heavy rain was highly underestimated with a value of 0.422, although frequency of No rain was slightly underestimated with 0.96. In seasonal timescale however the satellite rainfall estimate slightly overestimated the frequency of light rain and extremely underestimated the frequency of heavy rain. No rain type was also underestimated with 0.818. Generally, Underestimation of No rain and overestimation of light rain was examined in all timescales.

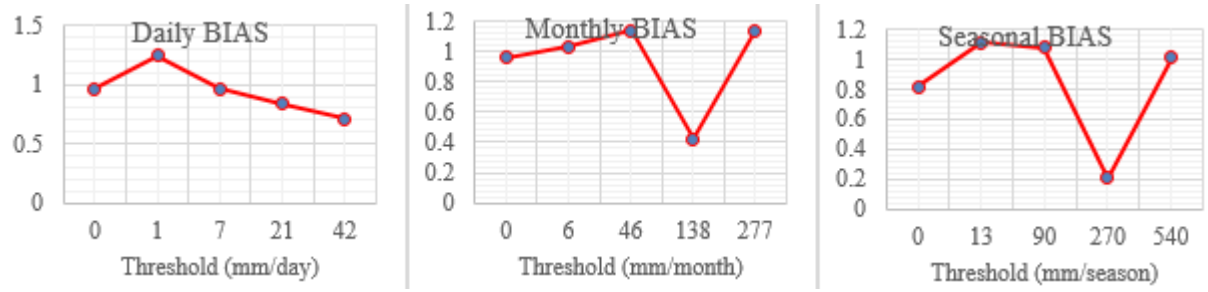

Figure 4.12: Catagorical BIAS plot

In Daily POD plot (Figure 4.13), except No rain type, observed rain events of all rain types were poorly predicted by SREs about 10.8-36.2%; in No rain type however, the prediction skill was achieved with 85.5%. In monthly and seasonal POD plots, the observed rain events of heavy rain type was poorly predicted with 21.5% and 3.4% respectively, although all the rest rain types showed more than 65% and 59.1% forecast skill for monthly and seasonal

timescales respectively.

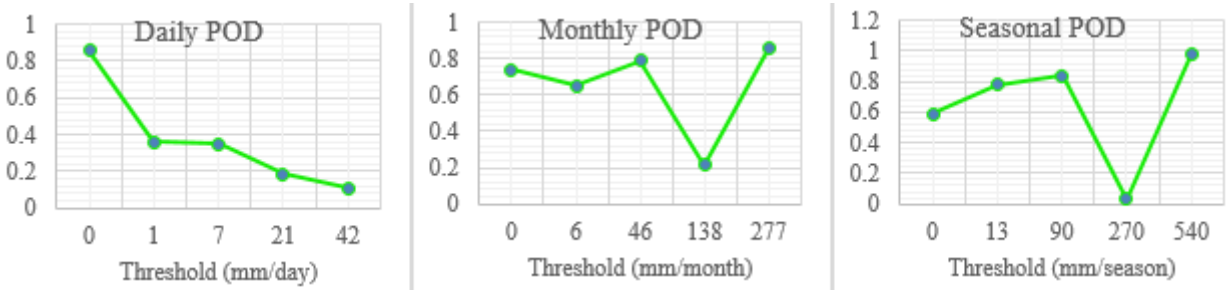

Figure 4.13: Catagorical POD plot

Based on Daily FAR plot (Figure 4.14), except No rain type, forecasted rain events of all rain types were incorrect with more than 64.1%; but in No rain type, 11.6% of forecasted rain events were not observed (were false alarms). In monthly timescale, less than 49.1% of forecasted rain events of all rain types were not observed; which implies the false alarm was less than half for all rain types. Seasonal timescale is almost similar to monthly timescale, but 83.3% of forecasted rain events were not correct in case of heavy rain type. All the rest Seasonal FAR was less than 30.3%. Hence, in Daily timescale, the algorithm had faced special difficulty with false alarms. Hydrologically, daily data is preferred than monthly, seasonal and any other accumulations.

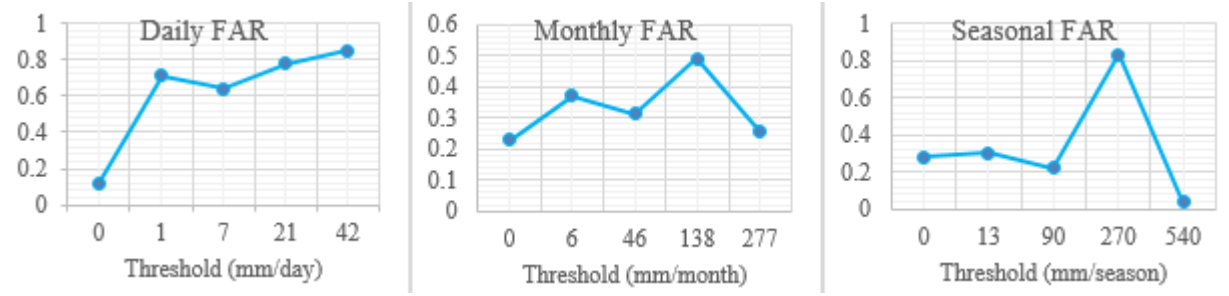

Figure 4.14: Catagorical FAR plot

In Daily CSI plot (Figure 4.15), except No rain type, all rain types of the rain events (observed and/or predicted) were correctly forecasted with less than 21.4%, but in No rain type about 76.9% of rain events (observed and/or predicted) were correctly forecasted. In Monthly CSI plot, Light rain and Heavy rain types of rain events were correctly forecasted with less than half percent. In the Seasonal CIS plot, No rain and Heavy rain types showed less than half percent accuracy with 48.1% and 2.9% respectively.

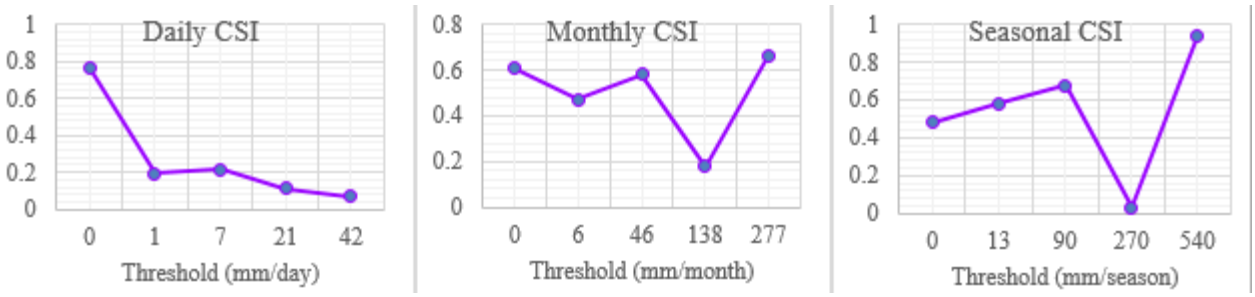

Figure 4.15: Catagorical CSI plot

4.4.3 Continuous statistics

Only a piece of information is obtained from each statistic about the error, and inspecting a number of statistics is necessary to get a complete picture (Levizzani et al., 2007). Thus, recommended continuous statistics such as Correlation coefficient (r), Bias or Mean Error (ME), Mean Absolute Error (MAE) and Root Mean Square Error (RMSE) are calculated (Table 4.3) and discussed as follow;

The correlation coefficient (r) between satellite based rainfall estimate and ground rain gauge values are 0.52, 0.915, 0.926 and 0.004 for daily, monthly, seasonal and annual timescales respectively. Hence, direct positive correlation is observed in all timescales. In monthly and seasonal accumulation, correlation is very strong. In daily timescale, it is an intermediate, and in annual timescale, the correlation was unimportant. The Best positive correlation was observed in accumulated seasonal timescale.

The Mean Error (ME) indices for daily, monthly, seasonal and annual timescales are -0.16, -5.03, -17.61, and -60.38 respectively. The negative signs of this index indicate an average underestimation of Satellite based rainfall data in comparison to observed rain gauge data. As it can be observed in Figure 4.16, except 2005, this average underestimation is supported by annual average time-series plot.

From Table 3.4, 0.16, 5.03, 17.61, and 60.38 are magnitudes of mean absolute errors for daily, monthly, seasonal and annual timescales. Thus, highest average forecast error was observed in annual timescale, while lowest average forecast error is being observed in daily timescale. When there are a compensating errors, perfect score may be obtained for bad estimation, which means, it does not indicate the association between observations and estimations.

Once again from the table 6.9, 48.57, 112.59 and 318.47 respectively are magnitudes of Root Mean Square Errors for daily, monthly, seasonal and annual timescales. The error magnitude became exaggerated with timescale aggregation both in MAE and RMSE.

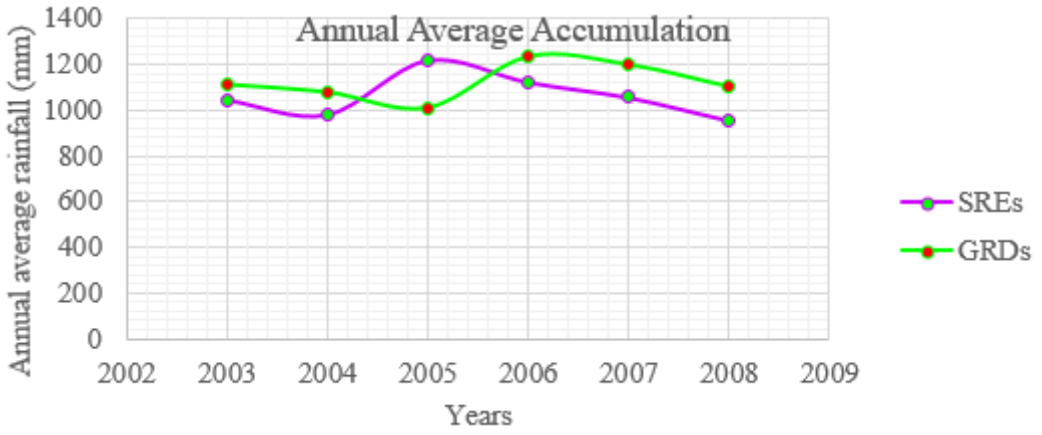

Figure 4.16: Annual average accumulation plot of SREs and GRDs

Table 4.3: Continuous verification Statistical result

	Continuous Statistical indices			
Timescales	r	ME (Bias)	MAE	RMSE
Daily	0.52	-0.16	0.16	6.9
Monthly	0.915	-5.03	5.03	48.57
Seasonal	0.926	-17.61	17.61	112.59
Annual	0.004	-60.38	60.38	318.47

4.5 Hydrological model results with raw satellite data

4.5.1 Sensitivity analysis

Before calibrating and validating HEC-HMS model, sensitivity analysis was done so as to understand the effect of each model parameters. For this purpose, seven HEC-HMS model parameters were considered, and these are: Initial abstraction ratio (I.ab), Potential max retention factor (S), Time of concentration (T), Storage coefficient (SC), Muskingum K, Muskingum X and No sub reaches (NoSR).

Figure 4.17 shows sensitivity analysis result of raw Satellite rainfall estimate in-terms of Nash-Sutcliffe efficiency (NSE). Based on this result, Potential max retention factor (S) was the most sensitive parameter as shown by highest gradient. The parameters Time of concentration (T) and Storage coefficient (SC) were the second and third sensitive parameters respectively. Initial abstraction ratio (I.ab) was the fourth sensitive parameter. The remaining three parameters not showed significance change on values of NSE. However, their level of sensitivity were ranked as K, X and NoSR from highest to the least. Parameters like Potential max retention factor (S), Time of concentration (T) and Storage coefficient (SC) showed a

non-linear model performance, while all the rest show nearly linear model performance.

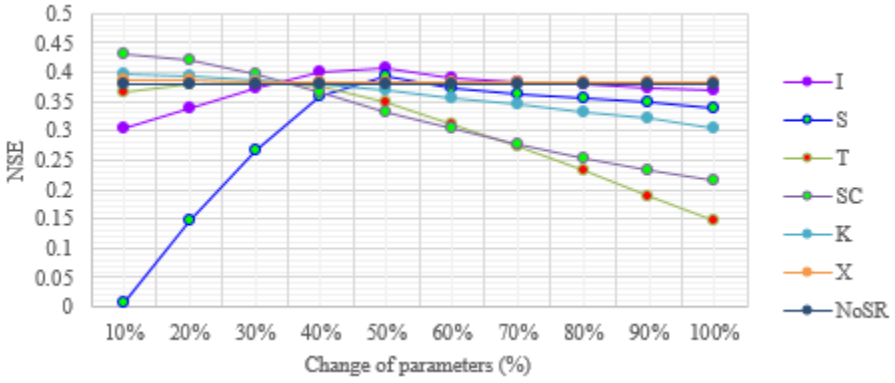

Figure 4.17: Sensitivity analysis result in-terms of NSE (Raw SREs)

In-terms of percent bias (PBIAS), Potential max retention factor (S) was the most sensitive parameter. Initial abstraction ratio (I.ab) was the second sensitive parameter which controls the PBIAS. All the remaining parameters not showed significant influence on the values of PBIAS. As it can be referred from Figure 4.18, Potential max retention ratio (S) followed non-linear model performance; Initial abstraction ratio (I.ab) on the other hand showed a linear trend.

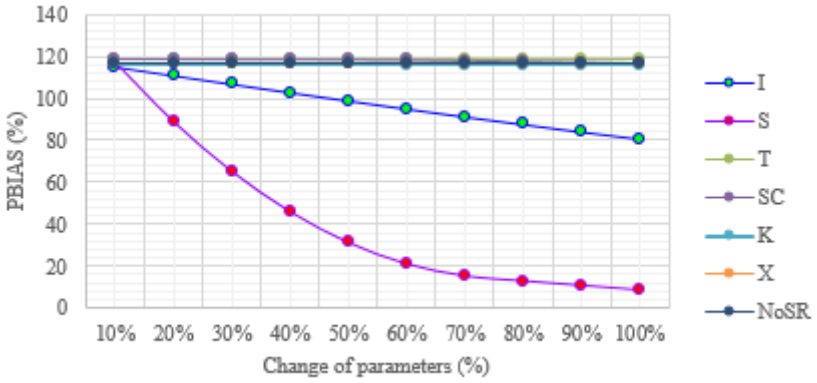

Figure 4.18: Sensitivity analysis result in-terms of PBIAS (Raw SREs)

4.5.2 Calibration

The HEC-HMS hydrological model was calibrated and validated in Gumerow catchment for the period of four years (2003-2006) and two years (2007-2008) respectively. Figure 4.19 shows the observed and simulated hydrographs for both calibration and validation periods simultaneously. The model almost captured the trend of daily based observed flow during

calibration period of (2003-2006). However, the model highly underestimated the observed peak flows during this period. It may be due to an average underestimation of SREs.

Other graphical technique called Flow Duration Curve (FDC) is shown in Figure 4.20 for further illustration. Thus, the model had a good agreement during low flows (>40%). However, it tended to slightly overestimate the observed data during medium flows (>10% and <40% probability), and highly underestimate during high flows (<10% probability).

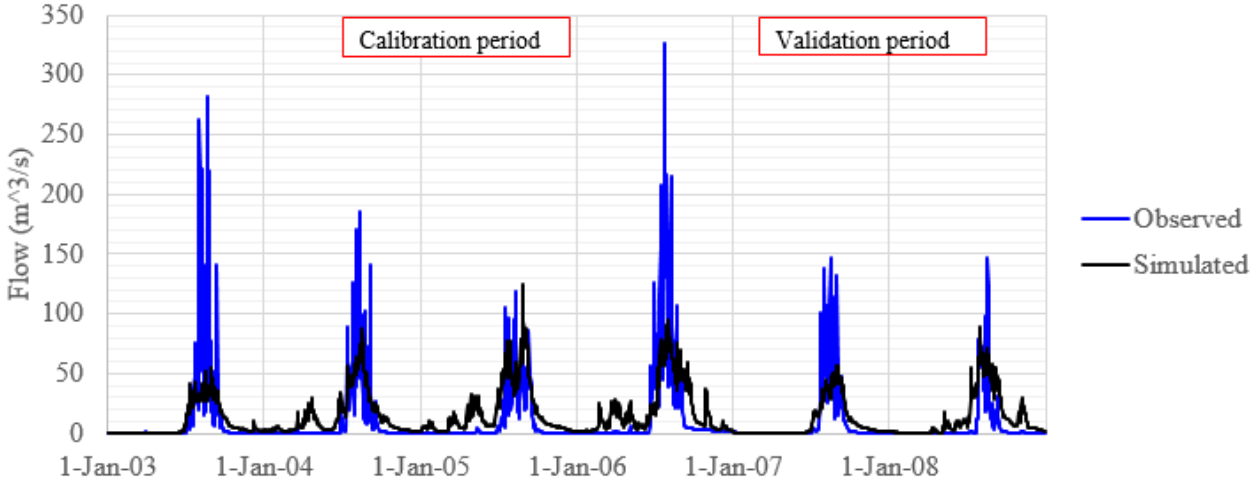

Figure 4.19: Observed and simulated hydrograph (Raw SREs)

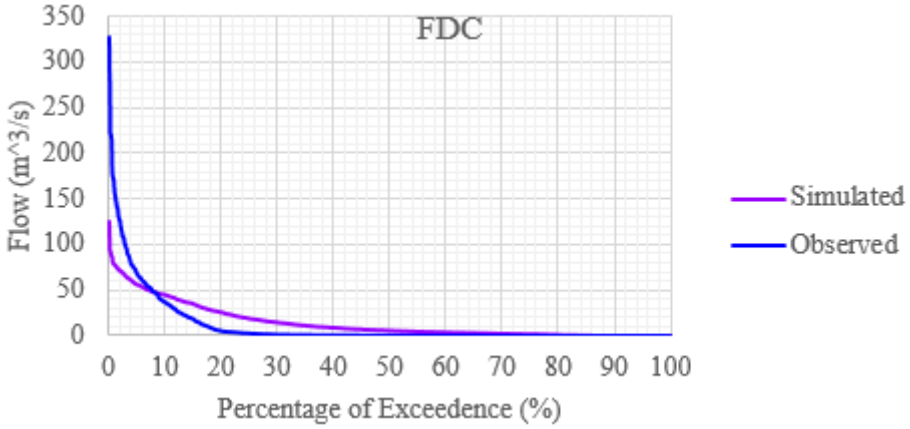

Figure 4.20: Observed and simulated FDC (Raw SREs)

The quantitative statistical measures such as Nash-Sutcliffe efficiency (NSE), Percent bias (PBIAS), RMSE to standard deviation ratio (RSR), Pearson's correlation coefficient (r) and coefficient of determination (R^2) were used to evaluate the model performance both during the calibration and validation periods. As summarized in table 4.5, the NSE, PBIAS, RSR, r and R^2 were found as 0.406, 24.26%, 0.771, 0.646 and 0.417 respectively during calibration.

Table 4.4: Fitted model parameter values selected for calibration of raw SREs

	Fitted model parameter values						
Elements	I.ab	S	T	SC	K	X	NoSR
Sub4	0.78	10	11.5	967	*	*	*
Sub1	0.89	10	240	8	*	*	*
Sub3	0.99	7.5	55.5	38.5	*	*	*
Sub2	0.94	5.2	167.5	9.5	*	*	*
Sub6	0.98	5.1	5	28	*	*	*
Sub5	1	4.65	12.5	44	*	*	*
Sub7	0.98	5.1	187	71	*	*	*
Reach2	*	*	*	*	30.5	0.25	1
Reach3	*	*	*	*	37.5	0.3	1
Reach1	*	*	*	*	2.56	0.2	1

Based on the model performance ratings summarized in table 3.6, the results indicated a poor agreement between simulated and observed datasets with NSE of 0.406 and R^2 of 0.417. Even if the result was rated as fair with PBIAS of 24.26%, an average underestimation of model can be clearly understood with this value. The result was rated as poor with RSR of 0.771. Zero RSR can be obtained as a result of zero RMSE, which is the perfect value. Better model performance is defined with lower RSR. The correlation coefficient is good with r of 0.646 for calibration period. During this situation, where raw satellite rainfall estimate is used, the fitted HEC-HMS model parameter values were tabulated in table 4.4.

4.5.3 Validation

In Figure 4.19, Observed and Simulated hydrographs of validation period were shown from 01, Jan2007 to 31, Dec2008. The Figure shows that, the model almost captured the trend of daily observed flows; however, it underestimated the observed peak flows as with in the calibration period (01, Jan2003 to 31, Dec2006). But, it seems that, the two hydrographs showed better agreement in validation period relative to calibration period. An overestimation of flows are also observed both in calibration and validation periods. As a result, the observed and simulated hydrographs were more illustrated by FDC (Figure 4.20).

The Statistical measures used in calibration period were also used to test validation model performance. Thus, the NSE, PBIAS, RSR, r and R^2 were found as 0.452, 41.53%, 0.74, 0.691 and 0.477 respectively during validation period.

Based on the model evaluation criteria summarized in table 3.6, the validation model results also showed a poor agreement between simulated and observed hydrograph datasets with

NSE of 0.452 and R^2 of 0.477. An average underestimation of model result become worse with PBIAS of 41.53%. The standardized error index still showed a poor performance with RSR of 0.74. The correlation coefficient is good with r of 0.691. However, except the PBIAS, all statistical results showed an improvement in validation period relative to the calibration period.

4.6 Hydrological model result with combined version satellite data

4.6.1 Sensitivity analysis

Before HEC-HMS model is calibrated and validated, sensitivity analysis was done so as to understand the effect of each model parameters. The Seven model parameters considered are: Initial abstraction ratio (I.ab), Potential max retention factor (S), Time of concentration (T), Storage coefficient (SC), Muskingum K, Muskingum X and No sub reaches (NoSR).

Figure 4.21 shows sensitivity analysis result in-terms of Nash-Sutcliffe efficiency (NSE). Based on this result Potential max retention factor (S) was the most sensitive parameter. The parameters Storage coefficient (SC) and Time of concentration (T) were the second and third sensitive parameters respectively. Initial abstraction ratio (I.ab) and Muskingum (K) were ranked at fourth and fifth level of sensitivity. The remaining two parameters (X and NoSR) not showed a significance change on value of NSE. Potential max retention factor showed non-linear trend.

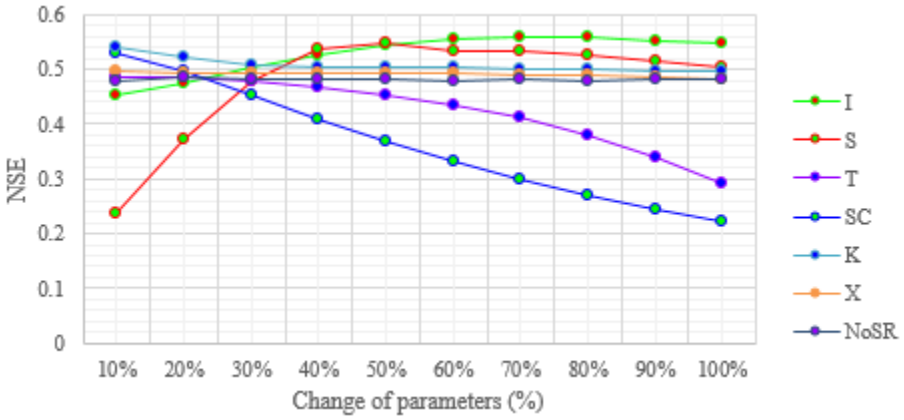

Figure 4.21: Sensitivity analysis in-terms of NSE (combined version SREs)

In-terms of percent BIAS (PBIAS), Potential max retention factor (S) is the most sensitive parameter. Initial abstraction ratio (I.ab) was ranked at second level of sensitivity which controls the PBIAS. Both Potential max retention factor and Initial abstraction ratio showed

non-linear model performance. All the remaining model parameters not showed a significant change on PBIAS values. The sensitivity analysis result in-terms of percent BIAS (PBIAS) could be referred in Figure 4.22.

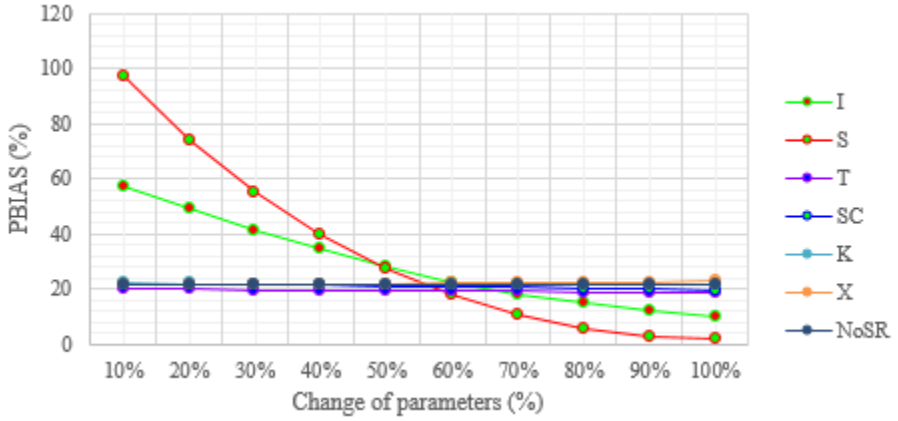

Figure 4.22: Sensitivity analysis in-terms of PBIAS (combined version SREs)

4.6.2 Calibration

The HEC-HMS hydrological model was calibrated and validated in Gumerow catchment for the period of four years (2003-2006) and two years (2007-2008) respectively. Figure 4.23 shows the observed and simulated hydrograph for both calibration and validation periods together. The hydrograph shows that, the model captured the trend of daily based observed stream flow during calibration period of (2003-2006). However, the model underestimated the observed peak flows during this period. As it can be seen in the Figure, the simulated flow hydrograph is fluctuating smoothly, while the observed one showed rapid fluctuation.

Flow Duration Curve (FDC) is shown in Figure 4.24, and the model has a good agreement during low flows (>30% probability). However, it tended to slightly overestimate the observed data during medium flows (>10% and <30% probability), and highly underestimate during high flows (<10% probability).

Statistical measures such as Nash-Sutcliffe efficiency (NSE), Percent bias (PBIAS), RMSE to standard deviation ratio (RSR), Pearson's correlation coefficient (r) and coefficient of determination (R^2) were used to evaluate the model performance both during the calibration and validation periods. As summarized in table 4.5, the NSE, PBIAS, RSR, r and R^2 were found as 0.532, 14.83%, 0.684, 0.744 and 0.554 respectively during calibration.

Based on the model performance criteria summarized in table 3.6, the simulated model result

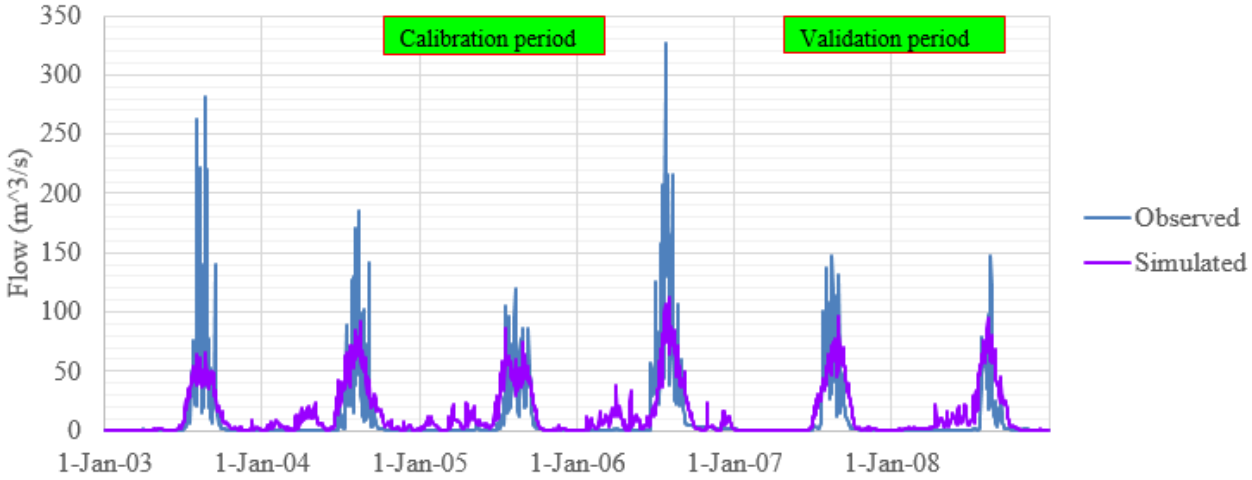

Figure 4.23: combined version hydrograph (combined version SREs)

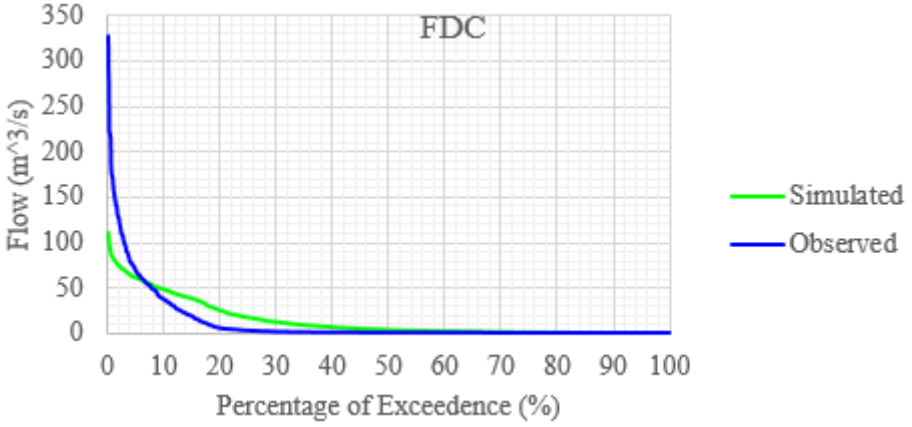

Figure 4.24: Observed and simulated FDC (combined version SREs)

Table 4.5: Summary of statistical model performance evaluation result for calibration and validation.

	Raw SREs		combined version SREs	
Statistics	Calibration	Validation	Calibration	Validation
NSE	0.406	0.452	0.532	0.56
PBIAS	24.26%	41.53%	14.83%	55.09%
RSR	0.771	0.740	0.684	0.663
r	0.646	0.691	0.744	0.786
R^2	0.417	0.477	0.554	0.618

Table 4.6: Fitted model parameter values selected for calibration of combined version SREs

	Fitted model parameter values						
Elements	I.ab	S	T	S.C	K	X	NoSR
Sub4	0.55	8.7	403	13	*	*	*
Sub1	1	8.4	280	16.5	*	*	*
Sub3	0.62	9.8	164	19	*	*	*
Sub2	0.83	9.5	160	43	*	*	*
Sub6	0.87	7.5	13	6	*	*	*
Sub5	0.58	8.8	10	8	*	*	*
Sub7	0.68	9.3	7	8	*	*	*
Reach2	*	*	*	*	99	0.4	1
Reach3	*	*	*	*	26.5	0.33	1
Reach1	*	*	*	*	7	0.21	1

was rated as Fair with NSE of 0.532 and R^2 of 0.554. Although an average underestimation is still obtained, the combined version model result showed good performance with PBIAS of 14.83%. The model performance is fair with RSR of 0.684 and good with r of 0.744 for calibration period. During this situation, where combined version SREs is used, the fitted HEC-HMS model parameter values were tabulated in table 4.6.

4.6.3 Validation

In Figure 4.23, Observed and Simulated hydrographs of validation period are shown from 01, Jan2007 to 31, Dec2008. The Figure shows that, the model almost captured the trend of daily observed flow. However, the model underestimated the observed peak flows like in the calibration period. Relative to hydrographs with raw SREs, combined version hydrographs (Figure 4.23) showed an agreement in low flows, and furthermore information can be discovered from FDC.

The Statistical measures used in calibration period were also used to test the model performance of validation period. Thus, these statistical measures such as NSE, PBIAS, RSR, r and R^2 were found as 0.56, 55.09%, 0.663, 0.786 and 0.618 respectively during validation period.

Based on the model evaluation criteria summarized in table 3.6, the model simulated the observed stream flow as Fair with NSE of 0.56, as poor with PBIAS of 55.09%, as Fair with RSR of 0.663, as Good with r of 0.786 and as Fair with (R^2) of 0.618. In comparison to calibration period, all statistical values show an improvement in validation except PBIAS. Generally, combined version performance is improved in comparison to raw SREs.

5 CONCLUSIONS AND RECOMMENDATIONS

5.1 CONCLUSIONS

The main objective of this study was to evaluate the performance of satellite based rainfall estimate, TRMM. The specific objectives of the study were: to verify the latest version of TRMM_3B42 satellite based rainfall estimate; to evaluate the performance of TRMM_3B42 as an input of distributed type of HEC-HMS hydrological model; and to realize the effect of Combined version of TRMM_3B42 on the model output. To succeed these objectives, appropriate data were processed and analyzed, and results were presented and discussed. From the results and discussions, the following conclusions were made:

Most of the seasonal and annual precipitation distribution of SREs and GRDs were nearly comparable except some important variations. The times series plots showed that, satellite rainfall estimates is fairly good in detection of GRDs, except occasional underestimation and overestimation of precipitation values for all rainfall stations.

Lowest overall accuracy of SREs was discovered in light rain, while highest accuracy was being observed in violent rain type. Underestimation of No rain and overestimation of light rain was examined in all timescales. No rain type showed best forecast skill in daily timescale; however in monthly and seasonal timescales, observed rain events of all rain types were correctly forecasted with more than 59% skill except heavy rain type. Relative to other timescales, the algorithm had faced special difficulty with false alarms in Daily timescale.

In between SREs and GRDs, Positive linear association was detected in daily, monthly and seasonal timescales with correlation coefficient values of 0.52, 0.915 and 0.926 respectively; however, no relation was detected in annual timescale with a value of 0.004. Moreover, an average underestimation of SREs was discovered in all timescales with the negative mean error signs. However, the average error magnitude showed an increment from daily to annual accumulation. As a result, daily timescale has lowest error magnitude in both MAE and RMSE indices.

For sensitivity analysis, seven HEC-HMS model parameters were considered like Initial abstraction ratio (I.ab), Potential max retention factor (S), Storage coefficient (SC), Time of concentration (T), Muskingum K. Among these parameters, Potential max retention factor (S), Initial abstraction ratio (I.ab), Storage coefficient (SC) and Time of concentration (T) were the most sensitive parameters, and X and NoSR were the least sensitive parameters for Gumerrow catchment.

Raw SREs were showed poor performance both in calibration and validation periods with NSE, PBIAS, RSR and R^2 values of 0.406, 24.26%, 0.771 and 0.417 in calibration and 0.452, 41.53%, 0.74 and 0.477 in validation periods respectively. Hence, the raw TRMM_3B42V7 data has poor performance to use as an input of HEC-HMS model in Gumerrow catchment.

Combined version SREs were showed satisfactory performance with NSE, PBIAS, RSR and R^2 values of 0.532, 14.83%, 0.684 and 0.554 in calibration and 0.56, 55.09%, 0.663 and 0.618 in validation periods respectively. Thus, the Combined version satellite rainfall estimate has an effect on HEC-HMS hydrological model outputs in Gumerrow catchment.

The model underestimated high flow vales both in raw satellite rainfall estimate and Combined version satellite rainfall estimates. Similar behavior was observed during calibration and validation periods also.

When the model was calibrated and validated with Combined version satellite based rainfall, its performance showed an improvement in all quantitative model evaluation statistics than raw satellite rainfall estimate. Relative to calibration period, the model performance of validation period was showed improvement in all statistics except PBIAS.

5.2 RECOMMENDATIONS

- As it is known, distributed type of models consider variation of spatial characteristic of study area. Following that, different characteristics give different hydrological response. Secondary LULC data was used for this study, and it in turn affects selection of CN values and hydrological model results. As a result, detail land use land cover map should be prepared to fill the gap of this research.
- Besides to TRMM_3B42, there are other multisatellite precipitation products on the web with high spatial and temporal resolutions. To select the best of all, and in turn to apply in hydrological models and any other water resource studies, the performance of these products need to be tested, evaluated and studied in detail.
- A spatial type of precipitation input data is required for distributed type of HEC-HMS rainfall runoff model. Conversion of the point rain gauge data to its spatial form, and running the model is important to compare its model output with respect to raw SREs and Combined version SREs model outputs.

6 APPENDIXES

6.1 Appendix A: Slice of gap filled daily recorded data

Year	Alemkete	Chacha	Debrebrh	Debresin	Debretsig	Degem	Deneba	Eneware	Fetera	Fiche	Gudoberet	Jihur	Kotu	Lemi	Mehalme	Mendida	Meragna	Muketuri	Sheno
2003	0	0	0	0	0	0	0	0	0	0	0	0	0	0	0	0	0	0	0
2003	0	0	0	0.0234	0	0	0	0	0	0	0	0	0	0	0	0	0	0	0
2003	0	0	0	0	0	0	0	0	0	0	0	0	0	0	0	0	0	0	0
2003	0	0	0	0	0	0	0	0	0	0	0	0	0	0	0	0	0	0	0
2003	0	0	0	0.7006	0	0	0	0	0	0	0	0	0	0	0	0	0	0	0
2003	0	0	0	0	0	0	0	0	0	0	0	0	0	0	0	0	0	0	0
2003	0	0	0	0	0	0	0	0	0	0	0	0	0	0	0	0	0	0	0
2003	0	0	0	0	0	0	0	0	0	0	0	0	0	0	0	0	0	0	0
2003	0	0	0	0	0	0	0	0	0	0	0	0	0	0	0	0	0	0	0
2003	0	0	0	0	0	0	0	0	0	0	0	0	0	0	0	0	0	0	0
2003	0	0	0	0	0	0	0	0	0	0	0	0	0	0	0	0	0	0	0
2003	0	0	0	0	0	0	0	0	0	0	0	0	0	0	0	0	0	0	0
2003	0	0	0	0	0	0	0	0	0	0	0	0	0	0	0	0	0	0	0
2003	0	0	0	0	0	0	0	0	0	0	0	0	0	0	0	0	0	0	0
2003	0	0	0	0	0	0	0	0	0	0	0	0	0	0	0	0	0	0	0
2003	0	0	0	0	0	0	0	0	0	0	0	0	0	0	0	0	0	0	0
2003	0	0	0	0	0	0	0	0	0	0	0	0	0	12.6	0	0	0	0	0
2003	0	0	0	0	0	0	0	0	0	0	0	0	0	0	0	0	0	0	0.1
2003	0	0	0	0	0	0	0	0	0	0	0	1.2	0	0	0	0	0	0	0
2003	0	0	0	0	32.8	5	1.8	2.2	0	2.3	0	1	9.2	0	0	0.2	0	0.6	0
2003	0.8	0	0	0	8.3	16.7	3.9	1.9	0	11.2	0	0	0.8	0	0	0	0	0	0
2003	6.2	0	0	0.5605	3.9	0.4	1.3	0	0.3	0	0	0	0	0	0.5	0	0	0	0
2003	0	0	0	1.0041	0	0	4.9	0	0	0	0	0	0	0	0.5	0	0	2.5	0
2003	0	0	0	1.4478	4.5	0.8	0	0	0	1.7	0	0	0.2	0	2.8	3.5	6.9	5.1	0
2003	0	0	2.6	7.6648	0	0	0	0	0	0.9	10	0	0.8	0	0	0	0	6.5	0
2003	0	1	11.5	1.3797	3.2	1.9	13.8	9.8	0	0.4	1.8	8.2	1.5	0	5.3	4.2	0	19.3	2.4
2003	2	0	0	0	0.9	8.2	0	1.4	3	6.9	0	0	2.7	0	14.8	0	1	0	0
2003	0	0	1.5	0	0	0	0	0	0	0	0	0	0	0	0	0	0	0.3	0
2003	0	0	0	0	0	0	0	0	0	0	0	0	0	0	0	0	0	1.3	0
2003	0	0	0	0	0	0	0	0	0	0	0	0	0	0	0	0	0	0	0
2003	0	0	0	0	0	0	0	0	0	0	0	0	0	0	0	0	0	0	0
2003	0	0	0	0	0	0	0	0	0	0	0	0	0	0	0	0	0	0	0
2003	0	0	0	0	0	0	7.5	0	0	0	0	0	0	0	0	0	0	0	0

2008	0	0	0	0	0	0	0	0	0	0	0	0	0	0	0	0	0	0	0
2008	0	0	0	0	0	0	0	0	0	0	0	0	0	0	0	0	0	0	0
2008	0	0	0	0	0	0	0	0	0	0	0	0	0	0	0	0	0	0	0
2008	0	0	0	0	0	0	0	0	0	0	0	0	0	0	0	0	0	0	0
2008	0	0	0	0	0	0	0	0	0	0	0	0	0	0	0	0	0	0	0
2008	0	0	0	0	0	0	0	0	0	0	1	0	0	0	0	0	0	0	0
2008	0	0	0	0	0	0	0	0	0	0	12	0	0	0	0	0	0	0	0
2008	0	0	0	0	0	0	0	0	0	0	3	0	0	0	0	0	0	0	0
2008	0	0	1.6	28.8	0	1.5	0	0	0	0	1	0	0	0	0	0	0	0	0
2008	1	0	1.8	18	0	45.2	4.5	0.6	10.1	5.6	23.3	0	0	0	6.3	0	1.8769	5	3.5
2008	0	0	0	0	10.7	0	0	0	1.5	0	4.4	0	0	0	0	25	0.2077	0	0
2008	0	0	0	0	0	0	0	0	0	6.6	0	0	0	0	0	0	0	0	0
2008	0	4.2	0.8	28.7	1.4	0	0	0	0	0	3	0	0	8	11.4	0	0	0.1	1.4
2008	9.2	0	0	3.8	1.7	0	0	0	0	4.7	2.1	0	0	0	2.3	0	4.4013	0	0
2008	0	0	0	5	2.3	12.8	0	0	0	0	1	0	0	10	0	5	0	0	0
2008	2.1	1.1	3.7	6	10.4	0	18.2	9.4	1.5968	23.9	0	2.8	28.5	0	0	0	0	9.6	10.2
2008	4.1	2.4	3.4	39	20.3	46.3	10.5	15.6	6.3284	7.6	10.1	4.7	2.5	13.4	4.2	2.2	2	10.1	9.5
2008	6.6	3	8.8	8.1	11.4	24.3	13.7	20.2	7.4147	7.4	1.4	10.2	7.2	10	11.6	20	5.2	3.3	15.1
2008	20.7	2.1	2.9	28.2	1.9	12.5	2.6	6.7	17.705	8.1	4.8	0.8	4.9	8.2	35.2	22	10.3	14.2	2.6
2008	0	0	0	68.2	5.4	25.8	1.7	0.3	1.4856	6	5	0	0	6.2	1.4	24	0.2	28.5	0.2
2008	8.1	12.4	32.2	20.2	0.5	1.5	0	7.8	6.1591	4.1	10.1	21.2	45.5	0	1.8	22	15.2	9	0
2008	5.6	1.8	3.6	0	0.9	5.1	0	0	4.2582	1.5	3	0	0	0	7.6	30.2	0	0	1.2
2008	0	0	0	0	0	0	0	0	1.9169	0	0	0	0	8	0	0	0	0	0
2008	0	0	0	0	0	0	0	0	0	0	0	0	0	0	0	0	0	0	0
2008	0	0	0	0	0	0	0	0	0	0	0	0	0	0	0	0	0	0	0
2008	0	0	0	0	0	0	0	0	0	0	0	0	0	0	0	0	0	0	0
2008	0	0	0	0	0	0	0	0	0	0	0	0	0	0	0	0	0	0	0
2008	0	0	0	0	0	0	0	0	0	0	0	0	0	0	0	0	0	0	0
2008	0	0	0	0	0	0	0	0	0	0	0	0	0	0	0	0	0	0	0
2008	0	0	0	0	0	0	0	0	0	0	0	0	0	0	0	0	0	0	0
2008	0	0	0	0	0	0	0	0	0	0	0	0	0	0	0	0	0	0	0
2008	0	0	0	0	0	0	0	0	0	0	0	0	0	0	0	0	0	0	0
2008	0	0	0	0	0	0	0	0	0	0	0	0	0	0	0	0	0	0	0

6.2 Appendix B: Accumulated Seasonal spatial maps

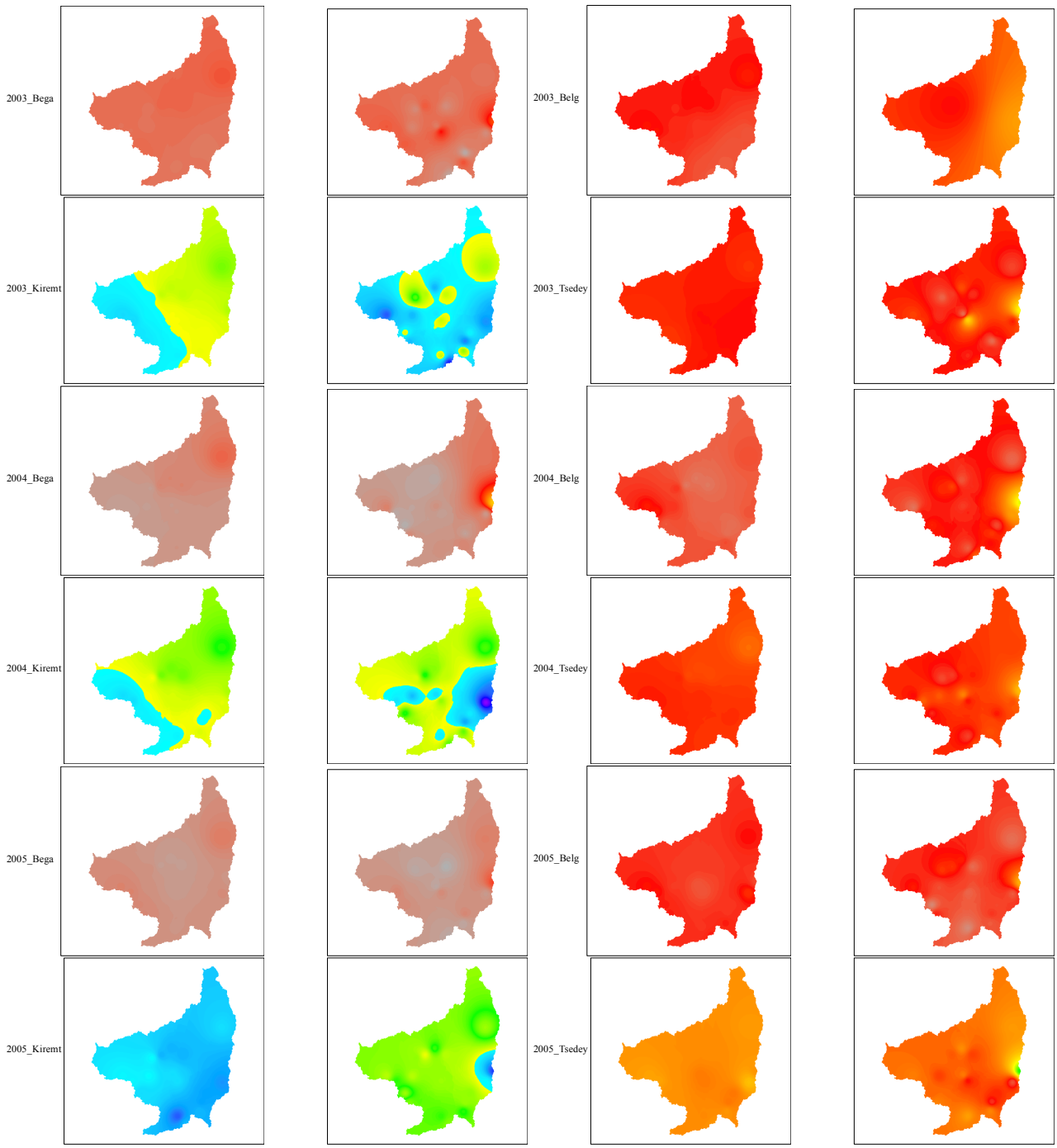

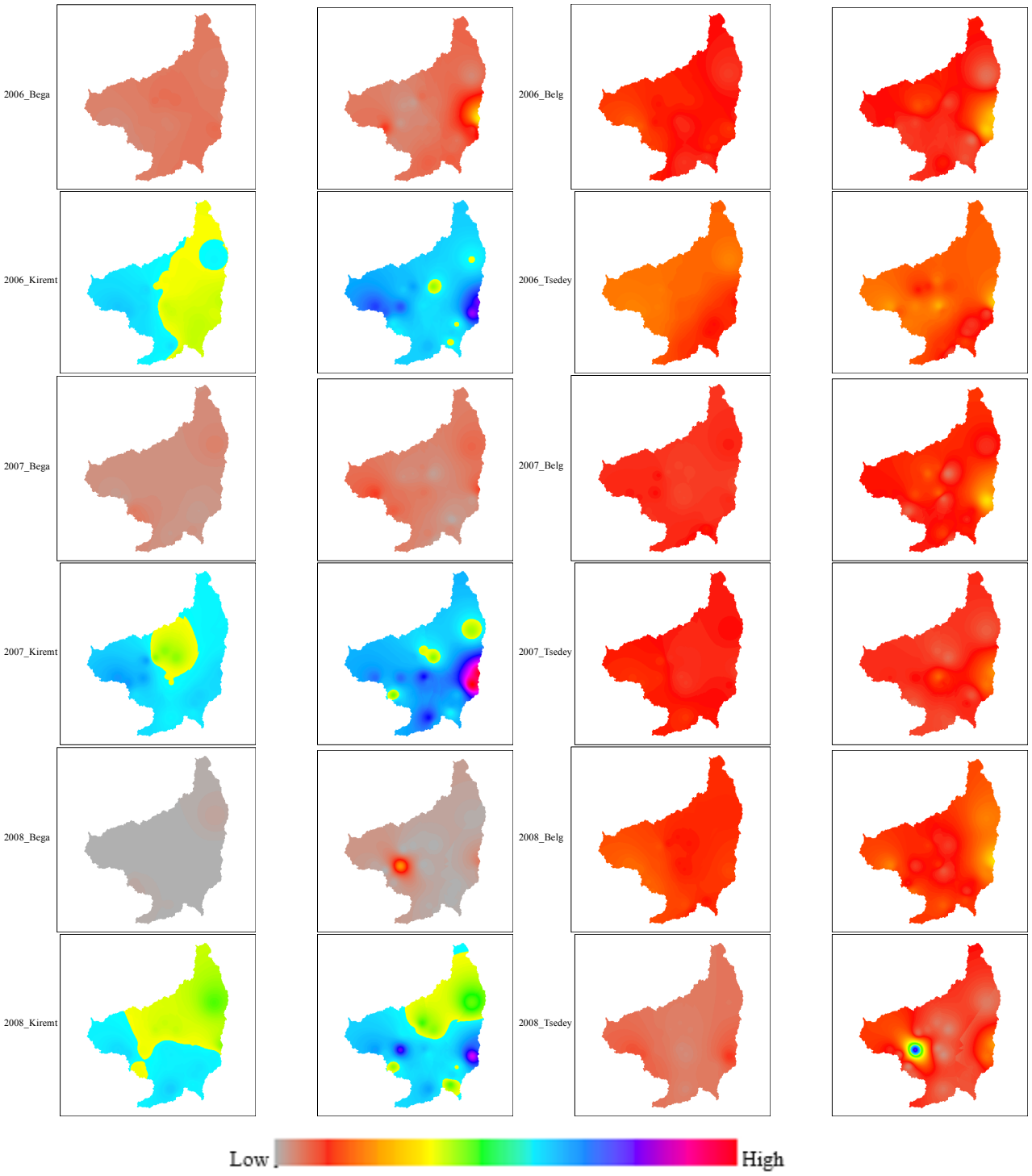
2006_Bega
2006_Belg
2006_Kiremt
2006_Tsedey
2007_Bega
2007_Belg
2007_Kiremt
2007_Tsedey
2008_Bega
2008_Belg
2008_Kiremt
2008_Tsedey
Low
High

6.3 Appendix C: Accumulated Annual average spatial maps

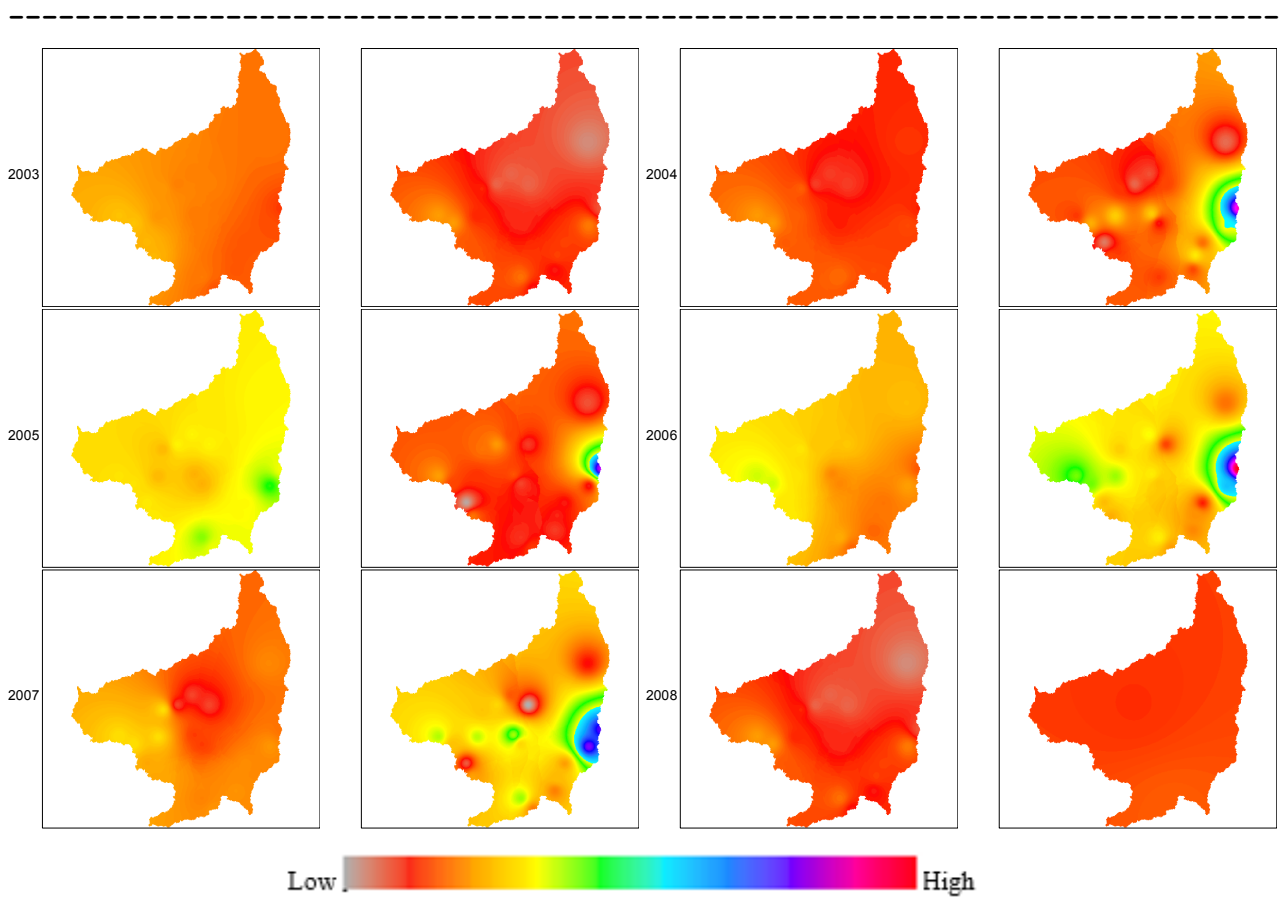

6.4 Appendix D: Accumulated monthly time-series plots of the stations

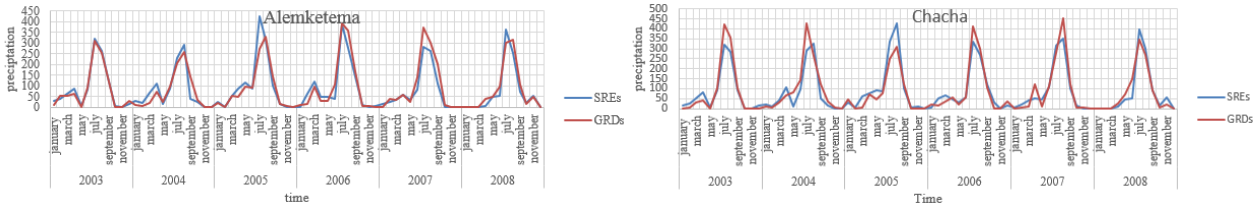

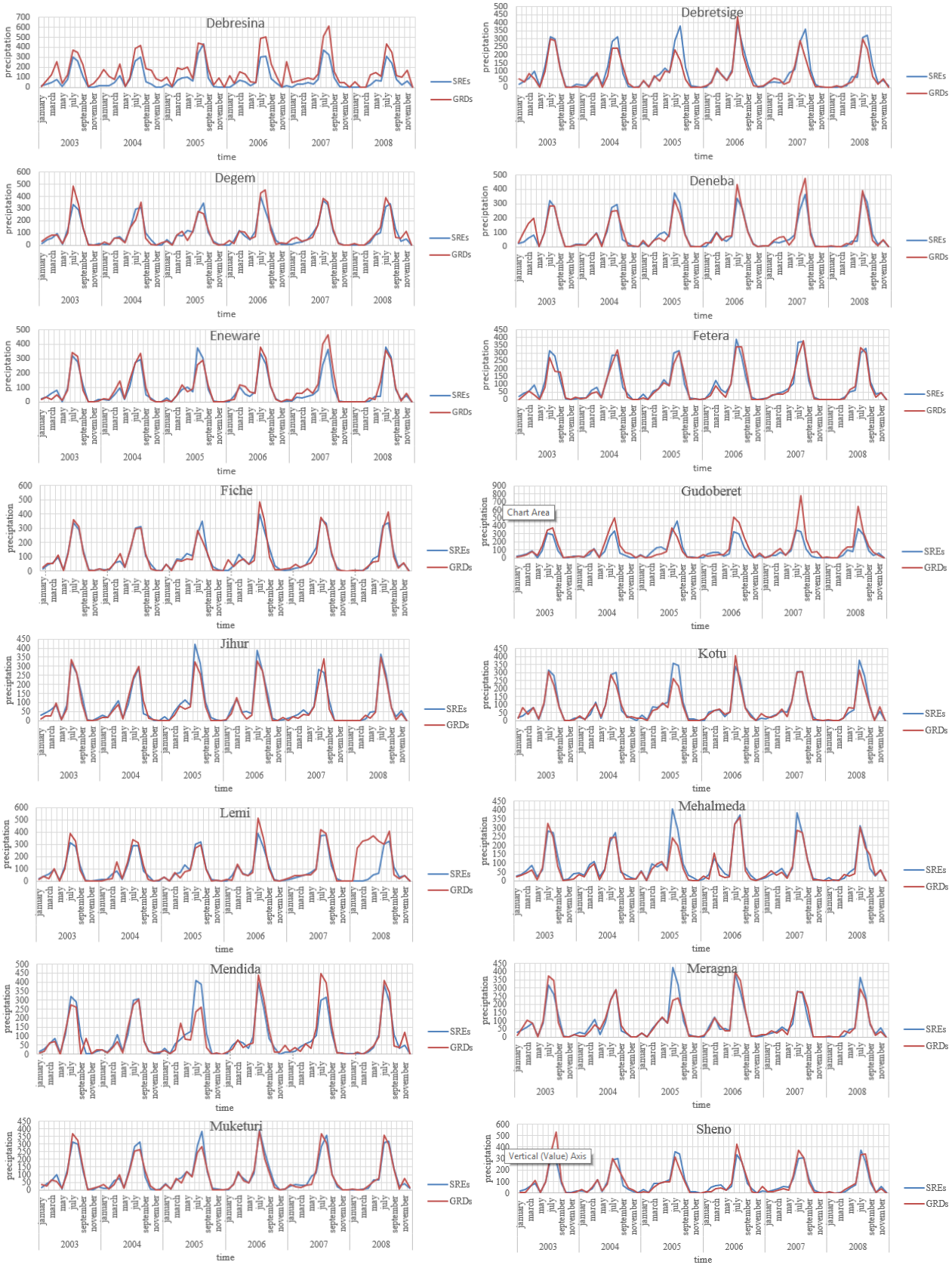
Debresina
Debretsige
Degem
Deneba
Eneware
Fetera
Fiche
Gudoberet
Chart Area
Jihur
Kotu
Lemi
Mehalmeda
Mendida
Meragna
Muketuri
Sheno
Vertical (Value) Axis
preciptation
time
SREs
GRDs
2003
2004
2005
2006
2007
2008

6.5 Appendix E: Accumulated Seasonal time-series plots of the stations

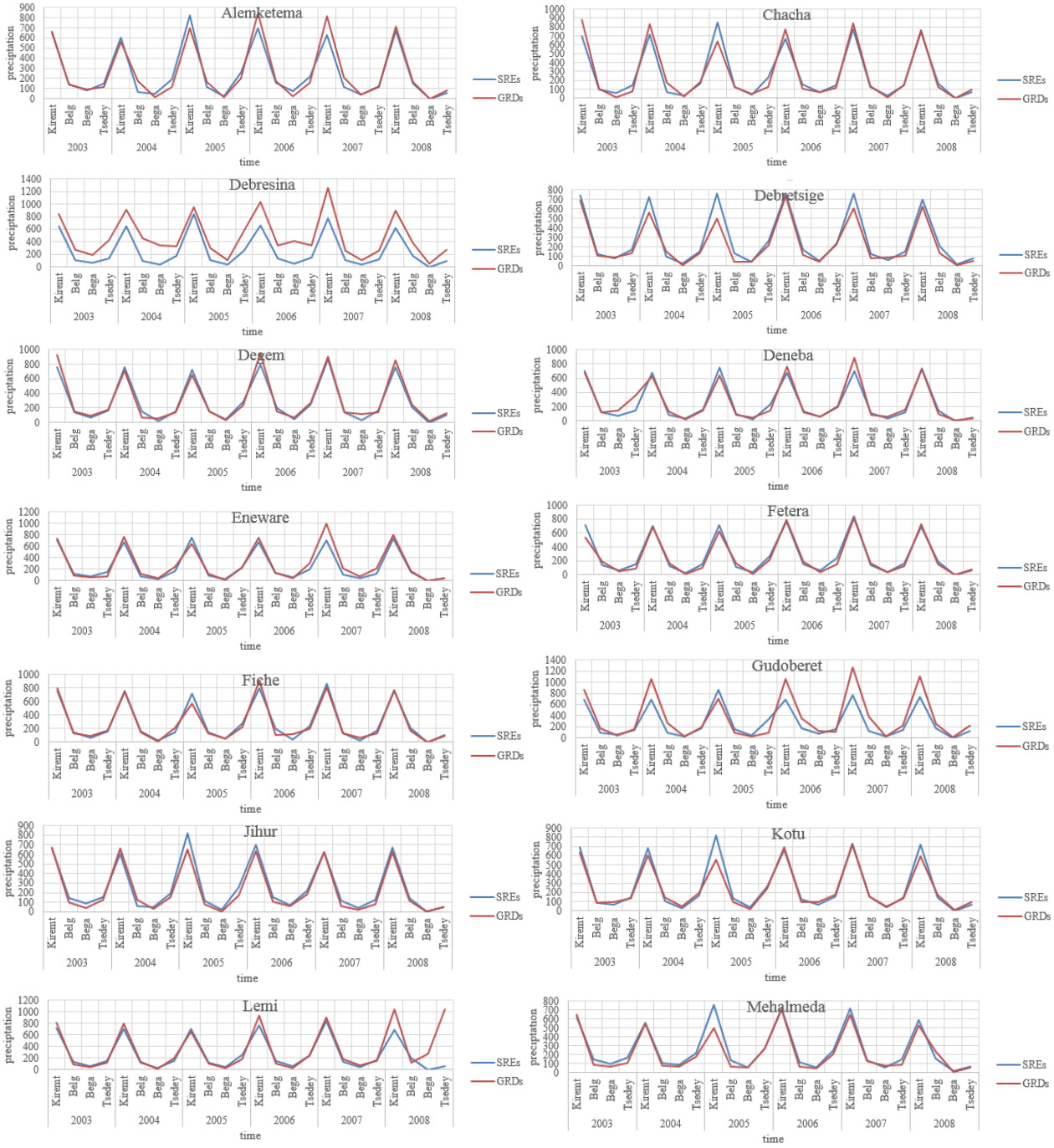

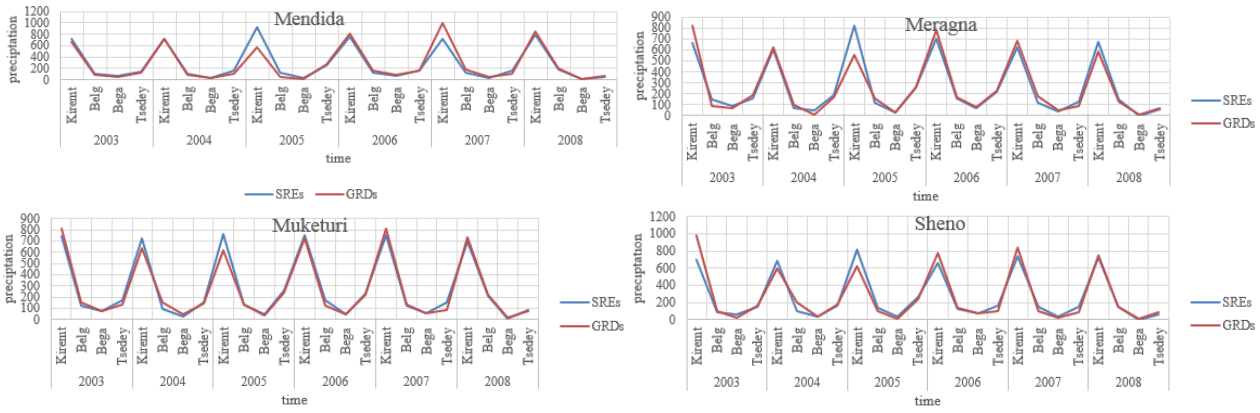
Mendida
Meragna
Muketuri
Sheno
preciptation
time
SREs
GRDs
Kiremt
Belg
Bega
Tsedey
2003
2004
2005
2006
2007
2008

REFERENCES

Ajmar, A., Albanese, A., Disabato, F. & Miotto, F. (2012). Integration of satellite and rainfall data for the identification of flood events in developing countries. *Italian Journal of Remote Sensing - 2012, 44 (1): 167-180.*

Alazzy, A.A., Lü, H., Chen, R. & Ali, A.B. (2017). Evaluation of satellite precipitation products and their potential influence on hydrological modeling over the ganzi river basin of the tibetan plateau. *Advances in Meteorology Volume 2017, Article ID 3695285, 23 pages.*

BARRETT, E.C. (2000). Satellite remote sensing of precipitation: Progress and problems. *Remots Sensing and Hydrology 2000 (Proceedings of a symposium held at Santa Fe, New Mexico, USA, April 2000). IAHS Publ. no. 267, 2001.*

Bashar, K.E. & Zaki, A.F. (2009). SMA based continuous hydrologic simulation of the blue nile. *FRIEND/Nile Project.*

Bayissa, Y., Tadesse, T., Demisse, G. & Shiferaw, A. (2017). Evaluation of satellite-based rainfall estimates and application to monitor meteorological drought for the upper blue nile basin, ethiopia. *Remote Sens. 2017, 9, 669.*

Bhattacharya, A.K., McEnroe, B.M., Zhao, H., Kumar, D. & Shinde, S. (2012). ModClark model: Improvment and application. *IOSR Journal of Engineering (IOSRJEN).*

Caldera, V.N., H.P.G.M.; Piyathisse. (2016). A comparison of methods of estimating missing daily rainfall data. *ENGINEER - Vol. XLIX, No. 04.*

Devi, G.K., P, G.B. & S, D.G. (2015). A review on hydrological models. *Aquatic Procedia 4 (2015) 1001 – 1007.*

Dinku, T., Hailemariam, K., Maidment, R., Tarnavsky, E. & Connor, S. (2013). Combined use of satellite estimates and rain gauge observations to generate high-quality historical rainfall time series over ethiopia. *Int. J. Climatol. 34: 2489–2504 (2014).*

Doan, C.D., Liu, J., Liong, S.-Y., Kim, D.E., Sanders, R. & Fewtrell, T. (2014). Combining satellite and gauge precipitation data with co-kriging method for jakarta region. *International Conference on Hydroinformatics.*

Feldman, A.D. (2000). *Hydrologic modeling system, technical reference manual.* US Army Corps of Engineers.

Gebre, S.L. (2015). Application of the hec-hms model for runoff simulation of upper blue

nile river basin. *Hydrol Current Res 6: 199*.

Gebremichael, M., Bitew, M.M., Hirpa, F.A. & Tesfay, G.N. (2014). Accuracy of satellite rainfall estimates in the blue nile basin: Lowland plain versus highland mountaine. *Water Resources Resesrch*.

GHARIB, M., M. (2018). EVALUATION of modclark model for simulating rainfall-runoff in tangrah watershed, iran. *APPLIED ECOLOGY AND ENVIRONMENTAL RESEARCH*.

Harris, A., Rahman, S., Hossain, F. & Easson, G. (2007). Satellite-based flood modeling using trmm-based rainfall products. *Sensors 2007, 7, 3416-3427*.

Hossain, S., Hewa, G.A. & Wella-Hewag, S. (2019). A comparison of continuous and event-based rainfall-runoff (rr) modelling using epa-swmm. *Water 2019, 11, 611*.

Huffman, G.J. (2018). The transition in multi-satellite products from trmm to gpm (tmpa to imerg). *TMPA-to-IMERG Transition*.

Huffman & Bolvin. (2018). TRMM and other data precipitation data set documentation.

Huffman, G.J., Adler, R.F., Bolvin, D.T. & Nelkin, E.J. (2009). The trmm multi-satellite precipitation analysis (tmpa). *TMPA - Rev. 3/2/09*.

Jajarmizadeh, M., Harun, S. & Salarpour, M. (2012). A review on theoretical consideration and types of models in hydrlogogy. *Journal of Environmental science and Technology*.

Japan-Aerospace-Exploration-Agency. (2017). *GPM data utilization handbook*. GPM/DPR Project team.

K, K. & V, H. (2014). APPLICATION of a continuous rainfall-runoff model to the basin of kosynthos river using the hydrologic software hec-hms. *Global NEST Journal*.

KIDD, C., KNIVETON, D.R., TODD, M.C. & BELLERBY, T.J. (2003). Satellite rainfall estimation using combined passive microwave and infrared algorithms. *JOURNAL OF HYDROMETEOROLOGY*.

Knebl, M., Yang, Z.-L., Hutchison, K. & Maidment, D. (2004). Regional scale flood modeling using nexrad rainfall, gis, and hec-hms/ras: A case study for the san antonio river basin summer 2002 storm event. *Journal of Environmental Management 75 (2005) 325–336*.

Kull, D. & Feldman, A. (1998). Evolution of clark's unit graph method to spatially distributed runoff. *Journal of Hydrologic Engineering, 3(1): 9-19*.

Lakew, H.B., Moges, S.A. & Asfaw, D.H. (2017). Hydrological evaluation of satellite and

reanalysis precipitation products in the upper blue nile basin: A case study of gilgel abbay. *Hydrology 2017, 4, 39.*

Levizzani, V., Amorati, R. & Meneguzzo, F. (2002). A review of satellite-based rainfall estimation methods. *A Research Project supported by the European Commission under the Fifth Framework Programme and contributing to the implementation of the Key Action 'Sustainable Management and Quality of Water' within the Energy, Environment and Sustainable Development.*

Levizzani, V., Bauer, P. & Turk, F.J. (2007). MEASURING precipitation from space. *ADVANCES IN GLOBAL CHANGE RESEARCH 28.*

Lillesand, T.M., Kiefer, R.W. & Chipman, J.W. (2004). *REMOTE sensing and image interpret ation.* John Wiley; Sons, Inc.

Liu, X., Liu, F.M., Wang, X.X., Dong, X., Fan, Y.Y., Cai, S.X. & Ao, T.Q. (2015). Combining rainfall data from rain gauges and trmm in hydrological modelling of laotian data-sparse basins. *Appl Water Sci (2017) 7:1487–1496.*

MARIANI, S. & CASAIOLI, M. (2008). FORECAST verification: A summary of common approaches and examples of application. *FORALPS Technical Report, 5.*

Mishra, A.K. (2012). Application of merged precipitation estimation technique to study intense rainfall events over india and associated oceanic region. *Atmospheric and Climate Sciences, 2012, 2, 222-229.*

Moriasi, D.N., Arnold, J.G., Liew, M.W.V., Bingner, R.L., Harmel, R.D. & Veith, T.L. (2007). MODEL evaluation guidelines for systematic quantification of accuracy in watershed simulations. *Transactions of the ASABE Vol. 50(30): 885-900.*

Moriasi, D.N., Gitau, M.W., Pai, N. & Daggupati, P. (2015). HYDROLOGIC and water quality models: PERFORMANCE measures and evaluation criteria. *Transactions of the ASABE Vol. 58(6): 1763-1785.*

NASDA. (2001). *TRMM data users handbook.* Earth Observation Center.

Paudell, M. (2010). An examination of distributed hydrologic modeling methods as compared with traditional lumped parameter approaches. *All Theses and Dissertations. 2219.*

PECHLIVANIDIS, I., JACKSON, B. & MCINTYRE, N. (2011). CATCHMENT scale hydrological modelling: A review of model types, calibration approaches and uncertainty analysis methods in the context of recent developments in technology and applications. *Global*

NEST Journal, Vol 13, No 3, pp 193-214, 2011.

Raghunath, H. (2006). *Hydrology principles analysis design.* New Age International (P) Ltd.

Rahmawati, N. & Lubczynski, M.W. (2018). Validation of satellite daily rainfall estimates in complex terrain of bali island, indonesia. *Theor Appl Climatol (2018) 134:513–532.*

Ren, P., Li, J., Feng, P., Guo, Y. & Ma, Q. (2018). Evaluation of multiple satellite precipitation products and their use in hydrological modelling over the luanhe river basin, china. *Water 2018, 10, 677.*

Romilly, T.G. & Gebremichael, M. (2010). Evaluation of satellite rainfall estimates over ethiopian river basins. *Hydrol. Earth Syst. Sci., 15, 1505–1514, 2011.*

Rossi, M., Kirschbaum, D., Valigi, D., Cesare, A. & Guzzetti, F. (2017). Comparison of satellite rainfall estimates and rain gauge measurements in italy, and impact on landslide modeling. *Climate 2017, 5, 90.*

Sahlu, D., Moges, S.A., Nikolopoulos, E.I., Anagnostou, E.N. & Hailu, D. (2017). Evaluation of high-resolution multisatellite and reanalysis rainfall products over east africa. *Advances in Meteorology Volume 2017, Article ID 4957960, 14 pages.*

Sattari, A.K., Mohammad-Taghi; Rezazadeh-Joudi. (2016). Assessment of different methods for estimation of missing data in precipitation studies. *Assessment of methods for estimating missing data in precipitation studies.*

Scharffenberg, B., Bartles, M., Brauer, T., Fleming, M. & Greg Karlovits. (2018). *Hydrologic modeling system hec-hms user's manual.* US Army Corps of Engineers.

SEARCY, J.K. & HARDISON, C.H. (1960). *Double-mass curves.*

Shrestha, M.S., Bajracharya, S.R. & Mool, P. (2008). Satellite rainfall estimation in the hindu kush-himalayan region.

Silva, N.R., R. P. De; Dayawansa. (2007). A comparison of methods used in estimating missing rainfall data. *The Journal of Agricultural Sciences, 2007, vol.3, no.2.*

Subramanya, K. (2013). *ENGINEERING hydrology.* McGraw Hill Education (India) Private Limited.

Suhaila, J., Sayang, M.D. & Jemain, A.A. (2008). Revised spatial weighting methods for estimation of missing rainfall data. *ASIA-PACIFIC JOURNAL OF ATMOSPHERIC*

SCIENCES, 44, 2, 2008, p. 93-104.

Tassew, B.G., Belete, M.A. & Miegel, K. (2019). Application of hec-hms model for flow simulation in the lake tana basin: The case of gilgel abay catchment, upper blue nile basin, ethiopia. *Hydrology 2019, 6, 21.*

Tesfatsion, Y. & Dinku, T. (2015). Rainfall estimation from satellite data in ethiopia: Calibration and application. *ResearchGate.*

Tiwari, M.K., Gaur, M.L., V., B.S. & K., N.J. (2013). Rainfall-runoff modeling using hec-hms, remote sensing and geographical information system in middle gujarat, india. *National Seminar on Climate Change Impacts on Water Resources Systems.*

Upadhyaya, S. & Ramsankaran, R. (2014). REVIEW of satellite remote sensing data based rainfall estimation methods. *Proceedings of HYDRO 2013 INTERNATIONAL, 4-6 Dec 2013, IIT Madras, INDIA.*

Wei, G., Lu, H., Crow, W.T., Zhu, Y., Wang, J. & Su, J. (2017). Evaluation of satellite-based precipitation products from imerg v04a and v03d, cmorph and tmpa with gauged rainfall in three climatologic zones in china. *Remote Sens. 2018, 10, 30.*

Woldemeskel, F.M., Sivakumar, B. & Sharma, A. (2013). Merging gauge and satellite rainfall with specification of associated uncertainty across australia. *Journal of Hydrology 499 (2013) 167–176.*

WWRP. (2009). Forecast verification - issues, methods and faq. *JWGFVR.*

WWRP. (2008). RECOMMENDATIONS for the verification and intercomparison of qpfs and pqpfs from operational nwp models. *RECOMMENDATIONS for the VERIFICATION AND INTERCOMPARISON.*

Xu, C.-y. (2002). *TEXTBOOK of hydrologic models.* Uppsala University Department of Earth Sciences Hydrology.

Zambrano-Bigiarini, M., Nauditt, A., Christian Birkel, Verbist, K. & Ribbe, L. (2017). Temporal and spatial evaluation of satellite-based rainfall estimates across the complex topographical and climatic gradients of chile. *Hydrol. Earth Syst. Sci., 21, 1295–1320, 2017.*

Zemadim, B. (2010). *Hydrology guide book.* ASWHI.

Zeng, Q., Wang, Y., Chen, L., Wang, Z., Zhu, H. & Li, B. (2018). Inter-comparison and evaluation of remote sensing precipitation products over china from 2005 to 2013. *Remote Sens. 2018, 10, 168.*